INVESTIGATION OF THE DISSIPATION OF THE TIP VORTEX OF A ROTOR BLADE BY MASS INJECTION

Richard P. White, Jr., et al

Rochester Applied Science Associates, Incorporated

Prepared for:

Army Air Mobility Research and Development Laboratory

August 1972

AD

USAAMRDL TECHNICAL REPORT 72-43

INVESTIGATION OF THE DISSIPATION OF THE TIP VORTEX OF A ROTOR BLADE BY MASS INJECTION

By

Richard P. White, Jr.
John C. Balcerak

August 1972

EUSTIS DIRECTORATE
U. S. ARMY AIR MOBILITY RESEARCH AND DEVELOPMENT LABORATORY
FORT EUSTIS, VIRGINIA

CONTRACT DAAJ02-71-C-0036
ROCHESTER APPLIED SCIENCE ASSOCIATES, INC.
ROCHESTER, NEW YORK

Approved for public release; distribution unlimited.

96

DISCLAIMERS

The findings in this report are not to be construed as an official Department of the Army position unless so designated by other authorized documents.

When Government drawings, specifications, or other data are used for any purpose other than in connection with a definitely related Government procurement operation, the United States Government thereby incurs no responsibility nor any obligation whatsoever; and the fact that the Government may have formulated, furnished, or in any way supplied the said drawings, specifications, or other data is not to be regarded by implication or otherwise as in any manner licensing the holder or any other person or corporation, or conveying any rights or permission, to manufacture, use, or sell any patented invention that may in any way be related thereto.

Trade names cited in this report do not constitute an official endorsement or approval of the use of such commercial hardware or software.

DISPOSITION INSTRUCTIONS

Destroy this report when no longer needed. Do not return it to the originator.

A

Unclassified
Security Classification

DOCUMENT CONTROL DATA - R & D

(Security classification of title, body of abstract and indexing annotation must be entered when the overall report is classified)

1. ORIGINATING ACTIVITY (Corporate author) Rochester Applied Science Associates, Inc. 140 Allens Creek Road Rochester, New York	2a. REPORT SECURITY CLASSIFICATION Unclassified 2b. GROUP

3. REPORT TITLE

INVESTIGATION OF THE DISSIPATION OF THE TIP VORTEX OF A ROTOR BLADE BY MASS INJECTION

4. DESCRIPTIVE NOTES (Type of report and inclusive dates)
Final Report

5. AUTHOR(S) (First name, middle initial, last name)
Richard P. White, Jr.
John C. Balcerak

6. REPORT DATE	7a. TOTAL NO. OF PAGES	7b. NO. OF REFS
August 1972	93	23

8a. CONTRACT OR GRANT NO.	9a. ORIGINATOR'S REPORT NUMBER(S)
DAAJ02-71-C-0036 b. PROJECT NO. c. Task 1F162203A14301 d.	USAAMRDL Technical Report 72-43 9b. OTHER REPORT NO(S) (Any other numbers that may be assigned this report) RASA Report 72-03

10. DISTRIBUTION STATEMENT

Approved for public release; distribution unlimited.

11. SUPPLEMENTARY NOTES	12. SPONSORING MILITARY ACTIVITY
Details of illustrations in this document may be better studied on microfiche	Eustis Directorate, U.S. Army Air Mobility Research & Development Laboratory, Ft. Eustis, Virginia

13. ABSTRACT

This report describes an experimental research program in which the outer section of a UH-1D helicopter blade was modified to incorporate a system for injecting the tip vortex produced by the blade with a mass of linearly directed air. The effects of nozzle geometry, the velocity of injection, the turbulence wavelength, and the angle of injection on the resulting strength of the trailed tip vortex were investigated, and the results are presented in terms of quantitative measurements of the circulation strength as a function of the injected mass of air. Data obtained from flow-visualization studies in which illuminated helium bubbles, smoke, and tuft grids were used to help understand the resulting changes in the circulatory flow associated with the tip vortex are also presented. In addition, comparisons are made with results of associated research investigations previously conducted by RASA, and with results of similar research conducted by other organizations.

The results of this investigation indicate that mass injection of the concentrated tip vortex is a practical approach to the elimination of the strong induced effects on a lifting surface of the circulatory flow associated with a concentrated vortex generated by a helicopter rotor blade.

I

DD FORM 1 NOV 68 1473 REPLACES DD FORM 1473, 1 JAN 64, WHICH IS OBSOLETE FOR ARMY USE.

Unclassified
Security Classification

14. KEY WORDS	LINK A		LINK B		LINK C	
	ROLE	WT	ROLE	WT	ROLE	WT
Mass Flow Injection						
Vortex Dissipation						
Vortex Instability						
Aerodynamics						
Acoustics						
Rotor Blades						
Tip Vortex						
Viscous Mixing						
Blade Loads						

II

8788-72

DEPARTMENT OF THE ARMY
U. S. ARMY AIR MOBILITY RESEARCH & DEVELOPMENT LABORATORY
EUSTIS DIRECTORATE
FORT EUSTIS, VIRGINIA 23604

This report has been reviewed by the Eustis Directorate, U. S. Army Air Mobility Research and Development Laboratory and is considered to be technically sound.

The research was performed to investigate the dissipative effect of air injected into the tip vortex core. The results appeared to be successful and the concept of air injection to dissipate the vortex appears to be feasible, although the practical application of the concept is yet to be investigated.

This report is published for the dissemination of the results of this investigation and for the stimulation of ideas relative to the basic subject. The program was conducted under the technical management of Mr. W. E. Nettles of the Aeromechanics Division of this Directorate.

Task 1F162203A14301
Contract DAAJ02-71-C-0036
USAAMRDL Technical Report 72-43
August 1972

INVESTIGATION OF THE DISSIPATION OF THE TIP VORTEX OF A ROTOR BLADE BY MASS INJECTION

Final Report

RASA Report 72-03

By

Richard P. White, Jr.
John C. Balcerak

Prepared by

Rochester Applied Science Associates, Inc.
Rochester, New York

for

EUSTIS DIRECTORATE
U. S. ARMY AIR MOBILITY RESEARCH AND DEVELOPMENT LABORATORY
FORT EUSTIS, VIRGINIA

IV

ABSTRACT

This report describes an experimental research program in which the outer section of a UH-1D helicopter blade was modified to incorporate a system for injecting the tip vortex produced by the blade with a mass of linearly directed air. The effects of nozzle geometry, the velocity of injection, the turbulence wavelength, and the angle of injection on the resulting strength of the trailed tip vortex were investigated, and the results are presented in terms of quantitative measurements of the circulation strength as a function of the injected mass of air. Data obtained from flow-visualization studies in which illuminated helium bubbles, smoke, and tuft grids were used to help understand the resulting changes in the circulatory flow associated with the tip vortex are also presented. In addition, comparisons are made with results of associated research investigations previously conducted by RASA, and with results of similar research efforts conducted by other organizations.

The results of this investigation indicate that mass injection of the concentrated tip vortex is a practical approach to the elimination of the strong induced effects on a lifting surface of the circulatory flow associated with a concentrated vortex generated by a helicopter rotor blade.

FOREWORD

The work described in this report was performed by the Rochester Applied Science Associates, Inc., for the Eustis Directorate of the U. S. Army Air Mobility Research and Development Laboratory, Fort Eustis, Virginia, under Contract DAAJ02-71-C-0036, Task 1F162203A14201. The research program was undertaken under the technical cognizance of Mr. William E. Nettles of the Eustis Directorate.

Appreciation is extended by the authors to Drs. Stephen A. Rinehart and Keith W. Shipman, and Mr. Robert Polvino of RASA for the valuable assistance in the successful completion of the research program, as well as to Mr. Donald Gross and his staff at the University of Maryland Wind Tunnel facility.

TABLE OF CONTENTS

LIST OF ILLUSTRATIONS

LIST OF TABLES

LIST OF SYMBOLS

A	cross-sectional area of the nozzle ($in.^2$)
AR	aspect ratio, nondimensional
C	blade chord, ft
m_i	injected mass flow, lb/sec
P_m	static pressure at orifice flow meter, inches of mercury
R	radius to blade tip, ft
T	thrust, lb
V	freestream velocity, ft/sec
v_i	velocity of injected mass flow, ft/sec
α_i	angle of injection with respect to chordline, degrees
α_T	aerodynamic angle of attack at tip of blade section
Γ	circulation strength of the trailed tip vortex, ft^2/sec
Γ_0	circulation strength of the unmodified trailed tip vortex, ft^2/sec
μ	advance ratio, nondimensional
ψ	azimuthal angle, degrees
Ω	blade rotational speed, rad/sec

I. INTRODUCTION

Since the first successful flight of the helicopter, the "dynamic" characteristics of this vehicle have been well-known to those who have been either riding in the aircraft or to those striving to construct a successful rotor system or vibration-free structure. During the early years of the development of the helicopter, the important dynamic effects produced by the vortex wake had to be ignored in deference to the more urgent need to solve problems of stability, control, performance and structural integrity. Once these goals were achieved, however, then vibrations, a more reasonable structural life, and most recently, noise considerations led to the need to define the nature of the vortex wake. In order that helicopter blades could be properly designed on the basis of these considerations, the aerodynamic loadings associated with the interaction of the blade with the nonuniform flow field arising from the trailed and shed vorticity had to be defined more precisely. While early theoretical attempts to predict the instantaneous induced-velocity field (Ref. 1) and the oscillatory aerodynamic loading (Refs. 2 and 3) of helicopter rotors represented significant advances in that era, the work of Miller (Ref. 4) and DuWaldt and Piziali (Ref. 5) undertook the problem with all its complexities and provided the basis of the current state of the art.

The prediction of the dynamic loads of helicopter rotor systems continues to receive a great deal of attention in the V/STOL industry,and a majority of the investigators are concerned with the flow field in the vicinity of the rotor system and the helicopter fuselage which is immersed in the rotor vortex wake. Current research in the development of computational programs in this area allow the position of the "free, distorted wake" to be predicted in the vicinity of the helicopter rotor and fuselage for single, tandem and coaxial rotor systems. This research has been and continues to be aimed at improving significantly the prediction of the aerodynamic and dynamic loads generated by the rotor blades while the aircraft is in either a steady-state or a maneuver flight mode. Reference 6 and 7 present examples of the current state of the art in the prediction of the aerodynamic environment in which a helicopter blade operates in forward flight.

While these previously mentioned research programs have been associated with predicting the effects of the concentrated vortex, considerable effort has also been expended by the V/STOL industry in an attempt to understand the characteristics of the structure of the blade tip vortex and its interaction with a lifting surface because of its great influence on blade

dynamic loads problems, and the generation of rotor noise. For example, some of the approaches attempted by research engineers in V/STOL industry and, more recently, in the fixed-wing industry to modify the trailed concentrated tip vortex are categorized in Figure 1, and Figure 2 presents conceptual sketches of the various modifications to the lifting surfaces that have been attempted to test the validity of these diverse approaches.

Some of the approaches are categorized as hopefully accomplishing more than one kind of modification. For example, porous tips are listed both as capable of spreading concentrated vorticity and also dissipating the strength of the vorticity. Lifting surface tip spoilers are listed in the same category. End plates are categorized as both spreading and relocating the concentrated vorticity. The effect of gulled outer panels (Ref. 8) is to divide the total concentrated vorticity into two vortices, each of lesser strength, at two different spanwise locations (one at the juncture of the gulled tip and main lifting surface and the other at the tip), and also to relocate the tip vortex with respect to a dimension normal to the wing chord plane because of the deflection of the tip of the gulled section.

While the porous tip spreads the vorticity in the near wake (Ref. 9), it also has the potential of dissipating the vortex because of the turbulence generated by the flow passing through the porous sections. As might have been expected, the dissipation obtained with the porous tips was not significant because of the small turbulence wavelength generated, and thus investigators have found that the concentrated vortex reappeared downstream with its strength apparently unchanged. The wing tip spoilers, by which Chigier at NASA/Ames attempted to modify the tip vortex (Ref. 10), seems to produce the same end result as the porous tip at a downstream location, again apparently because of the small turbulence wavelength that was generated.

Spanwise blowing tried by Scheiman and others (Refs. 11 and 12), seemed to have no effect other than to relocate the position of the trailed vortex.

Investigations, to date, of the effect of jet engine location in the vicinity of the tip vortex have not been notably successful. Dr. John Olsen of Boeing (Ref. 13) and the NASA investigators (Refs. 14 and 15) who have tried this approach placed the turbulent jet in the irrotational regimes of the vortex. Thus, its potential dissipative action was weakly coupled with that part of the vortex which contains the concentrated rotational energy: the vortex core.

Based on research in which RASA had been engaged in the past, it was believed that the injection of a linearly directed aerodynamic mass flow into the core of a swirling tip vortex would significantly increase the viscous dissipation of that vortex. As indicated in Figure 1, this vortex modification technique has the sole objective of dissipating the strength of the concentrated vorticity rapidly by the action of eddy viscosity at the lower mass flows or by the generation of a jet flow instability at the higher mass flow.

In 1969 under ONR sponsorship, RASA conducted a theoretical analysis of the mixing of such an injected airflow in the core of the vortex. The results of this theoretical work conducted by Rinehart (Ref. 16) were extremely encouraging, in that they indicated that the concentrated vorticity of the trailed tip vortex could be significantly reduced by the input of a relatively small amount of mass flow if it were properly injected into the core of the vortex. The analysis also indicated that the performance parameters, such as lift and drag, would not be affected significantly and furthermore that the required mass flow was low enough so that in helicopter rotor systems, it could probably be obtained through centrifugal pumping in the rotor system. This theoretical research program also investigated the effects of suction and reverse swirl on the modification of the tip vortex, but the results showed that neither of these approaches was beneficial or practical.

In view of the encouraging results of this theoretical research, ONR sponsored an experimental program with RASA to determine if the predicted beneficial results of vortex injection were, in fact, realizable. The results of this experimental program (Ref. 17) generally confirmed the theoretical predictions up to specific values of injected mass flow. Beyond these mass flows, where the theory could not account for large-scale flow instabilities, the experimental results were even more encouraging than the theory. Thus, on the basis of these two research programs, it appeared that significant modification of the trailed tip vortex at its source could be realized for the helicopter. Thus the program reported upon herein was directed toward determining the most effective injection system for a practical helicopter rotor blade. The rotor blade tested during this program was from a UH-1D .

After the initial theoretical and experimental results obtained by RASA were presented, other investigators attempted to modify the concentrated tip vortex by the same or similar techniques with varying degrees of success. Yuan (Ref. 18) reported in May 1971 that he was able to eliminate the vortex 2-1/2 chord lengths downstream and gain an increase in the aerodynamic

performance characteristics of the three-dimensional lifting surface through the use of a curved chordwise slot(s) emitting air in the spanwise direction. While he presented quantitative data regarding the lift and drag, he presented no quantitative data substantiating the claim of the elimination of the concentrated trailed vorticity. Poppleton, in August 1971 (Ref. 19), reported on an experiment he conducted using a split airfoil and an injection tube to investigate the effect of air injection into the core of the trailing vortex. He noted that the effect of injecting air into the vortex is quite marked, although a great quantity of air was required to obtain these beneficial effects. Also, during August 1971, Kantha, Lewellen and Durgin at MIT (Ref. 20) reported on an investigation in which smoke was used to visualize the tip vortex and a vortex meter was used to obtain peak vorticity reading at 1, 3, and 13 chord lengths downstream. On the basis of the limited data that was obtained, the authors concluded that the effect of mass injection on the dissipation of the concentrated tip vortex was governed by the momentum and not the mass flow rate as originally concluded by Rinehart in Reference 16. These investigators also concluded that there seemed to be an optimum rate of injection beyond which increased injection did not bring about equally significant changes in the vortex core. In September 1971, Mason and Marchman at VPI (Ref. 21) reported on an investigation in which they used tuft grids located at 3.4, 14.2, 20 and 29.5 chord lengths downstream from the model to obtain a qualitative indication of the effect of mass injection on the characteristics of the vortex. On the basis of the qualitative results obtained, it was concluded that mass injection of the vortex core was an effective method of controlling the vortex, with the swirl velocity decreasing with increasing mass flow.

The results of the investigation reported herein will be compared with the results of previous investigations of vortex injection conducted by RASA and with those results obtained by other investigators in the hope that any differences in the interpretation of the results that have been obtained can be resolved.

II. DESCRIPTION OF MODEL AND INSTRUMENTATION

A. MODEL

The model used in this program was an outboard section of a blade from a UH-1D helicopter. The airfoil section of the blade was a NACA 0012 and the blade chord was 21.1 inches. The semispan of the section of the blade as installed in the wind tunnel measured approximately 5 feet. The blade section was untapered and the measured twist of the blade section was 0.35 deg/ft, which created an increasing angle of attack with span. The main structural member of the blade consisted of a "D" spar at the forward section of the chord. An aluminum skin was wrapped around the entire airfoil, and the skin was stabilized by aluminum honeycomb from the "D" spar to the trailing edge. The section of the helicopter blade was reworked to provide: (1) a support system for the wind-tunnel assembly; (2) an air-supply system from the support system at the base of the model to the tip; (3) a nozzle block at the tip of the model to which the various nozzles to be tested were attached, and a duct system for the air from the "D" spar to the nozzle; and (4) various tip-cap configurations.

A photograph of the supports at the base of the model is shown in Figure 3. Since the main structural member of the blade section was a "D" spar, the honeycomb material aft of the "D" spar was stripped from the model at its base to accommodate a clamp-type support which matched the contour of the "D" spar. This support was machined in a fashion so as to provide an air seal at the juncture of the base of the "D" spar and the support along the periphery of the "D" spar. The clamp was then conveniently bolted to a support which was attached to the balance table of the wind tunnel and which also had provision for supplying air to the model. An "O" ring between the clamp at the base of the model and the support on the balance table provided an air seal. The model was installed in the wind tunnel with the centerline of the "D" spar coincident with the centerline of the balance table to facilitate the routing of air through the assembly. In this installation, the model was pitched about the 15.5 percent chord.

At the tip of the model, the aft section of the "D" spar was cut out to provide for the passage of air to the nozzle. Turning vanes were also installed in this section to minimize the losses as the flow of air traversed the 90-degree turn from the "D" spar to the nozzle. A schematic diagram of the tip section of the model is shown in Figure 4, and a photograph of the turning vanes at the tip section of the models is shown in Figure 5. The inboard turning vane was positioned 3 inches

from the tip of the model, and it extended to the trailing edge of the model to provide a support for the installation of the nozzles. The inboard turning vane at the juncture of the "D" spar was formed by boring a 2-inch-diameter hole through one side of the model to the underlying skin, and then inserting a 2-inch-diameter plug into the hole. The plug stabilized the rib support which extended to the trailing edge, and an air seal between the inboard section of the model and the nozzle section was achieved by potting. An end rib was also machined to match the airfoil contour and to provide a support for the nozzle. The skin of the nozzle area was cut out from the 50 percent chord to the trailing edge of the model within the 3-inch spanwise width between the ribs to provide for the installation of the nozzles.

Physically, the nozzle could be up to 3 inches in spanwise width and from the 50 percent chord to the trailing edge in chordwise width. The end rib provided a square tip for the model, but provision was made to attach a developed half-round tip to the end rib or an additional squared-off tip which would essentially move the nozzle inboard. The semispan of the model, measured from the tunnel floor to the outboard edge of the end rib, was 59.28 inches. The square tip which could be attached to the end rib added 0.50 inch to the semispan, and the maximum thickness of the developed half-round tip section was 1.25 inches.

The concept of the nozzle design was to provide capability for varying the geometric shape of the model, the area of injection so that the velocity of injection could be varied while maintaining mass flow constant, the turbulence wavelength, and the angle of injection. These parameters were believed to be of primary importance with respect to providing the optimum nozzle to dissipate the tip vortex at minimum mass flow rates. In order to maintain the wind tunnel testing time within reasonable levels, the experimental study of the effect of these parameters was limited to one angle of attack, a root angle of 7.75 degrees, which, with model twist, corresponded to an angle of attack at the model tip of 9.5 degrees. This angle was selected to provide sufficiently high circulation strengths while also allowing for the study of variations in circulation strength due to angles of attack below stall.

The components comprising a typical nozzle and tip configuration are shown in Figure 6. In order to provide the versatility for the interchange of the various nozzles, an aluminum block was machined to fit the cutout at the tip of the airfoil, and further cutouts were machined in this block to accommodate the nozzles. The angle of injection was provided by machining a "ramp" corresponding to the desired angle of injection. The shape of

the nozzle could then be machined independently, and the proper angle of injection was obtained simply by placing the nozzle on the "ramp" and matching the exit face to the airfoil contour. The inlet to the nozzle from the plenum chamber which was formed by the duct system at the tip of the model was at a point 10.55 inches from the leading edge of the model, and the nozzles were positioned so that their centerline in the chordwise direction was approximately at the 75 percent chord location.

Two geometric shapes were considered for the nozzles, namely, circular and slotted jets. The circular shape was selected to provide a uniform injection velocity over the cross section of the core of the tip vortex. The slotted nozzle was selected to provide a greater chordwise distribution of uniform velocity of injection into the core of the vortex as it formed over the tip chord. (For each of these shapes, a coarse variation in the turbulence wavelength could be obtained from that corresponding to an open jet to the much smoother flow effected by equivalent nozzle shapes fabricated from honeycomb material.) A schematic diagram of the nozzles which indicates the pertinent dimensional data of all nozzles is shown as Figure 7, and a photograph of some of the typical nozzles is shown as Figure 8. The velocity of injection was varied while maintaining mass flow constant by fabricating nozzles with different areas. The areas of the nozzles were selected on the basis of expected mass flow requirements and to cover a range of average injection velocities from one to three times that of the freestream velocity. Provision was also made to restrict the entire nozzle area with a contoured block to provide a basic, unmodified blade section.

B. INSTRUMENTATION

The angle of attack of the model, tunnel conditions and balance data were recorded by the readout system of the University of Maryland Wind Tunnel. The mass flow of the injected air was computed from measurements of the pressures and temperatures across a sharp-edge orifice. The static pressure at the orifice was read out on a mercury manometer, the pressure drop across the orifice was read out on an alcohol manometer, and the temperature at the orifice was monitored by a thermocouple and read out on a potentiometer.

The swirl velocity in the trailed tip vortex was measured by an AEA[1] vortex meter, and the rotational speed of the meter was read out on an electronic counter. The signals generated by the vortex meter were also monitored on an oscilloscope. The wind tunnel facility at the University of Maryland provided a

[1]Aero Engineering Associates, State College, Pa.

two-dimensional, remotely controlled traverse mechanism to survey the wake normal to the model chord and along its span. The downstream position of the traverse mechanism could be varied manually; and for these tests, the traverse mechanism was positioned such that the vanes of the vortex meter were 6.5 chord lengths aft of the trailing edge of the model. The positions of the vortex meter along the span and normal to the chord plane were read out on counters. The resolution of the counter was ±0.01 inch in the spanwise direction and ±0.02 inch normal to the chord. The reference position for the vortex meter normal to the chord was the tunnel centerline, and the reference spanwise position for the vortex meter was the tip of the end rib of the model.

Three methods of flow visualization were used during the wind tunnel tests. Primarily, flow visualization in the proximity of the model was provided by neutrally-buoyant helium bubbles which were released upstream of the model over the tip section. The bubbles were illuminated by a collimated beam of light, observed visually and photographed. The trailed tip vortex was observed far downstream from a stream of smoke which was released upstream of the model over its tip section. Also, at approximately 15 chord lengths downstream of the model, indications of the swirl in the trailed tip vortex were observed visually and photographed on a tuft grid. The tuft grid was secured to the same frame assembly which housed the traverse mechanism.

III. CALIBRATION TESTS

Prior to the wind tunnel tests, the model was mounted horizontally to facilitate the acquisition of the distributions of the exit velocities across the nozzles. The exit velocities at the nozzles were measured with a 1/8-inch-diameter pitot tube, and the pressure differentials sensed by the pitot tube were read out either on an alcohol or a mercury manometer. Figure 9 is a photograph showing the setup for this calibration. The velocity distributions were obtained primarily for nozzles having an exit angle of 9.5 degrees; thus the model was mounted such that the tip was at a 9.5-degree angle with respect to the horizontal, with the jet then oriented horizontally. The velocities were measured at six chordwise positions of the jet; namely, at the 10, 20, 40, 60, 80 and 90 percent locations of the chordwise edges of the jet. In the spanwise direction, the velocities were measured in 0.10-inch increments near the center of the jet and in 0.05-inch increments near the spanwise edges of the jet. The velocity distributions for the slotted honeycomb jet nozzle (No. 5) which was used during the injection tests in which most of the detailed vortex surveys were made are shown in Figure 10.

The mass flow for each nozzle was obtained as a function of the density of the air at the orifice. The flow rate, which is a function of the density, the temperature and pressure drop across the orifice, varied for each nozzle, particularly as the area of the nozzle was changed. The mass flow of nozzle No. 5 as a function of the pressure at the orifice is shown in Figure 11; the flows of other nozzles used in the tests are shown in Appendix I.

IV. WIND TUNNEL TESTS

The wind tunnel tests under this program were conducted in the 7-3/4- x 11-foot Wind Tunnel at the University of Maryland. A photograph of the installation of the model and other appurtenances in the wind tunnel is shown in Figure 12.

In the first phases of the test program, flow-visualization tests were conducted for various tip configurations in order to determine which tip configuration would enhance the vortex-injection process. The criterion for these observations was the position of the centerline of the vortex with respect to the position of the nozzles at the model tip. The optimum position was viewed as that at which the centerline of the vortex was closest to the centerline of the nozzle. Various nozzle configurations were then tested to determine the effects of nozzle geometry, velocity of injection, turbulence wavelength and angle of injection on the circulation strength of the trailed tip vortex. This phase of the program was conducted primarily at a tip angle of attack of 9.5 degrees and a tunnel velocity of 100 fps. The tunnel velocity was limited to facilitate the flow-visualization studies. Acoustic data at zero airspeed for various nozzles at several mass injection rates were also obtained as a basis for optimum nozzle selection.

On the basis of the results of the initial tests, one nozzle was selected as the basic nozzle for the second phase of the test program, in which the primary data to be obtained were the vorticity distributions in the trailed tip vortices at 6.5 chord lengths behind the trailing edge of the model. Vorticity distributions were obtained at tunnel speeds of 100, 150 and 225 fps, at tip angles of attack of 9.5 and 13.5 degrees. Balance data was taken concurrently during the wake surveys and flow-visualization tests, and balance tares were taken before and after each run. The Reynolds numbers for the three tunnel velocities were 10^6, 1.5×10^6 and 2.2×10^6, respectively.

The surveys of the vorticity in the trailed tip vortex were initiated with three vortex meters spaced 2 inches apart. Initially, performance tests were conducted on the meters; that is, comparisons of the rotational speeds of the meters with a "calibrator" attached to the body of the meters which imparted a known (specified by the manufacturer) rotational speed to the meters at specified tunnel velocities. These tests indicated that no mutual interference was imparted in the performance of the meters by their proximity to each other. During initial wake surveys, however, it was found that the outboard meters were indicating a swirl velocity in regions where the swirl velocity was known to be negligible, and at which the center meter had indicated the absence of swirl flow.

The remainder of the tests were then conducted using only one meter. Performance tests on the vortex meter were performed periodically during the test period, and no degradation in the performance of the meters occurred during the test period.

The output from the vortex meter was read out on an electronic counter, and the signals from the meter were monitored continuously on an oscilloscope. The signals on the oscilloscope indicated that the trailed tip vortex oscillated normal to the model and along its span, particularly with no mass injection. The oscillations were detected from the changes in the rotational speed of the meter at a fixed position of the meter which could be observed on the oscilloscope. The rotational speed of the meter for a particular position was that recorded from a series of averages taken over a 10-second interval. The number of averages taken varied from approximately three to six, depending on the repeatability of the measurements made over the 10-second intervals. By this method, it was felt that the rotational speed of the meter could be averaged to within ±5 counts at high rotational speeds, say, 400 counts per second, and to within ±2 counts at low rotational speeds, say, below 50 counts per second.

Attempts were also made to measure the swirl velocities in the trailed tip vortex approximately 15 chord lengths downstream, but a series of difficulties precluded any quantitative measurements at this downstream position. These traverses were not pursued to a great extent, as at this point in the test program the allocated testing time was virtually expended. In lieu of attempting to overcome the difficulties in completing these surveys, the vortex was observed by injecting smoke into the core, and a tuft grid was mounted in the wind tunnel at the 15-chord length downstream position. Photographs of the tuft grid with and without mass injection were taken from a position downstream of the tuft grid at a test section velocity of 100 fps.

The primary flow visualization data that were taken were still photographs of the helium bubbles, but movies of the formation and dissipation of the tip vortex were also obtained. Photographs of the smoke-illuminated tip vortex were also taken, but these photographs were of poor quality and showed less detail than those of the helium bubbles.

V. DISCUSSION OF RESULTS

A. INITIAL PARAMETRIC INVESTIGATIONS

Effect of Tip Shape on Trailed Tip Vortex

One of the objectives in the first phase of the wind tunnel program was to determine which tip configuration of those selected for testing would be most likely to enhance the vortex-injection process. The tip shape was selected on the basis of the observation of the visualized flow using the helium-bubble technique. The criterion for selection was the position of the centerline of the vortex with respect to the position of the nozzle, and the optimum position was viewed as that at which the centerline of the vortex was closest to the centerline of the nozzle. For these tests, the nozzle area was filled with a contoured block in order to negate the passive effects of any particular nozzle on the formation of the tip vortex.

Three tips were considered. The first was a squared-off tip whose outboard edge was the end rib of the model. For the squared-off tip, the vortex which ultimately became the trailed tip vortex was formed by the mixing of two vortices across the tip of the model. The primary vortex was formed in the "classic" manner with the expected centerline of the vortex easily distinguished over the chord. It was also observed that a secondary vortex formed in the chord plane of the tip section which seemed to originate at the stagnation point and rolled up with the normal vortex behind the trailing edge of the model. The helium bubbles indicated that the centerline of the vortex formed approximately one chord length behind the trailing edge of the model. Photographs of the secondary vortex in the chord plane and in the planform views are shown in Figure 13.

The second tip considered was that described above with a 1/2-inch extension in span. The formation of the trailed tip vortex obviously remained the same, but the vortex then formed outboard from the position of the nozzle, and it was felt that this arrangement would tend to minimize the effectiveness of the injected air.

The third tip considered was a developed half-round tip whose contour was formed by rotating a template of the airfoil section about the centerline of the chord. With this tip, only the "classic" formation of the tip vortex could be detected, with no evidence of a secondary vortex. The centerline of the vortex could be observed visually to approximately the quarter chord of the model during its formation. Photographs of the vortex formation for this tip in the chord plane and in the planform views are shown as Figure 14.

On the basis of these observations of the flow, it was believed that the developed half-round tip would be more amenable to the vortex-injection mechanism with application to vortex dissipation, since it appeared that the injected air would be entrained more efficiently in the flow field of the vortex.

Methods of Quantitative Data Acquisition in the Wake

The measurement of the vorticity distributions in the tip vortex were made at 6.5 chord lengths downstream of the model. This position was chosen since earlier theoretical and experimental results, References 16 and 17, indicated that sufficient mixing of the injected air with that normally entrained by the tip vortex would have occurred at this point to indicate the effects of injection. Measurements at positions farther downstream which would indicate the variation of the circulation strength with time would have been desirable as well, but the requisite traverses at this downstream position were more difficult and time-consuming to a point where the effort expended in acquiring the data was not commensurate with additional data which would have been acquired.

In defining the test program, it was recognized that a tremendous amount of test time would be required if detailed vorticity surveys were made to evaluate the relative efficiency of the various nozzle designs, the effect of injection angle, injection velocity, and mass flow. For this reason it was deemed important to determine means by which the effects of mass injection on the total vorticity could be measured with a minimum of detailed vorticity data.

On the basis of an earlier test program that was conducted by RASA in which detailed vorticity contours were obtained (Ref. 17), it was noted that the change in the peak vorticity reading, as measured by a vorticity meter, properly reflected the change in circulation strength as various amounts of mass injection were used. This was found to be true, however, only if the vortex were not spread. If the vortex were spread, it was found that the peak vorticity reading could be reduced with the total circulation strength remaining constant.

In order to illustrate the relationship between the peak vorticity and the circulation in the tip vortex, the data obtained for one of the model test conditions are compared in Figure 15, which presents the variation of the circulation and the peak vorticity versus mass flow for a tunnel velocity of 150 fps and a tip angle of 9.5 degrees. The similarity between the variation of the peak vorticity reading and the circulation is apparent, particularly at flow rates in the range of approximately $0.1<m_i<0.3$. At the low injection rates, it is noted

that the peak vorticity drops more sharply than the circulation. This result occurs since only the vorticity in the proximity of the peak appears to drop at low mass flow rates, while the remaining vorticity remains relatively unaffected. Since the circulation is the first moment of the vorticity about the centerline of the vortex, the comparatively short moment arm associated with the higher vorticity readings contributes very little to the total circulation; thus the circulation also remains relatively unchanged for the range of mass flows. At the higher mass flow rates, the vortex begins to spread, and the drop in circulation is not commensurate with the drop in peak vorticity readings because the circulation remains relatively constant, although the peak vorticity decreases since the vortex size increases.

In the previous test program conducted by RASA (Ref.17), it was noted that the variation of the vortex circulation strength as a function of mass injection was adequately represented by integrating the vorticity across a traverse made through the peak vorticity reading in the spanwise direction or in a direction perpendicular to the freestream. Since these conclusions were drawn from data obtained by testing a rectangular wing of a different aspect ratio and spanwise loading, an initial set of traverses was made behind the UH-1D blade section and a detailed set of vorticity contours was constructed to determine whether the traverses could also be limited to the two directions for the UH-1D blade.

The data that was obtained to test the accuracy of the integration of the vorticity are presented in Figures 16 and 17. The spanwise distributions of vorticity at approximately 1/2-inch increments across the vortex are shown in Figure 16, and the contour distributions of constant vorticity readings constructed from these data are shown in Figure 17. For the noted parameters in this particular case, the circulation strength of the vortex obtained from the detailed wake surveys was 27.1 ft^2/sec and that obtained from two traverses normal to each other across the vortex was 26.2 ft^2/sec, a difference of approximately 3%. On the basis of these results, it was concluded that the correct integration of the vorticity distributions in the spanwise direction and in the direction perpendicular to the freestream would provide a measure of the total circulation in the tip vortex within the accuracy of the experimental data.

On the basis of the data discussed above, three different levels of surveys were conducted in the wake. In order to determine the optimum nozzle configuration for a given set of tunnel conditions but for various mass flows, the wake was surveyed at a given downstream location to determine the peak vorticity readings and the size of the vortex. The size of the vortex was determined from the position of the points nearest the vortex where no

swirl could be detected by the vorticity meter. In order to determine the passive effects (no mass injection) of the nozzle configurations as well as the injection angle, and the independent effects of velocity of injection and mass flow, spanwise traverses through the center of the core were made and the resulting vorticity distributions were integrated to obtain the circulation in the tip vortex. Once the optimum nozzle design was selected on the basis of these parameter variations, the variation of circulation with mass injection for various angles of attack and tunnel velocities was determined by integrating the vorticity traverses made through the center of the core in the spanwise direction, and in a direction perpendicular to the freestream.

Passive Effect of Nozzles on the Trailed Tip Vortex

In order to establish the proper base upon which to evaluate the effect of mass injection on the dissipation of the tip vortex, the passive (nonoperating mode) effect of the nozzles on the characteristics of the concentrated tip vortex was evaluated initially. Figure 18 presents the results of these tests. These results show that the passive effect of the nozzles was to decrease the overall strength of the trailed tip vortex and that the decrease in strength was dependent upon the geometric shape and cavity size of the nozzle. The open slot (Nozzle No. 10) which had the largest dimension in the chordwise direction of the nozzles tested in this series, and thus created the largest open cavity in a varying pressure field, caused the largest reduction in the trailed vorticity field. The honeycomb nozzles caused the smallest effect on the trailed vortex, and the difference in the passive effect between the honeycomb and the open cavity nozzles was attributed to the degree and wavelength of the turbulence generated by cavities of various sizes and depths.

Effect of Nozzle Geometry and Construction on Vortex Dissipation

The results of the series of tests that were conducted to determine the effect of geometric shape and construction of nozzles having the same exit area and for the same wind tunnel and model conditions are presented in Figure 19. At the lower values of injected mass flow, the results show that there is a reasonable difference in the peak vorticity readings among nozzles, particularly between the open configurations and those constructed of honeycomb. At the higher injected mass flows ($0.25 \leq m_i \leq 0.40$), the difference between the various nozzle configurations was minimal. It is believed that the larger difference in the peak vorticity noted at the lower values of the injected mass flows was due to the greater turbulence level and wavelength associated with the jet flow in the open nozzles

which decreases to the level of the honeycomb nozzles at the higher values of injected mass flows. Since at this stage of the test program it was believed that the higher values of injected mass flow would be required to dissipate the vortex to the desired levels, it was concluded that since nozzle geometry was not a decisive factor in the dissipation of the vortex, the acoustic output of the various nozzles should be considered in the choice of the optimum nozzle geometry.

In order to obtain a qualitative comparison of the acoustic output of the various nozzles, a B&K sound level meter was first used to determine the location of the maximum acoustic output of the nozzle at a distance of 6 feet behind the trailing edge. (It should be noted that these measurements can be considered on a qualitative basis only, as the data were conducted in a hard-wall facility and the sound analyzer was located close to one of the walls.) It was determined from these tests that the maximum overall acoustic output of the nozzles was at a location approximately 45 degrees to the nozzle chord plane. Octave band measurements were then made at this location for all the nozzle configurations at five values of the injected mass flow. It was noted from these test results that the honeycomb slotted nozzle was the lowest in acoustic output by 5 to 10 db depending upon the nozzle or octave band at which it was compared with the other nozzle configurations.

Figure 20 presents the change in the acoustic output of the slotted nozzles as a function of mass flow. It can be seen that the acoustic output of the honeycomb nozzle was always less than the open nozzle and that there was a more rapid increase in the acoustic output of the nozzles at the lower mass flows than at the higher mass flows. It is believed that the difference in the acoustic output between the nozzles at the lower and higher values of mass flow was caused by honeycomb-cell resonances that occurred at these mass flows. The spectrum of the acoustic output of the honeycomb slotted nozzle is shown for two mass flows in Figure 21. It can be seen that the spectrum changed as the mass flow changed and that for the octave band centered at 1000 Hz there seemed to be a peak at a mass flow of 0.135 lb/sec and not for a mass flow of 0.35 lb/sec. It was noted during the tests that at the lower mass flow there was a pure tone generating from the nozzle, and it is believed that the noted peak is a measure of that pure tone which was caused by a resonance of one of the honeycomb cells.

Figure 22 presents the spectrum of the slotted nozzle configuration at a mass flow of 0.350 lb/sec. It can be seen that the spectrums are very similar, with the honeycomb slot having a lower output throughout the frequency range over which data were obtained.

While the acoustic output of even the slotted honeycomb nozzle is fairly high (100 db) at 6 feet in a wind tunnel, its measurable acoustic output would be less in a free environment and would be greatly attenuated at a reasonable distance from the rotor system. In addition, it is not expected that the crew would notice the noise, as it is projected upward and away from the fuselage. On the basis of these acoustic results and those presented in Figure 19, the honeycomb nozzle configuration was, therefore, selected for further testing.

B. THE EFFECTS OF VARIOUS INDEPENDENT PARAMETERS ON VORTEX DISSIPATION

Independent Effect of Injection Velocity and Mass Flow

The independent effects of injection velocity and mass flow were determined by testing honeycomb nozzles having different exit areas at a constant mass flow. For the nozzles that were used, three different injection velocities were tested at various mass flows. The results of these tests are shown in Figure 23.

At an injected mass flow of m_i=0.200 lb/sec, the effect of increasing the injection velocity (decreasing nozzle area) was always found to be beneficial; whereas at an injected mass flow of 0.281 lb/sec, the vortex circulation strength decreased as the nozzle area was decreased from 1.65 in.^{2} to 1.24 in.^{2}, and increased as the nozzle area was decreased further to 0.83 in.^{2}. This apparent discrepancy in the results can be accounted for by inspection of the vorticity distributions that were obtained. Figure 24 presents the vorticity distribution for the various nozzles at injected mass flows of 0.200 and 0.281 lb/sec. The vorticity distributions for an injected mass flow of 0.200 lb/sec show that the peak vorticity decreases with increasing mass flow and that the vortex core dimension is not increased. At an injected mass flow of 0.281 lb/sec, the peak vorticity decreases as the injection velocity increases from 383 fps to 438 fps without increasing the size of the core of the vortex. As the injection velocity is increased further to 585 fps, however, the peak vorticity is decreased and the vortex core size is increased considerably. Since the circulation is the first moment of the vorticity distribution, the integration of the vorticity distribution at V_i=585 fps results in a circulation strength higher than that measured at an injection velocity of 438 fps. This somewhat unusual result is believed to be due to the higher energy in the jet which causes vortex spreading as well as dissipation. In other words, the energy that the turbulent jet was depositing in the core of the vortex was greater than that which could mix with the swirling flow. It is believed that

this excess energy was forcing the vortex to spread. At the downstream location where the measurements were made, the data indicates that the dissipative process of the higher energy was less efficient than that of the lower energy jet. However, at greater downstream distances the vortex injected with the higher energy jet should be weaker than if it were injected with the lower energy jet.

On the basis of the range of mass flows which could be expected to dissipate the circulation strengths of the tip vortex, for the range of parameters to be investigated, the nozzle having an area of 1.24 $in.^2$ was selected for further test.

The solid data points shown in Figure 23 are those at which the velocity of injection was a constant. The decrease in circulation with increasing mass flows for a constant injection velocity indicates that while the injection velocity seems to be of primary importance, the magnitude of the injected mass flow is also an important parameter in regard to vortex dissipation.

Since both mass flow and velocity of injection were found to be important to the dissipative process, an attempt was made to correlate the data in terms of thrust. The data presented in Figure 23 as well as all other data that were obtained using these nozzles in the tests were correlated on the basis of thrust, and the results are presented in Figure 25. These data show that the majority of the dissipative action occurs over a very narrow range of thrust, $1\text{-}1/2 \leq T \leq 2\text{-}1/2$ pounds. In addition, it is noted that below $T < 1\text{-}1/2$ pounds very little dissipative action occurs, and for $T > 2\text{-}1/2$ pounds almost no additional dissipative action is obtained. These results indicate that there is an optimum amount of injection momentum to achieve the desired dissipative action. This conclusion is very interesting, as it indicates that within practical limits it would be desirable to maximize the velocity of injection, which, in turn, would minimize the mass flow requirements. For example, if the velocity of injection were increased by 40% over that used in these tests, the required mass flow could be cut in half - possibly a very beneficial result! If on the other hand the air supply was being obtained from a high-mass-flow device such as a jet engine, it might be desirable to minimize the velocity and maximize the mass flow.

Effect of Injection Angle

During the flow visualization tests that were previously conducted by RASA (Ref. 17) using helium bubbles, the area over the wing tip section at which the vortex was forming was blanked out by light reflection. However, it was noted that if a straight edge were placed along the trailed vortex, the straight edge always intersected the lifting surface at the

75% chord with the angle between the chord plane and freestream the same as the angle of attack. Based on this information, the nozzles for the series of tests discussed herein were designed so that the nozzle center was at the 75% chord and so that the angle of injection was in the freestream direction regardless of the angle of attack. On the basis of the results presented by Chigier and others in Reference 12, however, it was noted that the line of the vortex center was not always in the freestream direction during the latter stage of its formation over the lifting surface and before it became a free vortex. Therefore, one of the parameters that was investigated early in the test program was the effect of the injection angle on the efficiency of vortex dissipation. This investigation was conducted by orienting the model at a tip angle of attack of 9.5 degrees and injecting the airflow at 5.5, 9.5 and 13.5 degrees. The results of these tests are presented in Figures 26 and 27. The data presented in Figure 26 show that the most efficient injection angle is that in which the airflow is injected in the freestream direction, and that it is less efficient to inject the vortex at an angle larger than that between the chord plane and the freestream direction than it is at a smaller angle. The reason injection at angles other than the freestream direction is less efficient is shown in Figure 27. These data indicate that injecting at the freestream angle decreases the peak vorticity but does not spread the vortex, whereas injecting the vortex at an angle smaller than the freestream angle reduces the peak vorticity by about the same amount but also spreads the concentrated vortex slightly. Injecting the vortex at a higher angle than the freestream angle does not reduce the peak vorticity as much as either of the other conditions and spreads the concentrated vortex significantly. It is believed that the reason injecting at a higher angle is less efficient than injecting at a lower angle than the freestream angle is that at a higher angle, the injected mass flow is acting on the portion of the vortex that has the least restraint from the lifting surface. A spanwise view of the vortex formation is presented in Figure 28, which shows the influence of the lifting surface on the vortex during its latter stages of formation. As can be seen in the photograph, the initial formation of the vortex can be noted at about the 25% chord. As more of the circulatory flow is concentrated in the tip vortex, the centerline of the vortex moves farther away from the surface of the blade. In the vicinity of the trailing edge, the vortex becomes a free vortex and streams away from the lifting surface in the freestream direction. If the flow was injected at an angle less than that of the axis of the vortex, a majority of the injected mass could still be expected to mix with the swirling flow. If the injection angle were larger than the axis of the vortex, it could be expected that more of the injected mass flow would escape and not mix with the swirling flow, and thus the dissipative action would be less.

The results of calculations conducted using the "free-wake blade loads" analysis (Ref. 6), which are shown in Figure 29, shows that the maximum angle of attack and trailed circulation strengths occur over the same azimuthal range, $180 \leq \psi \leq 360$ degrees. Therefore, if the nozzle is designed to dissipate the vortex in the range of $180 \leq \psi \leq 360$ degrees, then while the efficiency of vortex dissipation will be significantly less in the range of $0 \leq \psi \leq 180$ degrees, the strength of the vortex is also significantly less. Therefore, the injection system that is designed on the basis of the angle of attack and vortex strength that exists in the azimuth range $180 \leq \psi \leq 360$ should be adequate to dissipate the vortex that is generated anywhere in the rotor disk.

C. THE EFFECTS OF VARIOUS OPERATIONAL PARAMETERS

Summary of Results for Various Test Conditions

A summary of the effects of mass injection on the dissipation of the tip vortex for the various conditions at which the UH-1D blade section was tested is shown in Figure 30. These data show that a significant reduction in the strength of the concentrated vortex was achieved for all the conditions that were tested. While the trends of the reduction in circulation strength with increasing mass flow were similar for all cases, there are some noteworthy differences among the results. For example, the circulation strengths of the trailed vortex with no mass injection for the blade section at an angle of attack of 9.5 degrees and a wind tunnel velocity of 150 ft/sec were calculated to be approximately the same as for the blade section at an angle of attack of 13.5 degrees and a wind tunnel velocity of 100 ft/sec. The measurements that were made indicated that this estimate was essentially correct. The same type of correlation was also expected for the blade section at an angle of attack of 9.5 degrees and a wind tunnel velocity of 225 ft/sec, and for the blade section at an angle of attack of 13.5 degrees and a wind tunnel velocity of 150 ft/sec. The experimental results show that this correlation was not realized. The reason for this difference is shown in Figure 31, which presents the measured distributions of vorticity in the spanwise and normal directions for the two test conditions. The data at an angle of attack of 9.5 degrees and a wind tunnel velocity of 225 ft/sec indicate that the expected single-peak distribution of vorticity in the vortex core was obtained, but that at an angle of attack of 13.5 degrees and a wind tunnel velocity of 150 ft/sec a double-peak distribution was obtained. It is believed that this peculiar distribution was caused by a secondary vortex, which was formed about the tip section of the blade in a manner similar to that noted for the squared-off tip. The vorticity distribution suggests that at 6-1/2 chord lengths downstream, the secondary vortex had mixed with, and was centered in, the main vortex; the vorticity distribution

also suggests that the strength of the secondary vortex was much less than that of the main vortex. The existence of the double vortex was not confirmed by flow visualization during these tests.

Figure 31 also shows the vorticity distributions when mass injection was applied to the double-vortex configuration. It is noted that when mass injection was applied the distribution associated with a double vortex was no longer apparent. The data shown in Figure 30 tend to confirm the elimination of the secondary vortex, as the dissipated strengths of the vortices for the two test conditions (with and without the double vortex) are about the same for an injected mass flow of 0.298 lb/sec.

The existence of the double vortex was also noted for the non-injected configuration at an angle of attack of 13.5 degrees and a wind tunnel velocity of 230 ft/sec. From the vorticity distributions that were measured for this configuration, it was estimated that the strength of the secondary vortex was less than that for the same angle of attack but for a wind tunnel velocity of 150 ft/sec. On the basis of the measured distributions, the strength of the secondary vortex for this case was estimated to be 9 ft^2/sec; therefore, the strength of the main tip vortex was approximately 153 ft^2/sec. Using the same technique to estimate the strength of the secondary vortex for the model at 150 ft/sec and at 13.5 degrees angle of attack, the strength of the secondary vortex was estimated to be very close to the difference in the measured values. The reason for the difference in the strengths of the secondary vortex is not known. The data point for this case has been shown by a solid symbol with a flag at $m_i=0$ (Figure 30).

The usual manner in which the vorticity distributions were altered as the injected mass flow was increased is illustrated in Figure 32. The angle of attack for this case was 9.5 degrees and the wind tunnel velocity was 225 ft/sec. These data show that the peak vorticity was reduced without spreading the vortex as the mass flow was increased from 0 to 0.421 lb/sec. For a mass flow of 0.562 lb/sec, the peak vorticity was reduced further but the vortex core had been spread. Since the circulation is the integral of the moment of vorticity about the center of the vortex, the circulation would be expected to decrease as the mass flow was increased from 0 to 0.421 lb/sec, and for a mass flow of 0.562 lb/sec the rate of decrease in circulation would be expected to be much less. This expectation is borne out by the results presented in Figure 30, which shows that the efficiency of the vortex-injection system decreased markedly when the injection system caused vortex spreading. The same result was noted when the effect of injection angle was investigated, that is, the injected mass flow was more efficient when it did not cause vortex spreading.

In comparing the results presented in Figure 30 for α=13.5 degrees, V=100 ft/sec with those obtained at α=9.5 degrees, V=150 ft/sec, it is noted that the effect of injected mass flow was much more pronounced in the lower range of mass flows for the lower velocity test conditions. It is believed that the more efficient dissipation realized for the lower velocity condition at an injected mass flow of 0.169 lb/sec was due to the higher relative velocity of the injected jet with respect to the freestream. When the velocity of injection reached the same relationship to the freestream velocity for the model when tested at 150 ft/sec, the rate of decrease of circulation also markedly increased and the circulation values of the modified trailed vortices approached each other at the higher values of mass flow.

In Figure 30 the test point for the blade section at 13.5 degrees, for a tunnel velocity of 100 ft/sec, and for a mass flow rate of 0.446 lb/sec is shown as a solid point. It is noted that the strength of the vortex for this mass injection rate is more than twice the value obtained for a mass flow rate of 0.281 lb/sec, and that its strength is only 25% less than the strength of the unmodified vortex. The vorticity distributions in the spanwise and normal directions for these test conditions are presented in Figure 33. These data show that the vortex has been spread a tremendous amount, more than three times its unmodified size. It is suspected that this large increase in the size of the vortex core is caused by the great excess of jet energy over that which can mix with the swirling flow of the vortex. As previously discussed, this excess energy forces the vortex to spread. Also, in Figure 30, a solid, flagged symbol is shown at a mass flow of 0.562 lb/sec for the blade section at a 13.5-degree angle of attack and a tunnel velocity of 230 ft/sec. These test conditions yield a circulation strength about one-half of that realized by the UH-1D flight vehicle. The cross-sectional area of the injection nozzle (No. 6) used for the model under these test conditions was 1.65 $in.^2$ in contrast to 1.24 $in.^2$ for the rest of the data presented in this figure. In addition, the angle of the injection nozzle was 9.5 degrees in contrast to 13.5 degrees. The solid flagged symbol represents an estimated value of circulation that would have resulted if the correct nozzle could have been used. The estimated value was obtained by applying the corrections involving injection velocity and angle that were previously discussed.

Effect of Mass Injection on Performance

The measured performance characteristics for one of the test conditions for various amounts of mass injection are presented in Figure 34. These results are typical of the results for all test conditions. The measured direct jet effect of the injected

mass flow has been subtracted from the total balance readings so that the aerodynamic performance parameters of the blade section alone can be inspected, and these data show that the injected mass flow did not affect the basic performance characteristics of the lifting surface. In addition, the fact that the rolling moment and the lift did not change indicates that the spanwise loading distribution did not change as it would have if the vortex were merely spread by the injection process as it was forming over the tip. The same comment can be applied to the distribution of the drag force. The balance data for all of the test conditions are listed in Appendix II. It should be noted that at the completion of the tests during which the optimum nozzle was being selected, the clearance between the floor plate and model had to be increased to eliminate a physical interference between the two when the model was at the maximum tunnel velocity and angle of attack. It was found that the increased clearance allowed bleed air from the balance room to enter the tunnel and create a steady vortex on the model near the root at the trailing edge. This separated flow noticeably increased the drag and slightly decreased the lift. Since the tests that were being conducted were relative in that the performance characteristics were being compared before and after vortex injection, this separation at the root of the model was not considered important to the test program.

The fact that the performance characteristics were unaffected by mass injection also indicates that the two flows, the jet flow and the normal flow about the lifting surface, can be superimposed, which indicates that the two flows do not mix during the formation of the tip vortex. Since the rapid dissipation of the vortex caused by the mass injection does not occur until the vortex has left the lifting surface, it is not too surprising that the performance characteristics of the lifting surface have not been altered. The results obtained during a previous test (Ref. 17) at one and one-half chord lengths behind the lifting surface also indicate the same results, in that the reduction in the circulation at that location was much less than it was at six and one-half chord lengths.

The photographs of the illuminated helium bubbles shown in Figures 35 through 37 demonstrate the manner in which the vortex is modified and dissipated by mass injection. These photographs were taken with the model at an angle of attack of 13.5 degrees and a wind tunnel velocity of approximately 50 ft/sec. The mass injection rate for these test conditions was commensurate with that obtained at the higher wind tunnel velocities.

Figure 35 shows a planform view of the tip of the blade section with and without mass injection. Without mass injection, the centerline of the vortex and the concentrated swirling flow can be seen right up the chord of the blade section during the vortex formation. The lines of the overall swirling flow around the vortex can also be seen. With mass injection, the vortex centerline and the concentrated swirling flow are no longer evident, but it can be seen that the overall swirling flow pattern around the tip section has not been altered to any appreciable degree. The nonchanging aspect of the overall swirl pattern over the tip section of the blade as mass injection is applied is more graphically illustrated in Figure 36. The picture visualizing the normal flow field shows the manner in which the induced effects of the lifting surface sweep the freestream flow field outboard ahead of the blade section, and then as the flow field reaches the tip section the induced effect of the swirling flow from the forming vortex brings the freestream flow over the tip section and entrains it into the vortex. As the flow moves downstream from the trialing edge, the swirl tightens rapidly into the concentrated vortex. When the mass injection is applied, the overall swirl pattern in the vicinity of the blade tip remains unchanged, but the downstream flow field can be characterized as basically an uncorrelated turbulent aerodynamic flow with a gross overall swirl. The radical change of the wake flow is clearly depicted in Figure 37, which shows the unmodified and modified flow fields looking directly up the line of the trailed vortex. This view of the trailed vortex shows clearly the manner in which the swirl pattern over the tip of the blade section tightens up rapidly into a concentrated swirling flow as the vortex leaves the blade section and trails downstream. The concentrated straight line depicts the center of the vortex, as the bubbles which are entrained therein are basically in rectilinear motion at the vortex center. When the injected mass flow was applied, the swirl pattern in the vicinity of the lifting surface was not altered. In the wake, this swirl pattern did not tighten up as it did without mass injection, but broke up into a random turbulent flow with a moderate overall swirl.

It is believed that the visualized flow has illustrated that the injected mass flow did not alter the basic flow pattern over the blade tip during the formation of the vortex, but had altered the concentrated vortex flow immediately behind the lifting surface into a highly turbulent viscous flow.

D. INSTABILITY CHARACTERISTICS OF THE TRAILED VORTEX - WITH AND WITHOUT MASS INJECTION

Near completion of the test program, the traverse mechanism was moved to a position 15 chord lengths downstream of the blade section so that quantitative vorticity surveys could be made to supplement all the data (presented in Figure 30) that were obtained at 6-1/2 chord lengths. The test conditions for these tests were the same as for one of the cases for which data were presented in Figure 30, namely, for a wind tunnel velocity of 225 ft/sec and an angle of attack of 9.5 degrees. With a mass injection rate of 0.30 lb/sec, a survey was made and no indication of a vortex could be found; although at 6-1/2 chord lengths, measurements indicated that a considerable amount of vorticity remained for the same test conditions. Smoke was then injected into the vortex core, and the injected concentrated vortex was visualized until it intersected the turning vanes more than 50 chord lengths downstream of the model. When mass injection was again applied and smoke was used to visualize the flow field, it was noted that the concentrated tip vortex was eliminated quickly and only a very turbulent flow field with an overall swirl pattern remained. However, at approximately 9 chord lengths downstream from the model, the remaining turbulent swirling flow burst and no characteristic flow pattern could be discerned. Pictures of the vortex breakdown as depicted by the smoke could not be obtained, as the entire tunnel had become filled with smoke and a suitable contrast between the concentrated smoke flow and the background smoke flow could not be obtained.

In order to document what had been witnessed visually, a tuft grid having a 2-inch spacing between tufts was placed in the tunnel at a position 15 chord lengths downstream from the blade section. Because of the equipment in the tunnel, the freestream velocity was limited to 100 feet per second when pictures were being taken to demonstrate the effect of vortex breakdown. One set of test conditions in these tests, $V=100$ ft/sec, $\alpha_T=13.5°$ and $m_i \approx 0.30$ lb/sec, corresponded to a set of conditions at which quantitative data at 6-1/2 chord lengths were presented in Figure 30. Figure 38 shows tuft grid pictures of the flow field of the unmodified vortex when the injected mass flow was 0.30 lb/sec. While the quantitative data indicated that the vortex strength was still equal to one-third the value of the unmodified vortex at 6-1/2 chord lengths (Figure 30), no indication of a vortex could be distinguished on the tuft grid. Figure 39 shows the tuft grid of the unmodified vortex when the blade section angle of attack was 9.5 degrees and also when a mass flow of 0.26 lb/sec was injected into the vortex core. Again it is noted that when the vortex was injected with the noted amount of mass flow, no indication

of a vortex could be distinguished on the tuft grid. On the basis of the quantitative data taken at 6-1/2 chord lengths downstream of the model and on observations of the visualized flow, it is believed that an instability was observed which was created by the mass flow of the injected jet. If, in fact, this were the case, then the most efficient means of generating this instability should be determined so that the advantage can be taken of the rapid-dissipation processes associated with the instability.

E. COMPARISON OF THEORETICAL AND EXPERIMENTAL RESULTS

In Reference 16, Rinehart presented a viscous dissipation theory for the mixing of a turbulent jet and a swirling flow. This theory was based on an eddy viscosity model, and the eddy viscosity was related to Schlichting's expression for the kinematic eddy viscosity (assumed constant) of a quiescent jet. In comparing the results of this theory with the experimental data presented in Reference 17, it was noted that the results correlated reasonably well in the lower range of injected mass flows but that at the higher values of mass flow the theory indicated much less of a dissipative effect of the mixing than was obtained experimentally. Figure 40 shows this comparison of the theoretical and experimental results. In Reference 17, it was suggested that this difference at the higher mass flows might have been caused by a flow instability which would have changed the eddy viscosity coefficient significantly. In fact, it was noted that the properties of the vortex for the test conditions at which the theoretical curve crossed the experimental data correlated very well with those noted for the breakup of the concentrated vortex associated with delta wings. This correlation seemed to substantiate the premise of a vortex instability, although it has not been detected during the rather extensive investigation of the physical characteristics of the modified flow using various flow-visualization techniques. During the tests associated with the UH-1D blade section, it is believed that the vortex instability was observed, but the conditions under which it occurred are not associated with the test conditions for which the data of Reference 17 were obtained. In addition, under a current ONR contract* in which the vortex flow instability and dissipation are being studied in more detail, it has also been concluded that the data of Reference 17 probably did not reflect a vortex instability at 6-1/2 chord lengths downstream. It was concluded therefore that the theory presented in Reference 16 was limited because of the assumption of a constant value of the eddy viscosity coefficient.

Rinehart, in conjunction with Sutton, has reformulated and extended the theory of Reference 16 so that the eddy viscosity

*ONR Contract No. N00014-71-C-0226.

coefficient can vary in the axial direction. This new inductive eddy viscosity theory is based somewhat on a turbulent three-dimensional jet mixing with a swirling flow, and the eddy viscosity coefficient varies in a manner similar to that which occurs in a turbulent three-dimensional jet. This new predictive technique was applied to the data of Reference 17 and is also presented in Figure 40. It is noted that the correlation between the experimental and theoretical results is markedly improved over that obtained with the original theory of Reference 16. The theory has been applied to the data that RASA obtained within the present tests, and the results of that correlation effort are presented in Figure 41. It can be seen that the correlation is excellent.

The theoretical curves indicate that as mass flow is applied, no dissipative action is predicted until a given mass flow is achieved, and then a very rapid dissipative action suddenly occurs as the mass flow is increased further. This break point in the theoretical curve is associated with the velocity of injection relative to the freestream or the axial velocity in the core of the vortex.

It is believed that the theory in its present form can be used to obtain a reasonable estimate of the effect of injected mass flow on the dissipation of a concentrated trailed vortex of a given strength and size. However, since the theory cannot predict the stability characteristics of swirling flow mixing with a highly turbulent, viscous jet, it cannot be used to determine the possible additional beneficial effects in regard to the rapid dissipation of the vortex that might be obtained by triggering the inherent flow instability which exists in such flows. While the excellent theoretical representation of a turbulent viscous vortex that was developed by Fernandez and Lubard (Ref. 22) results in equations which possess both regular wave-like and jet-like solutions, and solutions which become singular indicating vortex breakdown, it is not basically a stability theory. Mager (Ref. 23) obtained a solution across the singularity (assumed conditions for vortex breakdown) by assuming that the form of the vortex flow remained the same. The results of his investigation indicated that the vortex size would increase many times across the singularity. However, since the form of the flow generally changes when a jet-type instability occurs, it is not believed that either of these theories is applicable to the study of the true instability characteristics of the mixed-swirling and jet flows which are generated by mass injection.

The basis of a true stability theory of the mixed flow field that is needed to study the above noted problem has been formulated by RASA, and it is expected that in the near future it can be developed to the point where it can be used to investi-

gate the most appropriate means of generating an unstable flow and the benefits that will accrue from its generation.

Comparison of RASA's Results With Those of Other Investigators

It is somewhat difficult to compare the results obtained in this investigation with those obtained by other investigators, as much of the work of other investigators has been basically qualitative in nature. It is noted that the limited amount of quantitative data presented by Kantha and others in Reference 20 compares favorably with that obtained in the present investigation, although the efficiency of the dissipative action that was obtained by Kantha was not as great. It is believed that the reason the results presented in Reference 20 indicated that the mass injection was less efficient is that the angle and location of the vortex-injection system were not optimized for the test conditions. It is also believed that the qualitative results obtained by Mason (Ref. 21) using tuft grids would have been enhanced if the injection system had been optimized in regard to the angle of injection and its location. Neither of these investigators found an instability of the vortex due to mass injection, which is surprising in view of the visualization that was undertaken at great downstream distances. It is possible that the vortex spreading created by the mismatched angle of attack and angle of injection could have stabilized the vortex flow in regard to the jet instability.

The results obtained by RASA cannot be compared with Yuan's work (Ref. 18) as no real quantitative or qualitative data on the trailed vorticity was presented in that reference. On the basis of the comparisons that could be made with other investigations, it is believed that these results generally support the results obtained during the current investigation.

VI. CONCLUSIONS

On the basis of the research program RASA has conducted, it has been shown that mass injection rapidly dissipates the circulatory energy of the tip vortex. It has also been shown that the proper design of an injection system is dependent upon the angle of injection, the velocity of injection, the mass flow, and the tip shape.

The following specific conclusions were made on the basis of the results of this research program.

Flow-visualization studies showed that:

1. The blade with a squared-off tip developed a secondary vortex of moderate strength in the chord plane of the tip section.

2. The double vortices formed by the blade with a squared-off tip mixed to form a single vortex behind the trailing edge.

3. A single concentrated tip vortex was observed to form at approximately the quarterchord position on the blade with a developed half-round tip.

4. The flow across the blade tip chord was basically unaffected by the mass-injection process.

5. For all model and tunnel conditions that were tested, the swirling flow in the tip vortex was dissipated more rapidly with increasing mass flow.

6. For a wind tunnel velocity of 100 fps and tip angles of attack of 9.5° and 13.5°, vortex instabilities were generated by the application of mass injection.

Quantitative measurements taken during the wind tunnel tests showed that:

1. The presence of a nozzle had a passive effect which slightly decreased the strength of the tip vortex. The magnitude of the effect varied with geometric shape and cavity size of the nozzle.

2. As mass injection was applied, the peak vorticity in the vortex could be related to the total circulatory strength of the vortex only if the vortex size were preserved.

3. Nozzle geometry was not a primary parameter in the injection system. Nozzle geometry, however, did affect the acoustic signature of the injection system.

4. The velocity of injection and the mass flow are primary parameters in the vortex-injection technique, and within practical limits, it appears to be beneficial to maximize the velocity of injection.

5. The most efficient angle of injection is that which corresponds to the angle of attack on the blade section.

6. At 6-1/2 chord lengths downstream of the model, an optimum degree of viscous dissipation of the tip vortex was achieved at mass flow rates which did not cause vortex spreading.

7. The performance characteristics of the blade section were unaffected by the injection process.

8. The effects of Reynolds number based on wing chord are not important to the mass-injection technique. The Reynolds stresses that are important to vortex injection are those associated with the jet flow.

9. Significant reduction in circulation strength was achieved for all conditions tested. Comparison of the measured circulation strengths for the blade section tested and estimated strengths for flight vehicles indicates that the system can be used to realize significant reduction in the circulation strength of the tip vortex trailed by flight vehicles with practical mass flow rates.

The results that were obtained in this research effort have resolved many of the questions associated with the practical application of the vortex-injection technique to rotor blades or to fixed-wing aircraft. The research effort has not resolved operational problems that might exist in a full-scale application in a rotating environment, however. The acquisition of quantitative data in regard to the beneficial effects of mass injection for a full-scale system under controlled conditions in a whirl tower and in a full-scale wind tunnel would thus appear desirable before free-flight vehicle tests are undertaken.

VII. RECOMMENDATIONS

On the basis of the results of the research program which was conducted, it is specifically recommended that the investigation of the vortex-injection technique be continued to determine:

1. The effects of the "effective" sweep angle which a rotor blade experiences as it traverses the azimuth in forward flight;

2. The effects of Mach number on the vortex-injection technique;

3. The requirements for incorporating the system in flight hardware;

4. The change in the dynamic loads, acoustic signature, and performance characteristics of a rotor system resulting from the elimination of the trailed tip vortex;

5. The requirements for the elimination of vortices generated by fixed-wing flap system;

6. The conditions under which a vortex instability can be enhanced by mass injection.

In addition, a theoretical analysis of the vortex stability and dissipation characteristics including the effects of mass injection should be developed so that the applications to other flight systems, other than those tested, can be undertaken with confidence without resorting to detailed testing.

I. Spreading of Concentrated Vorticity
   - A. End plates
   - B. Gulled outer panels
   - C. Tip planform variations
   - D. Porous tips
   - E. Lifting surface tip spoilers
   - F. Spanwise or angled blowing

II. Dissipation of the Concentrated Vorticity
   - A. Porous tips (small-scale turbulence)
   - B. Lifting surface tip spoilers (small-scale turbulence)
   - C. Jet engine exhaust in the vicinity of the wing tip
   - D. Reverse swirl
   - E. Linear turbulent mass injection developed by RASA

III. Relocation of the Concentrated Vorticity
   - A. End plates
   - B. Gulled outer panels
   - C. Spanwise or angled blowing

Figure 1. Categorization of Basic Approaches.

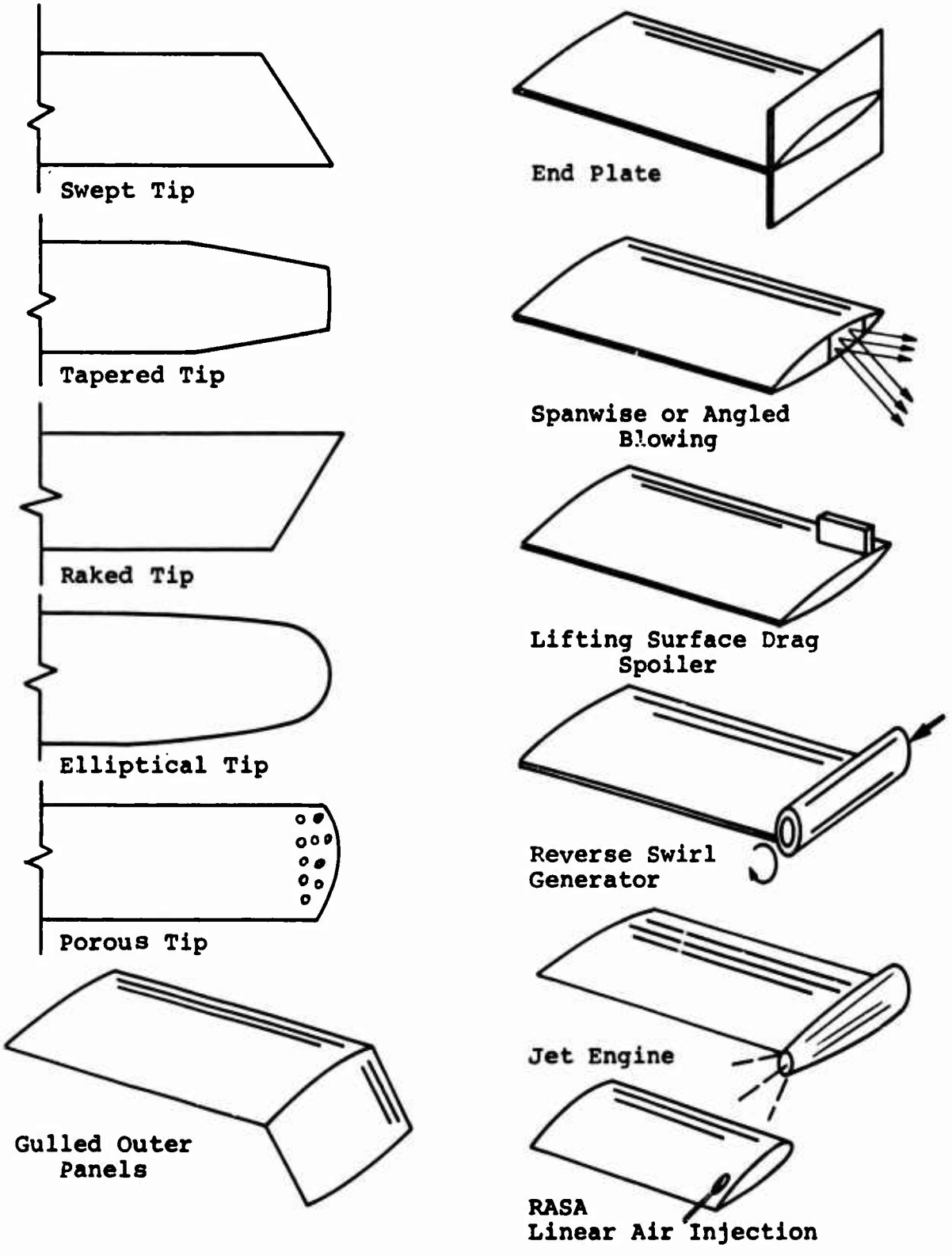

Figure 2. Wing Tip Configurations for Distributing, Dissipating or Relocating Tip Vortices.

Figure 3. Model Base Supports.

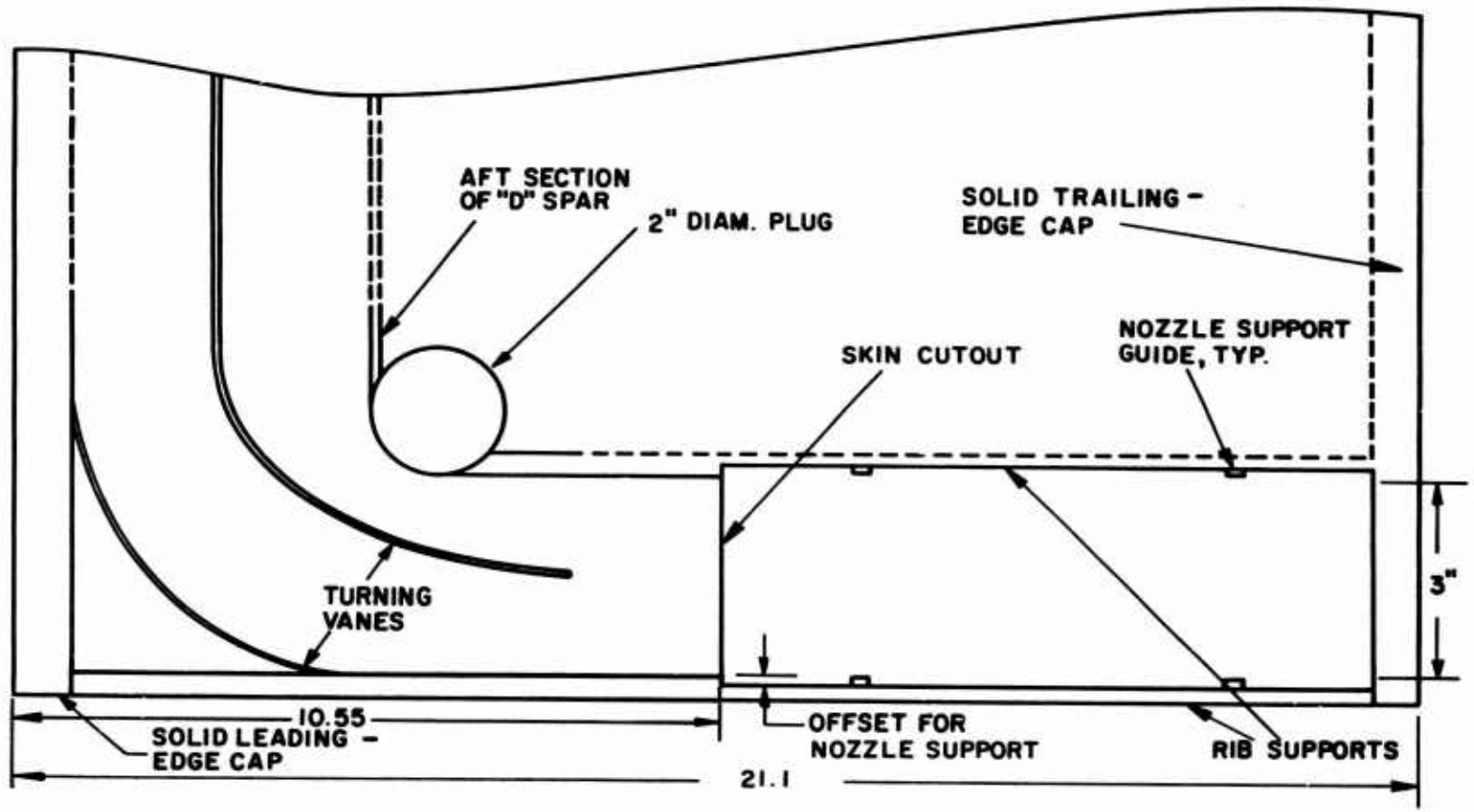

Figure 4. Schematic Diagram of the Tip Section of the Model.

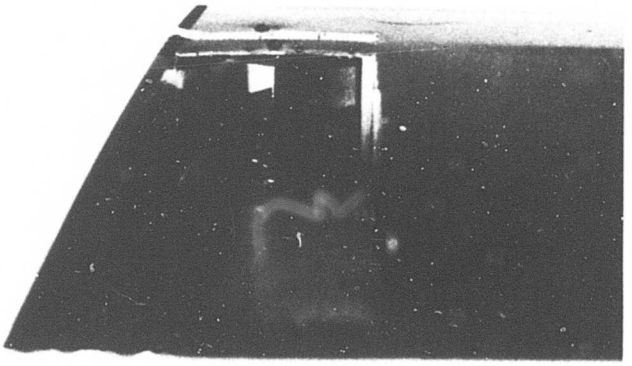

Figure 5. Tip Section of the Model as Viewed From Trailing Edge.

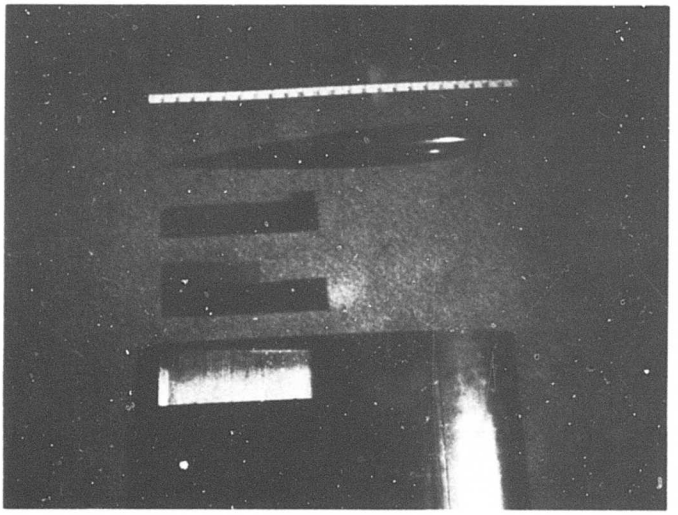

Figure 6. Exploded View of a Typical Nozzle and Tip Configuration.

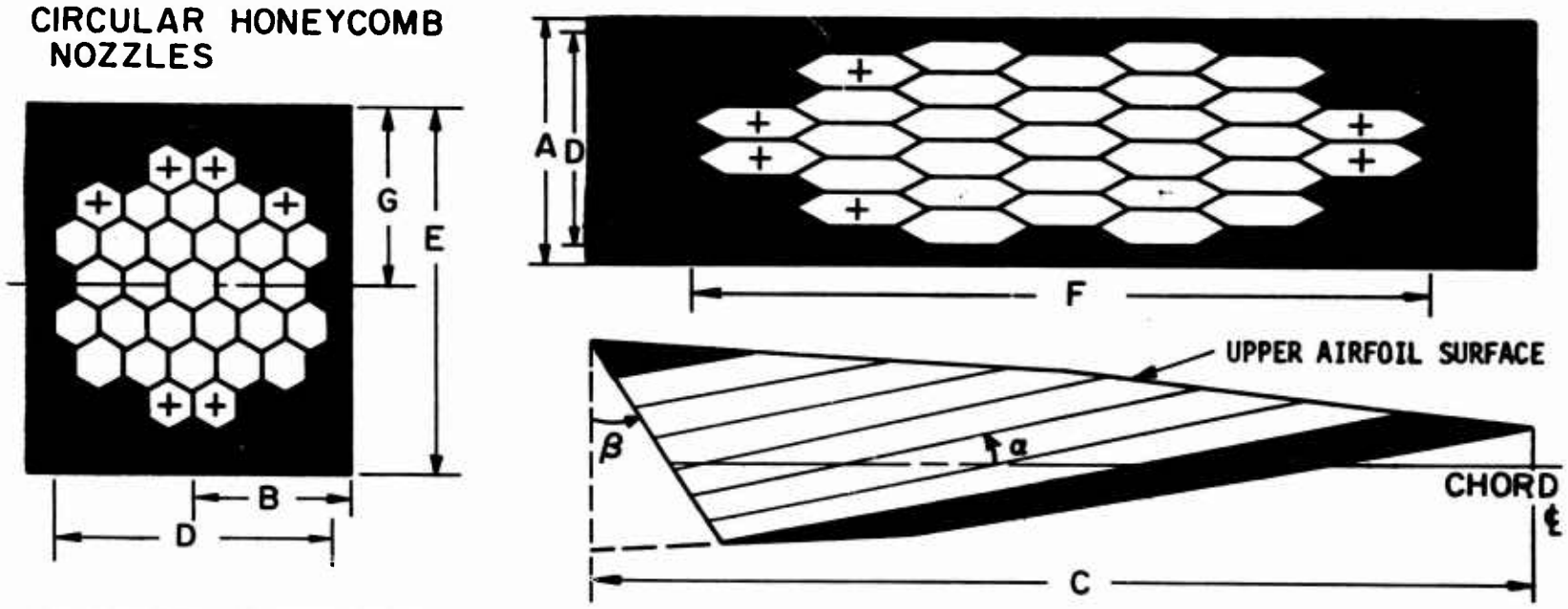

N = number of open cells

All dimensions are in inches

No.	N	Area (in^2)	α (deg)	β (deg)	A	B	C	D	E	F	G
1	16	0.83	9.5	0	1.75	0.75	9.4	1.5	2.1	4.9	1.4
2	24	1.24	9.5	0	1.75	0.75	9.4	1.5	2.1	6.7	1.4
3	31	1.60	9.5	0	1.75	0.85	9.4	1.5	2.1	6.6	1.4
13	24	1.24	5.5	0	1.75	0.85	9.4	1.5	2.1	8.9	1.0
14	24	1.24	13.5	22	1.75	0.75	9.4	1.5	2.1	5.6	1.4

Figure 7. Schematic Diagrams of Nozzles and Dimensional Data.

SLOTTED HONEYCOMB NOZZLES

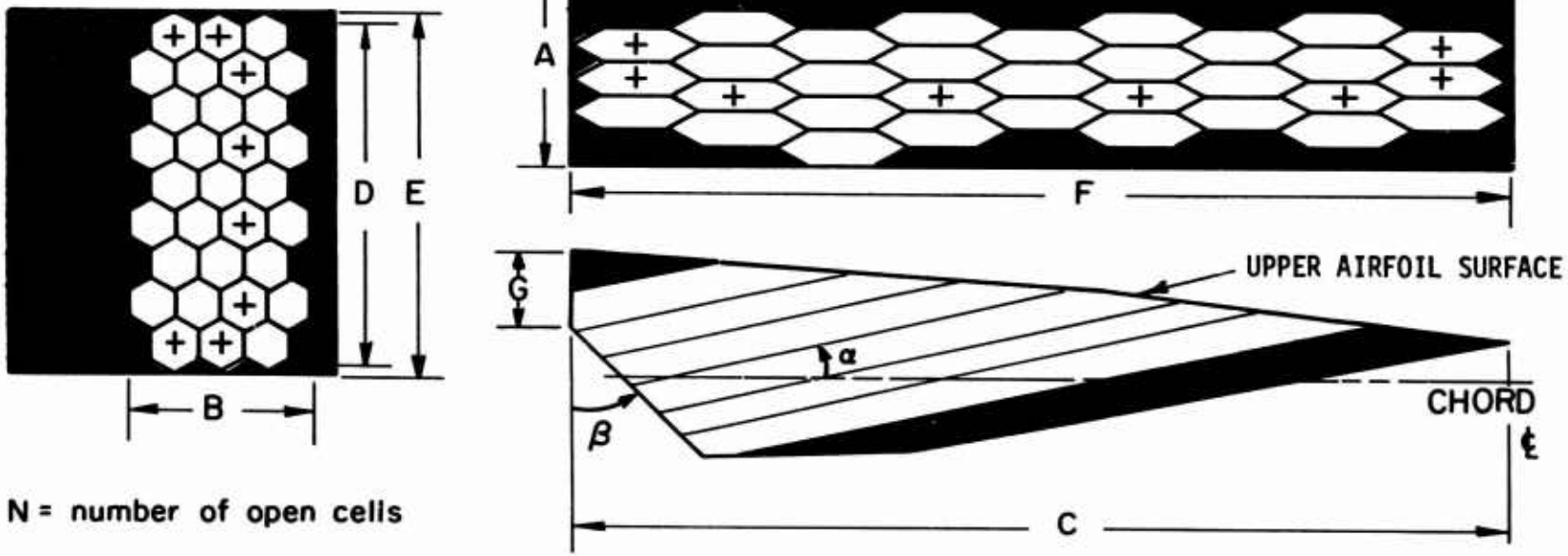

N = number of open cells

All dimensions are in inches

No.	N	Area (in^2)	α (deg)	β (deg)	A	B	C	D	E	F	G
4	16	0.83	9.5	68	1.75	0.9	9.4	1.8	2.1	8.5	0.4
5	24	1.24	9.5	68	1.75	0.9	9.4	1.8	2.1	8.5	0.4
6	31	1.60	9.5	68	1.75	0.9	9.4	1.8	2.1	8.5	0.4
17	24	1.24	5.5	0	1.75	0.9	9.4	1.9	2.1	9.1	1.9
18	24	1.24	13.5	47	1.75	0.9	9.4	1.9	2.1	6.9	0.4
16*	96	5.00	9.5	0	3.00	3.0	9.4	1.9	2.1	7.5	2.1

*#16 was left completely open to allow for on-site plugging to give any desired shape and area.

Figure 7. Continued.

OPEN CIRCLE NOZZLES

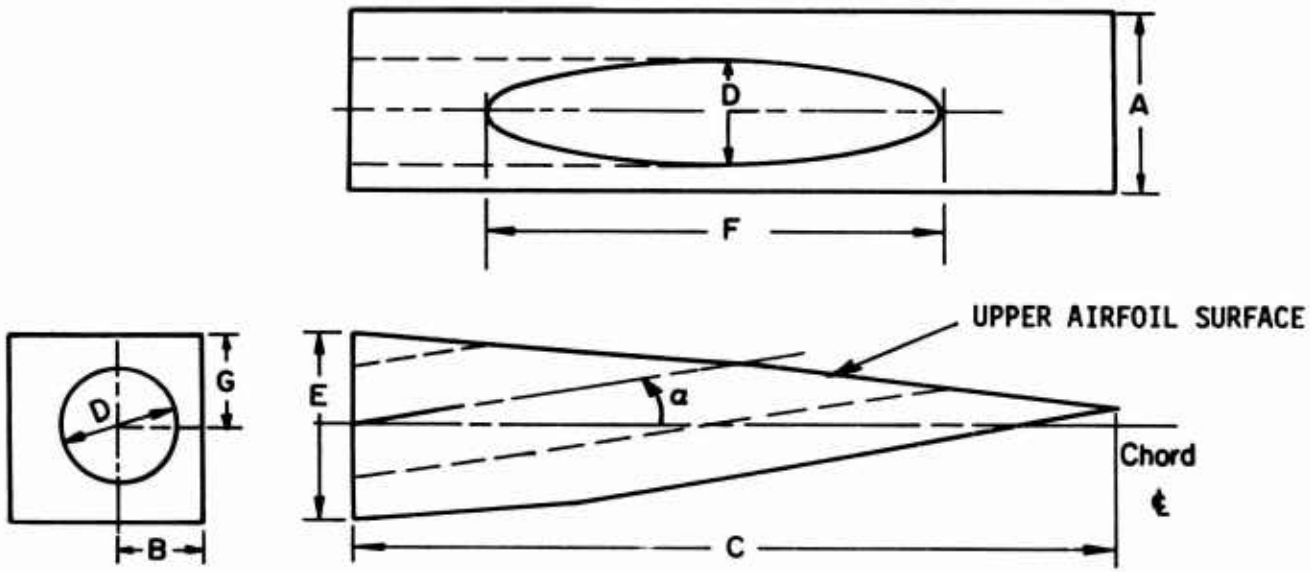

All dimensions are in inches

No.	N	Area (in^2)	α (deg)	β (deg)	A	B	C	D	E	F	G
7	-	0.93	9.5	-	1.75	0.79	9.4	1.09	2.1	4.15	1.10
8	-	1.23	9.5	-	1.75	0.85	9.4	1.25	2.1	4.82	1.10
9	-	1.54	9.5	-	1.75	0.85	9.4	1.40	2.1	5.35	1.10
19	-	1.23	5.5	-	1.75	0.85	9.4	1.25	2.1	6.35	1.00
21	-	1.23	13.5	-	1.75	0.85	9.4	1.25	2.1	3.88	1.25

Figure 7. Continued.

OPEN SLOT NOZZLES

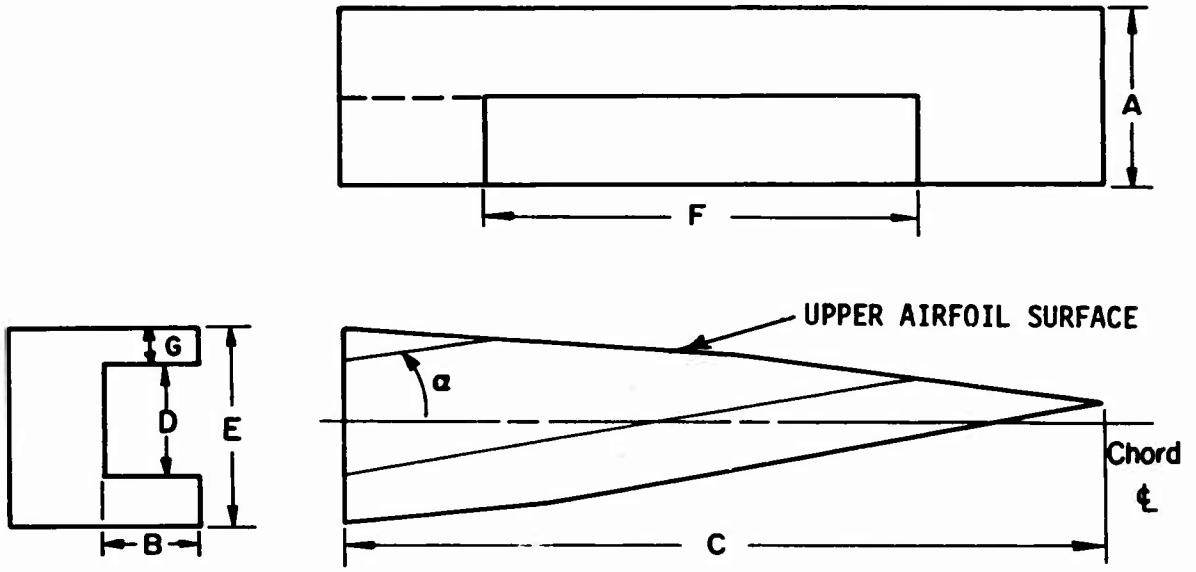

All dimensions are in inches

No.	N	Area (in^2)	α (deg)	β (deg)	A	B	C	D	E	F	G
10	-	0.93	9.5	-	1.75	0.64	9.4	1.28	2.1	5.00	0.42
11	-	1.23	9.5	-	1.75	0.79	9.4	1.58	2.1	6.10	0.30
12	-	1.54	9.5	-	1.75	0.91	9.4	1.82	2.1	7.74	0.16
20	-	1.23	5.5	-	1.75	0.79	9.4	1.58	2.1	7.75	0.30
22	-	1.23	13.5	-	1.75	0.79	9.4	1.58	2.1	4.86	0.46
15†	-	0.0	-	-	1.75	0	9.4	0	2.1	0	-

†#15 was a plug which essentially formed an unmodified airfoil.

Figure 7. Concluded.

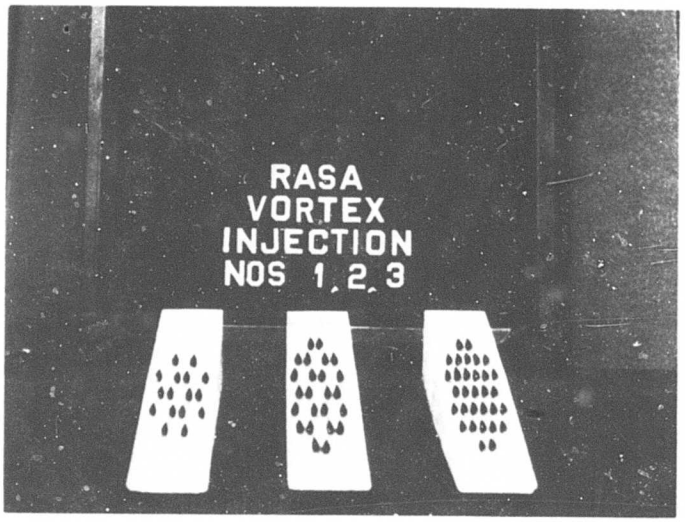

Figure 8. Circular Honeycomb Nozzles.

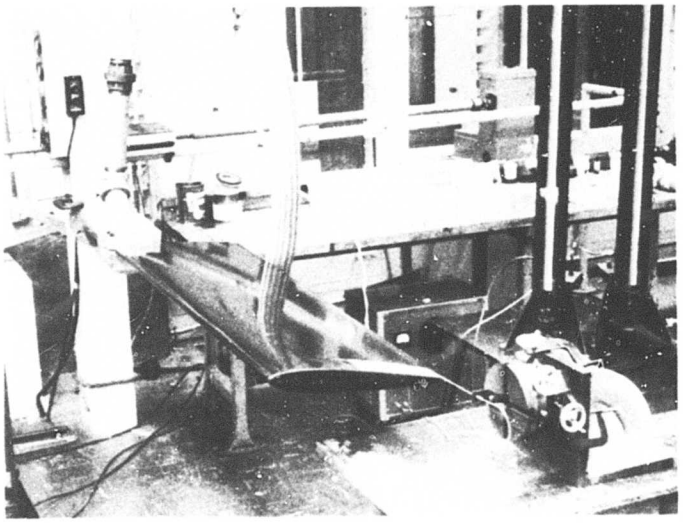

Figure 9. Calibration Setup for Obtaining Exit Velocity Distributions Across the Nozzles.

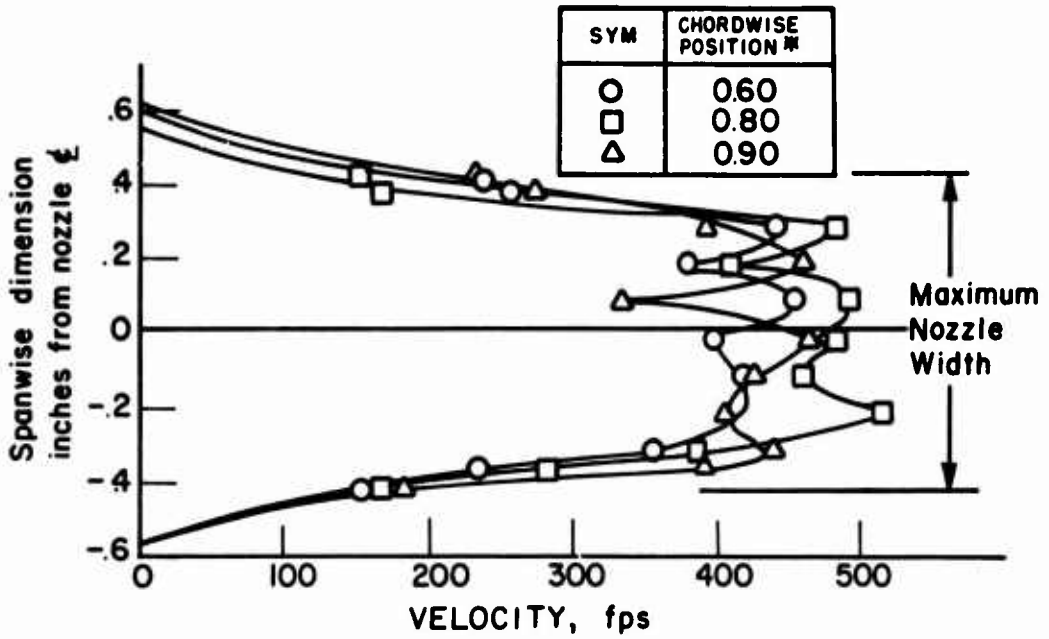

*Ratio of chordwise distance from forward edge of nozzle to the exposed chordwise length along contour.

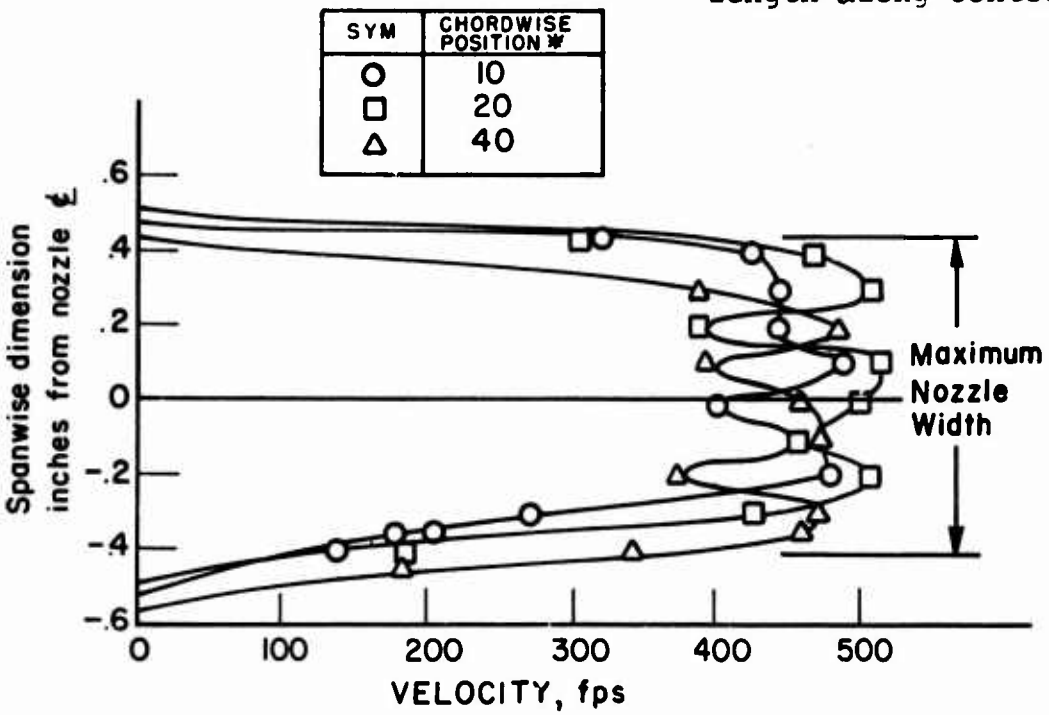

Figure 10. Velocity Distributions for Nozzle No. 5; Slotted Honeycomb; α_i=9.5°; A=1.24 in.^{2}; m_i=0.281 lb/sec.

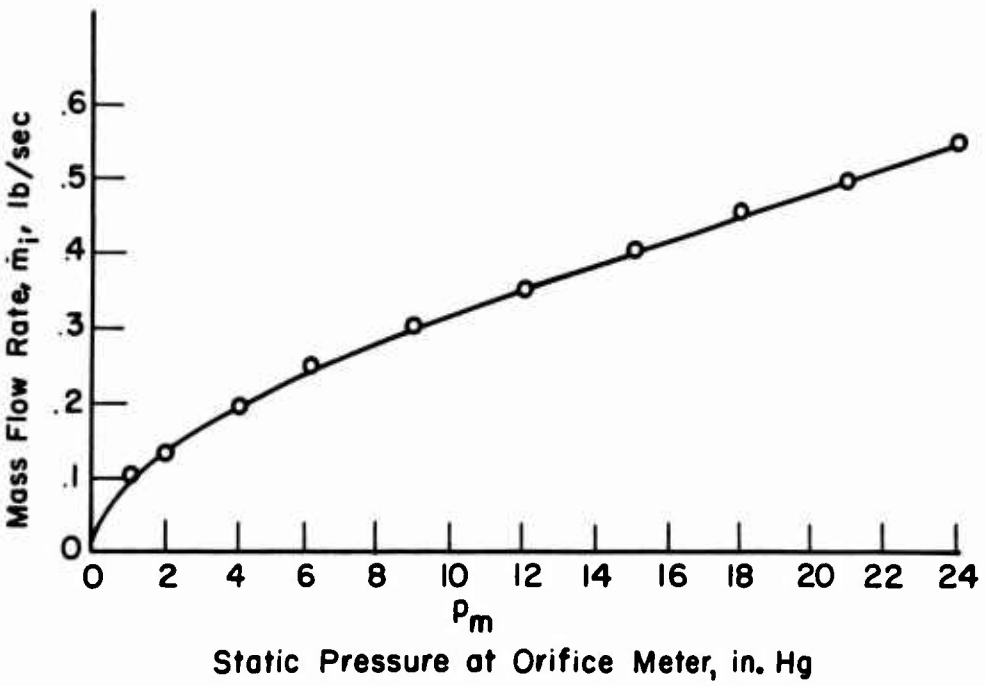

Figure 11. Mass Flow Rate Versus Static Pressure at Orifice. Nozzle No. 5; Slotted Honeycomb; α_i=9.5°; A=1.24 in.^{2}.

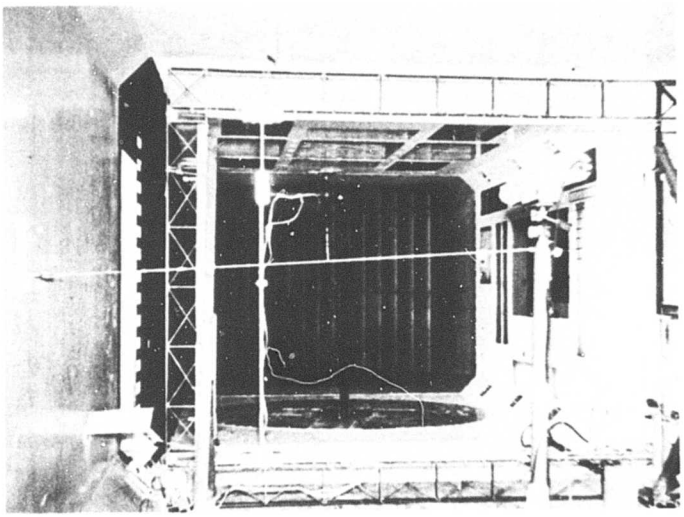

Figure 12. Installation of Model and Instrumentation for the Wind Tunnel Tests.

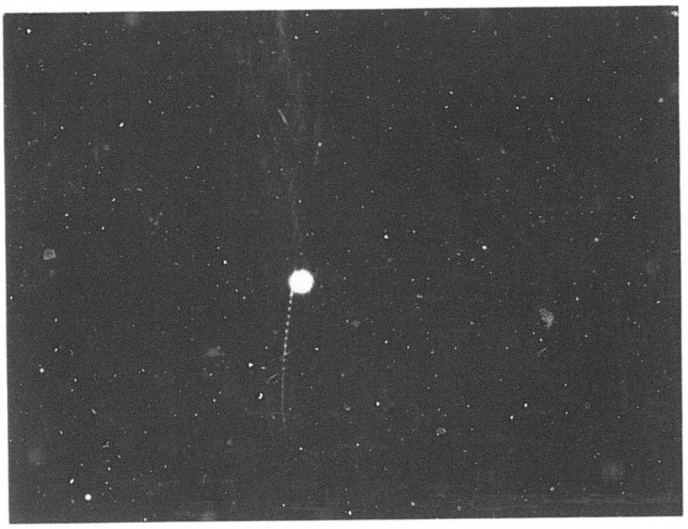

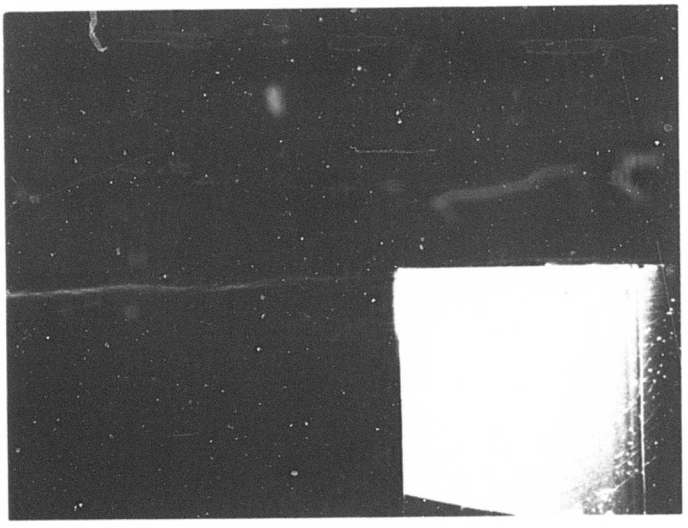

Figure 13. Formation of Vortex for Squared-off Tip Configuration.

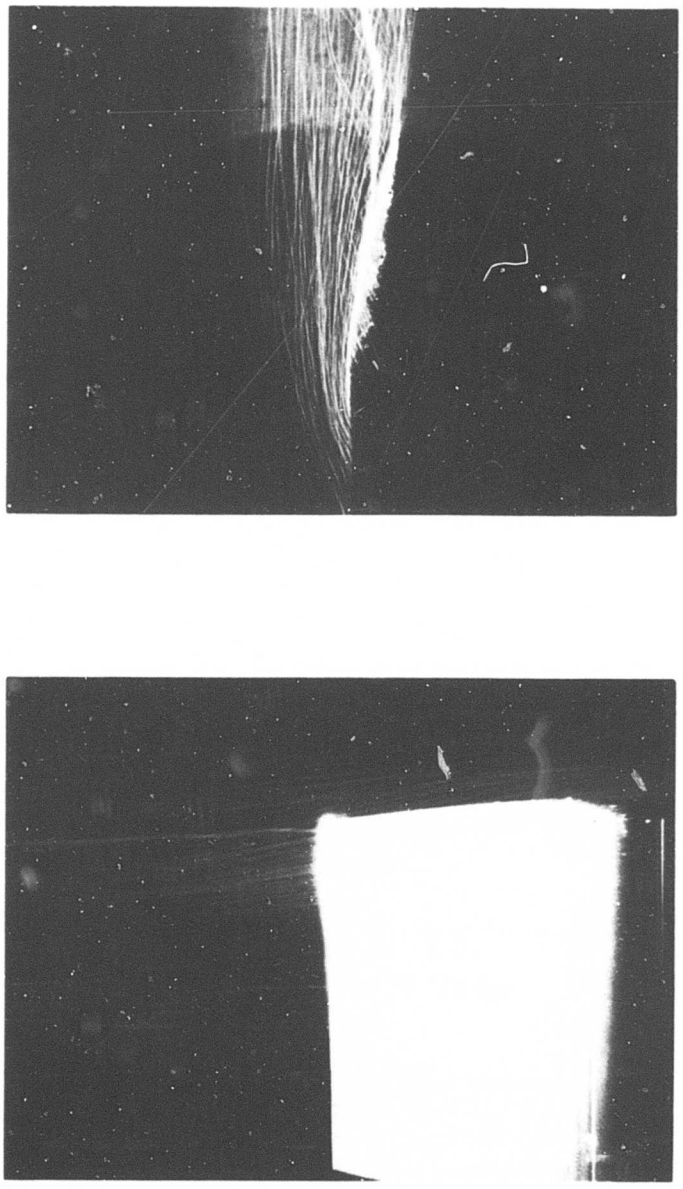

Figure 14. Formation of Vortex for Developed Half-Round Tip Configuration.

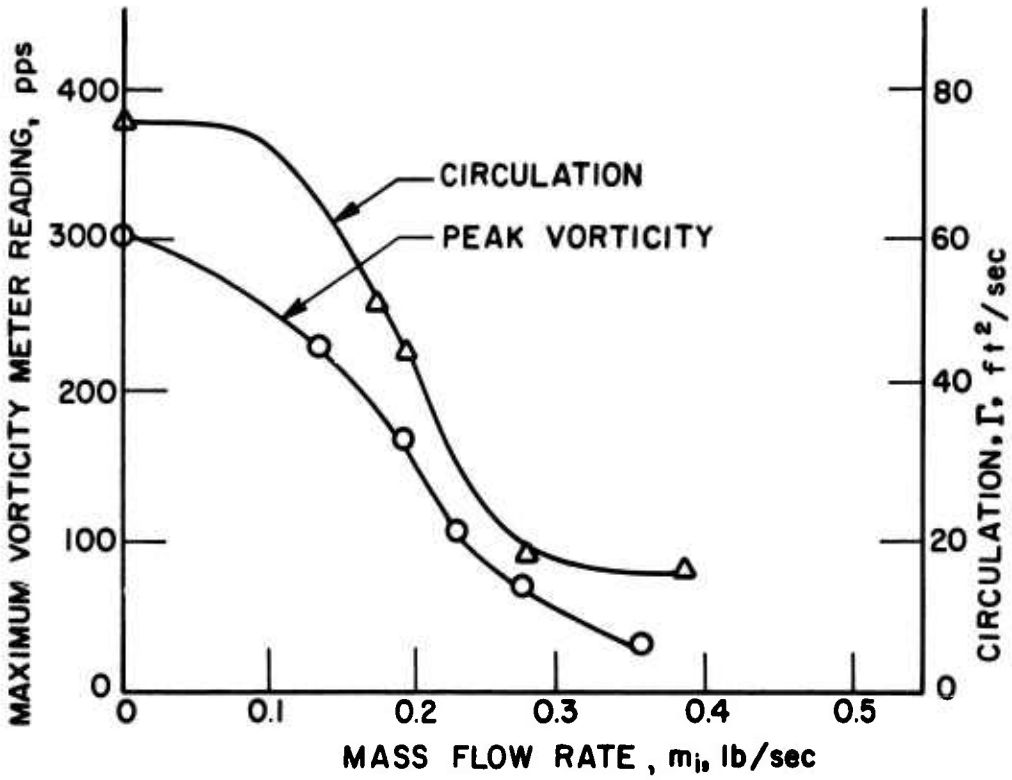

Figure 15. Comparison of Circulation and Peak Vorticity Versus Mass Flow Rate; V=150 fps, α_T=9.5°; Nozzle No. 5.

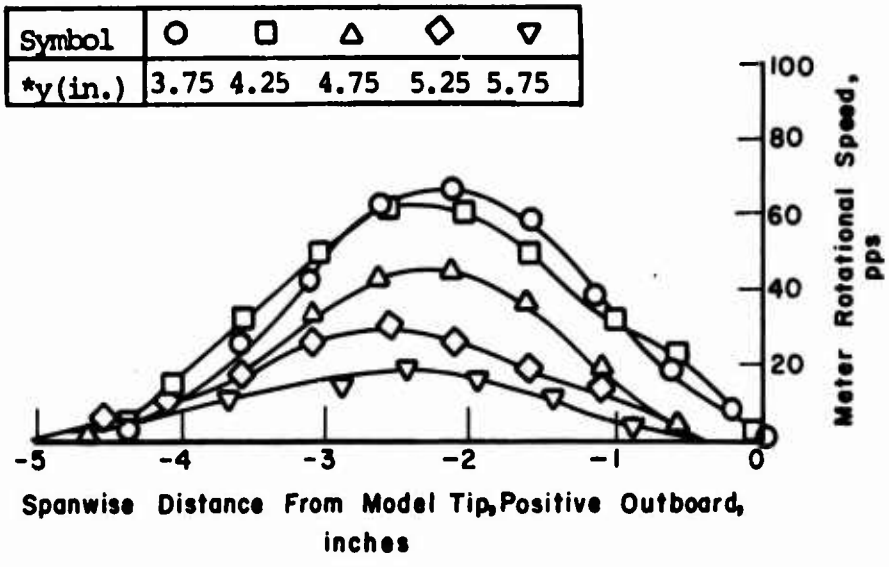

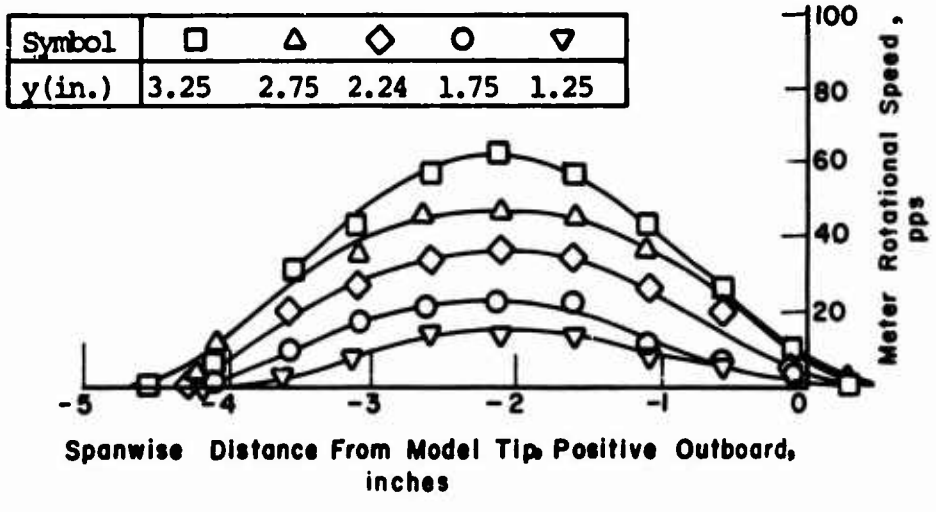

*y is the distance from the tunnel centerline, positive toward suction side.

Figure 16. Spanwise Distributions of Vorticity at Various Positions Across the Vortex; V=150 ft/sec, α_T=9.5°; Nozzle No. 5; m_i=0.281 lb/sec.

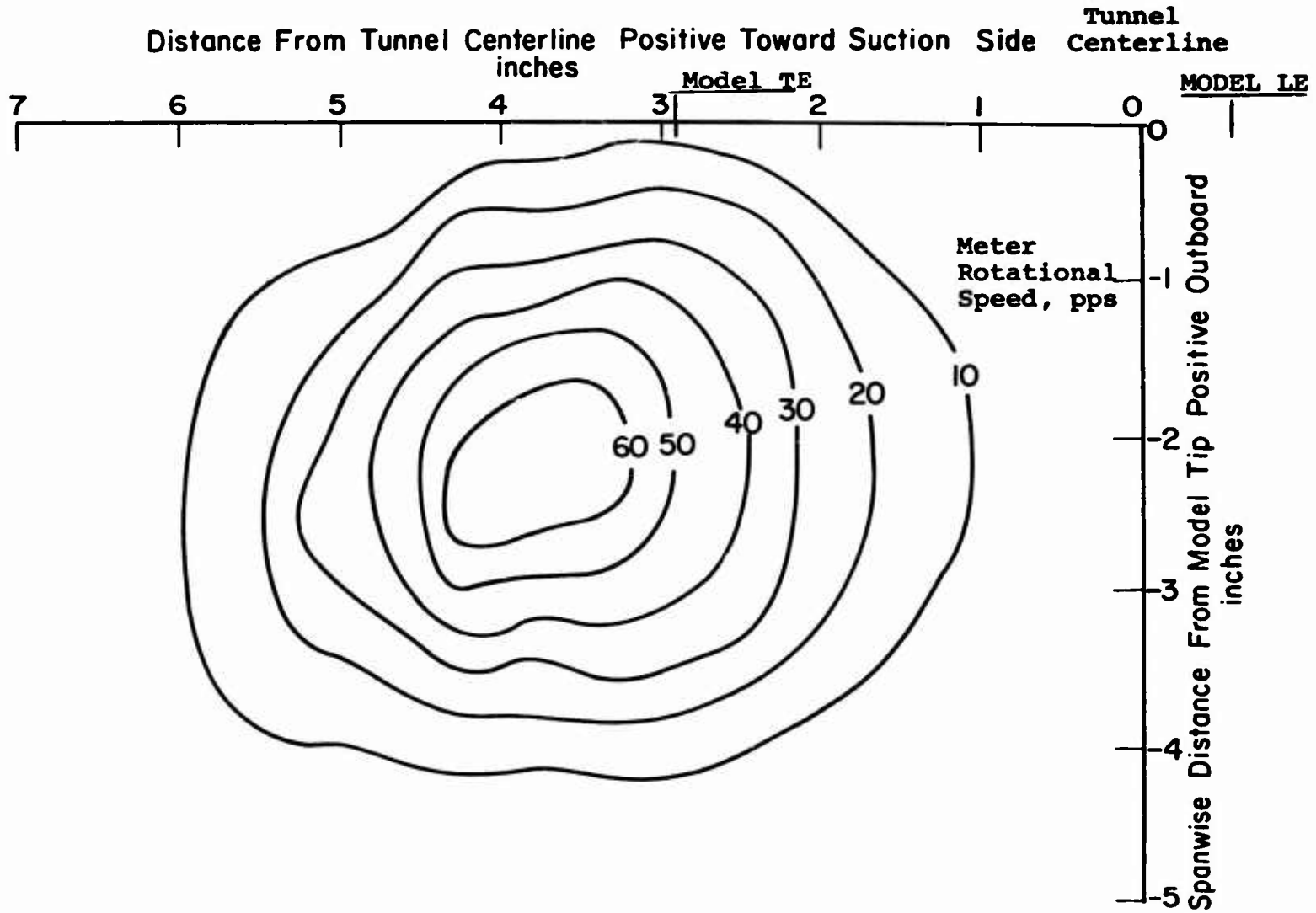

Figure 17. Contour Distribution of Vorticity Looking Upstream; V=150 ft/sec, α_T=9.5°; Nozzle No. 5; m_i=0.281 lb/sec.

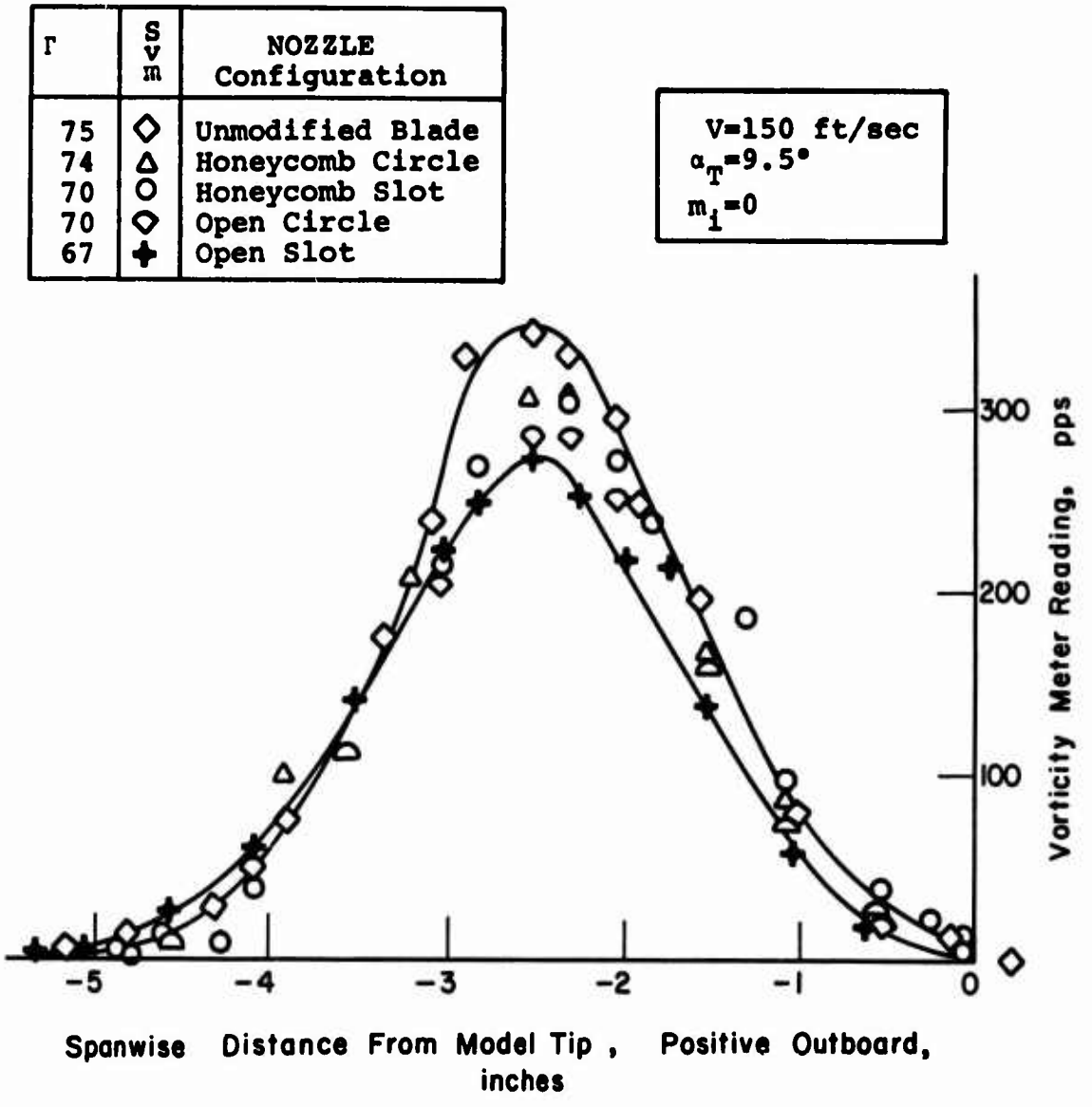

Figure 18. Spanwise Distribution of Vorticity for Various Nozzle Configurations.

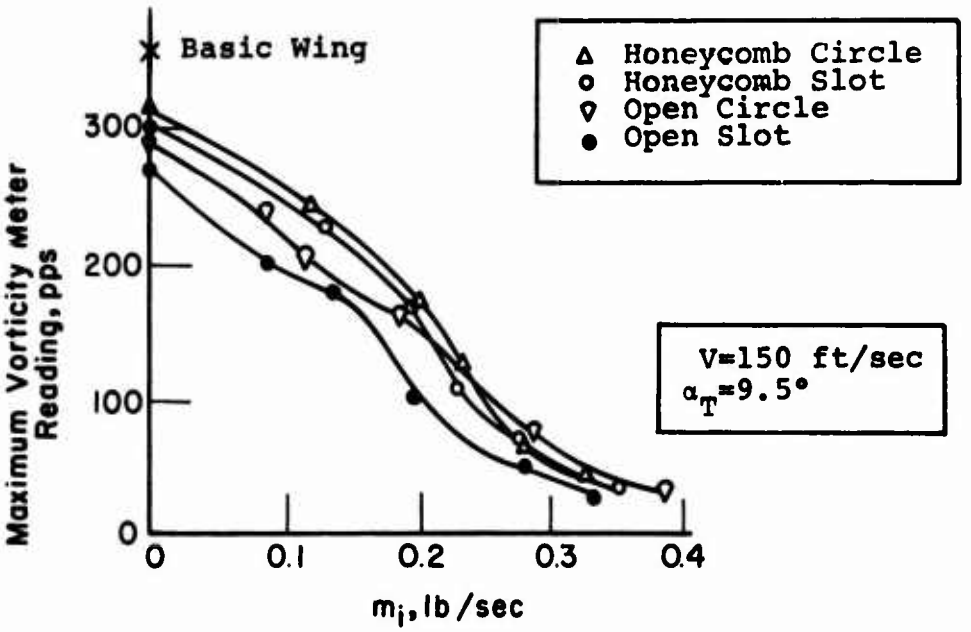

Figure 19. Peak Vorticity Versus Mass Flow Rate for Various Nozzles.

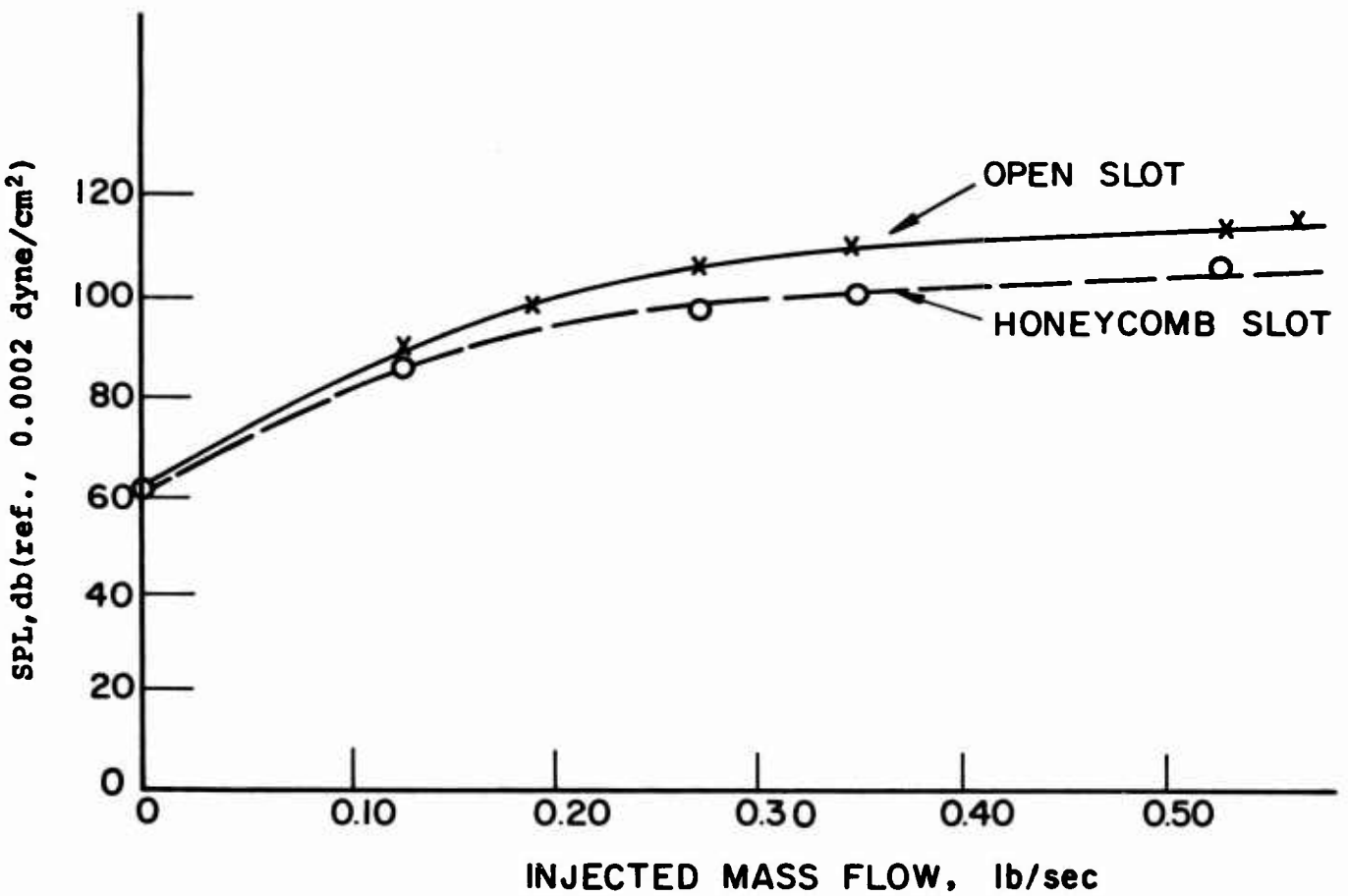

Figure 20. Variation of Overall Noise With Mass Flow.

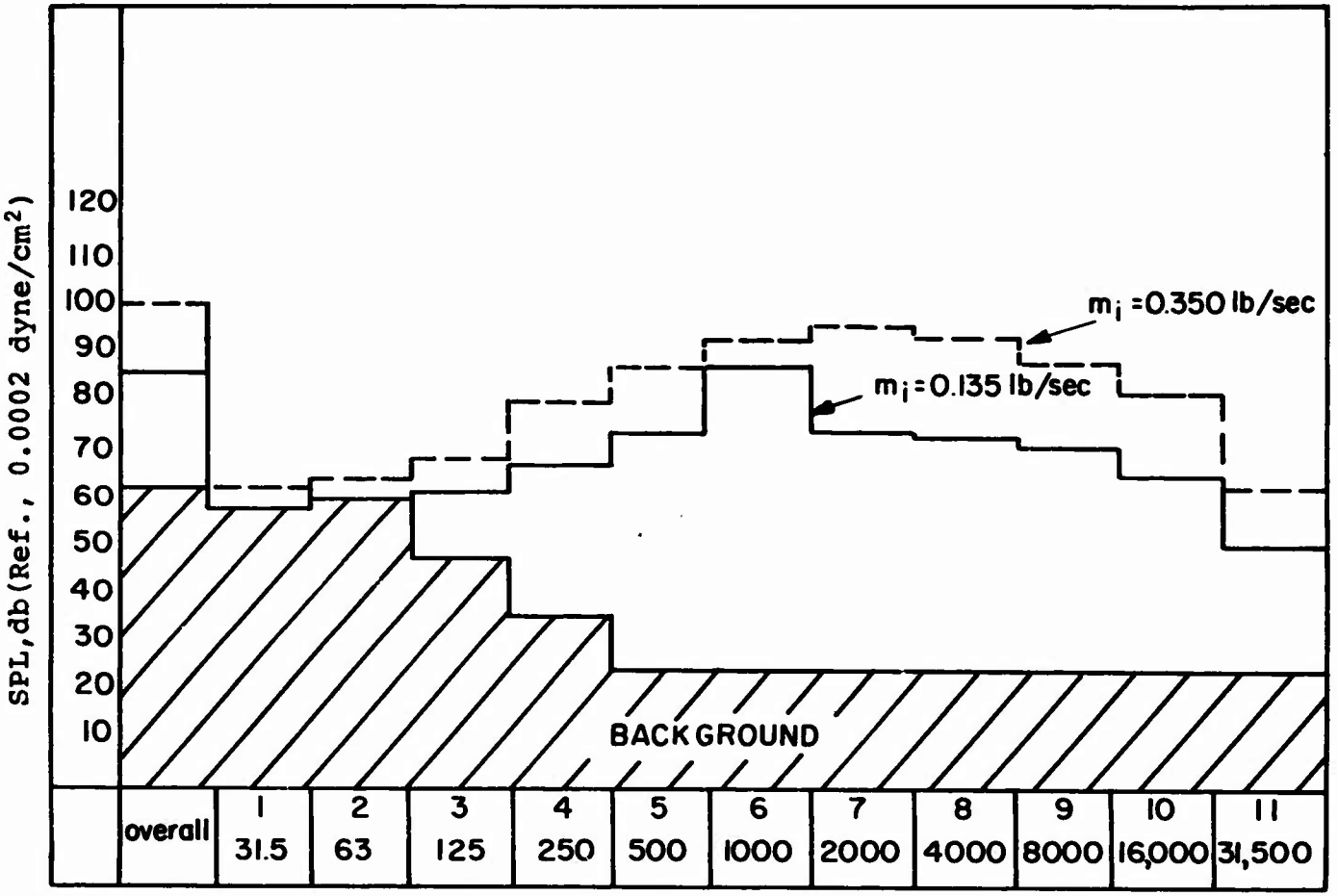

Figure 21. Spectrum of Honeycomb Nozzle for Two Different Mass Flows.

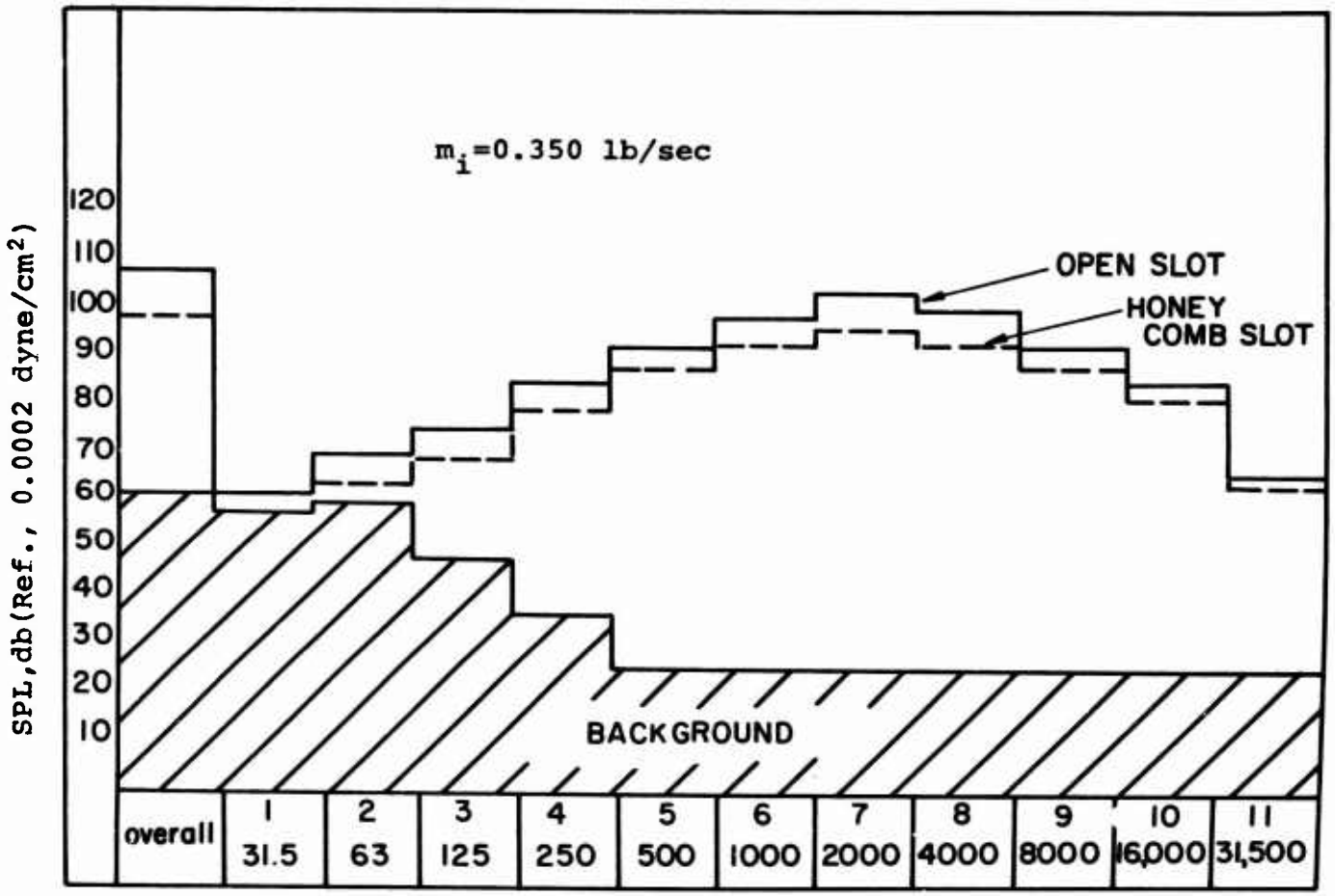

Figure 22. Spectrum of Acoustic Output of Slotted Nozzles.

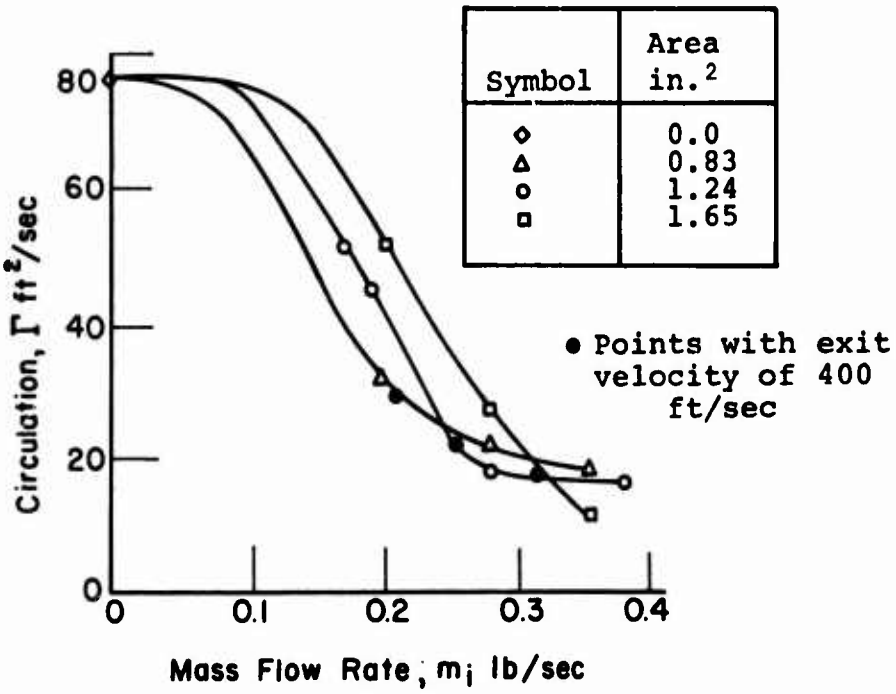

Figure 23. Circulation Versus Mass Flow for Various Constant-Area Nozzles.

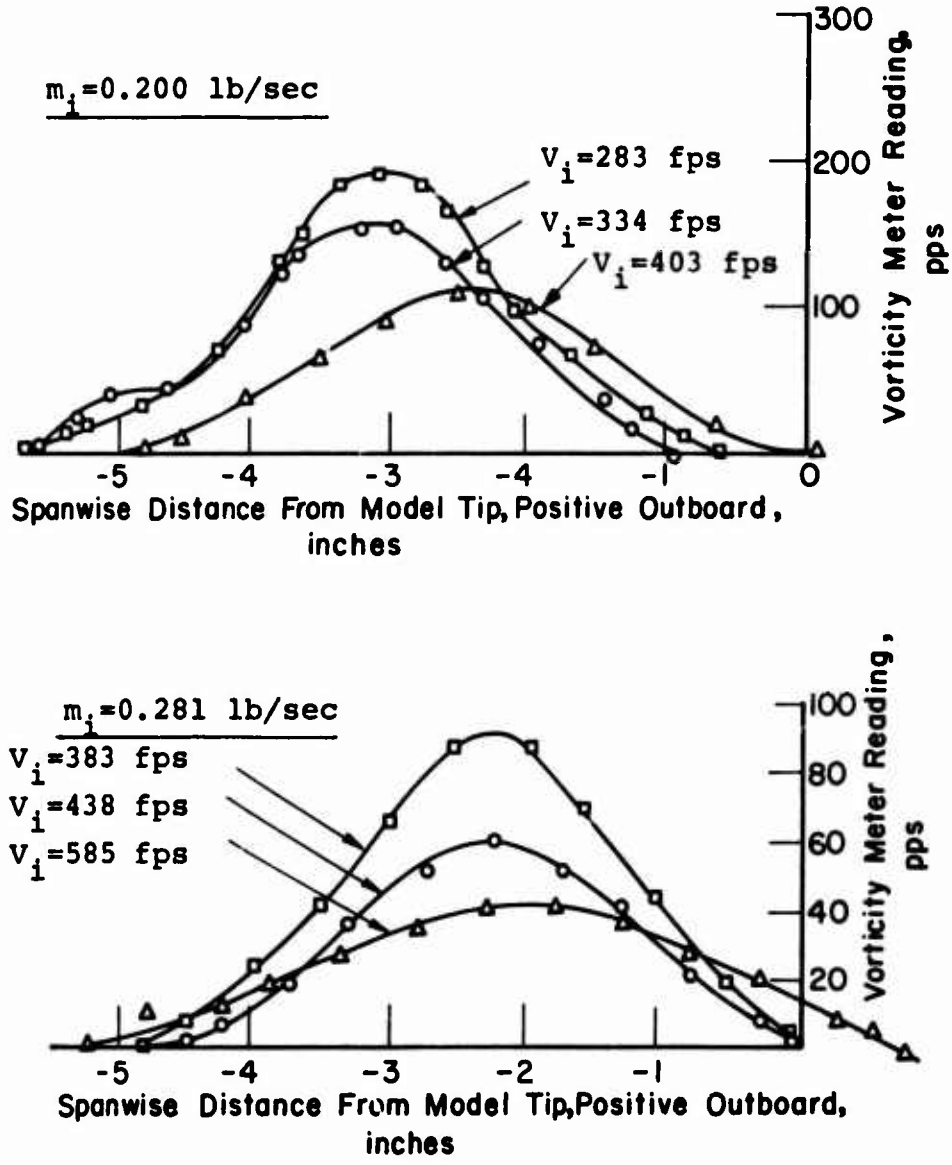

Figure 24. Distribution of Vorticity for Slotted Honeycomb Nozzles at V=150 fps and α_T=9.5°.

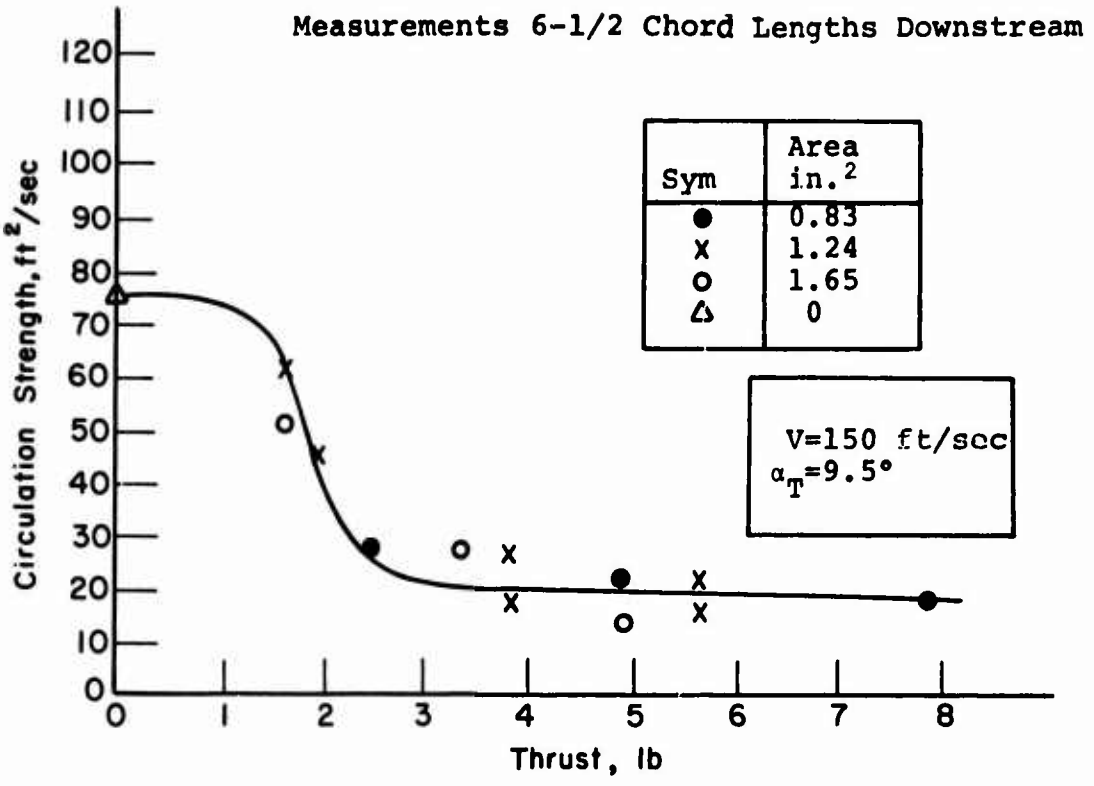

Figure 25. Circulation Strength Versus Thrust.

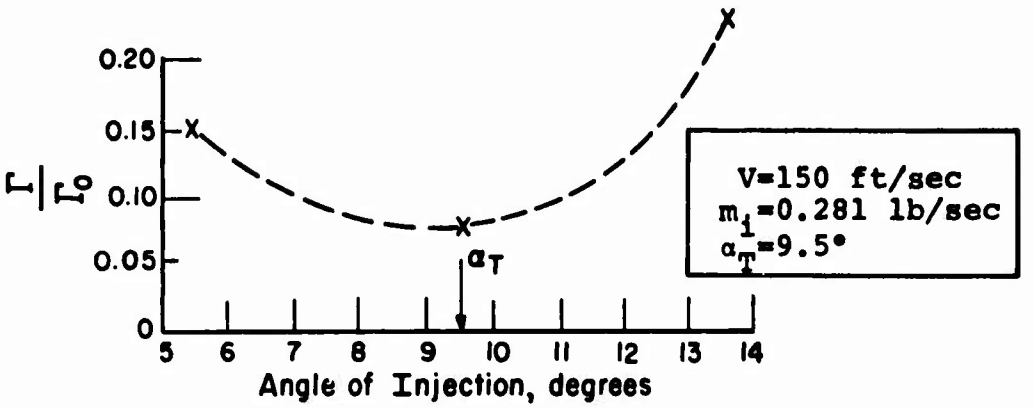

Figure 26. Variation of Circulation With Injection Angle.

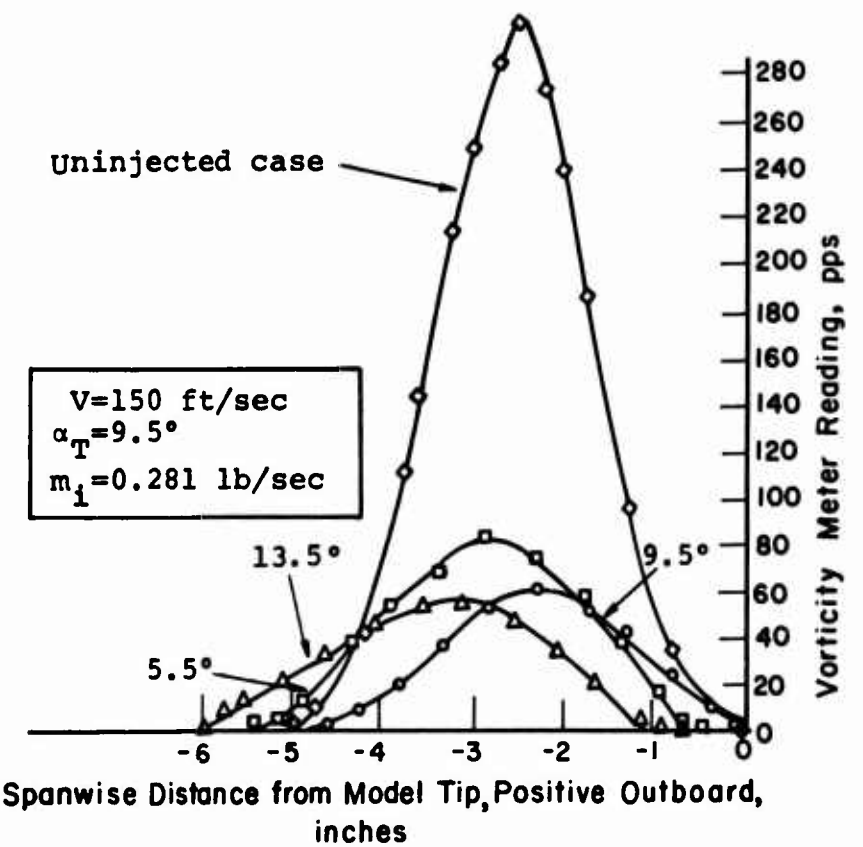

Figure 27. Spanwise Distribution of Vorticity for Honeycomb Nozzles for Various Angles of Injection.

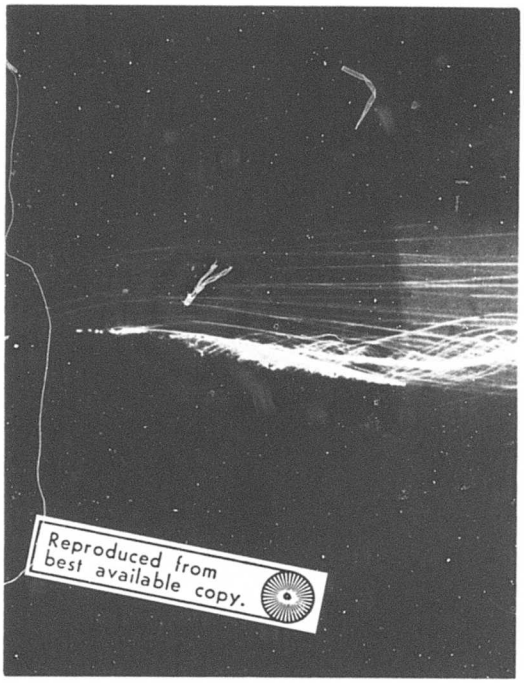

Figure 28. Spanwise View of Vortex Formation.

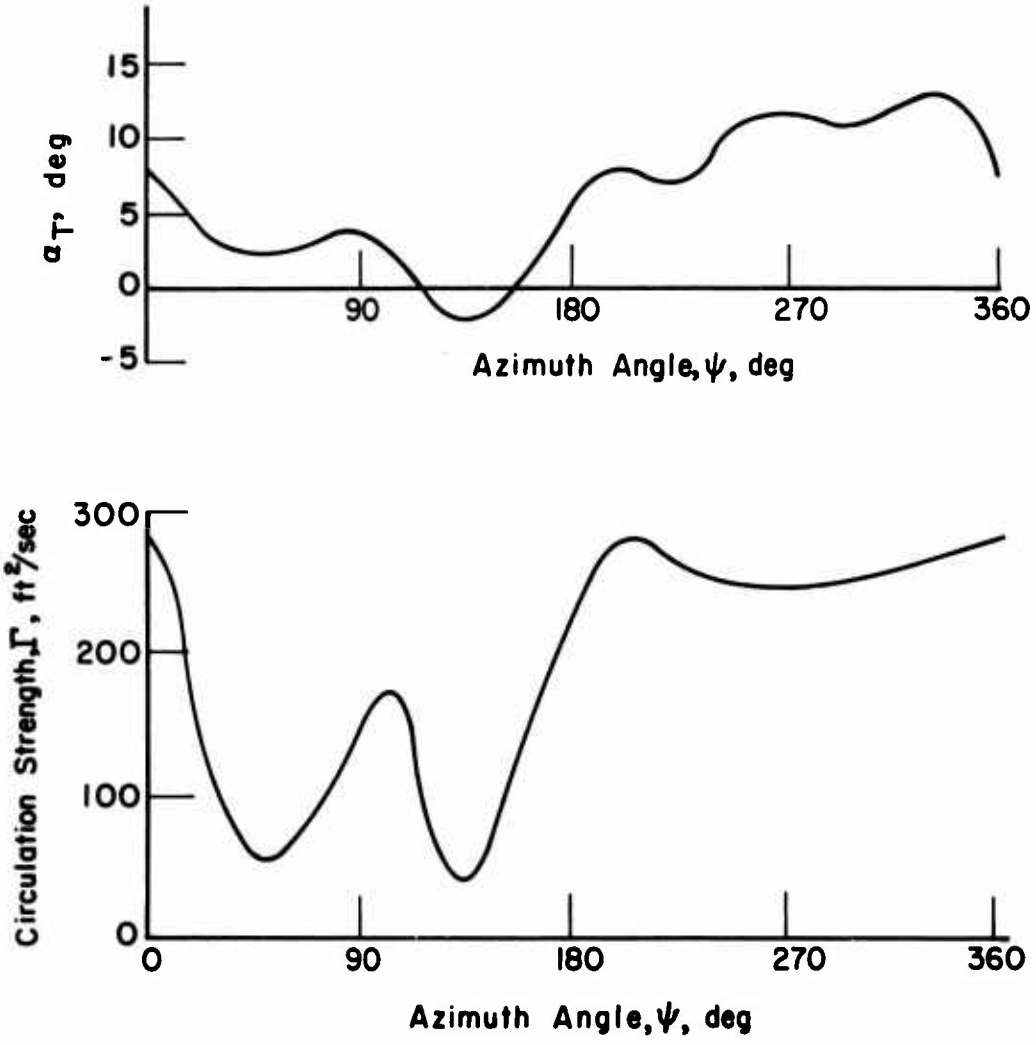

Figure 29. Variation of Angle of Attack and Circulation Strength for H-34 Helicopter at μ=0.20.

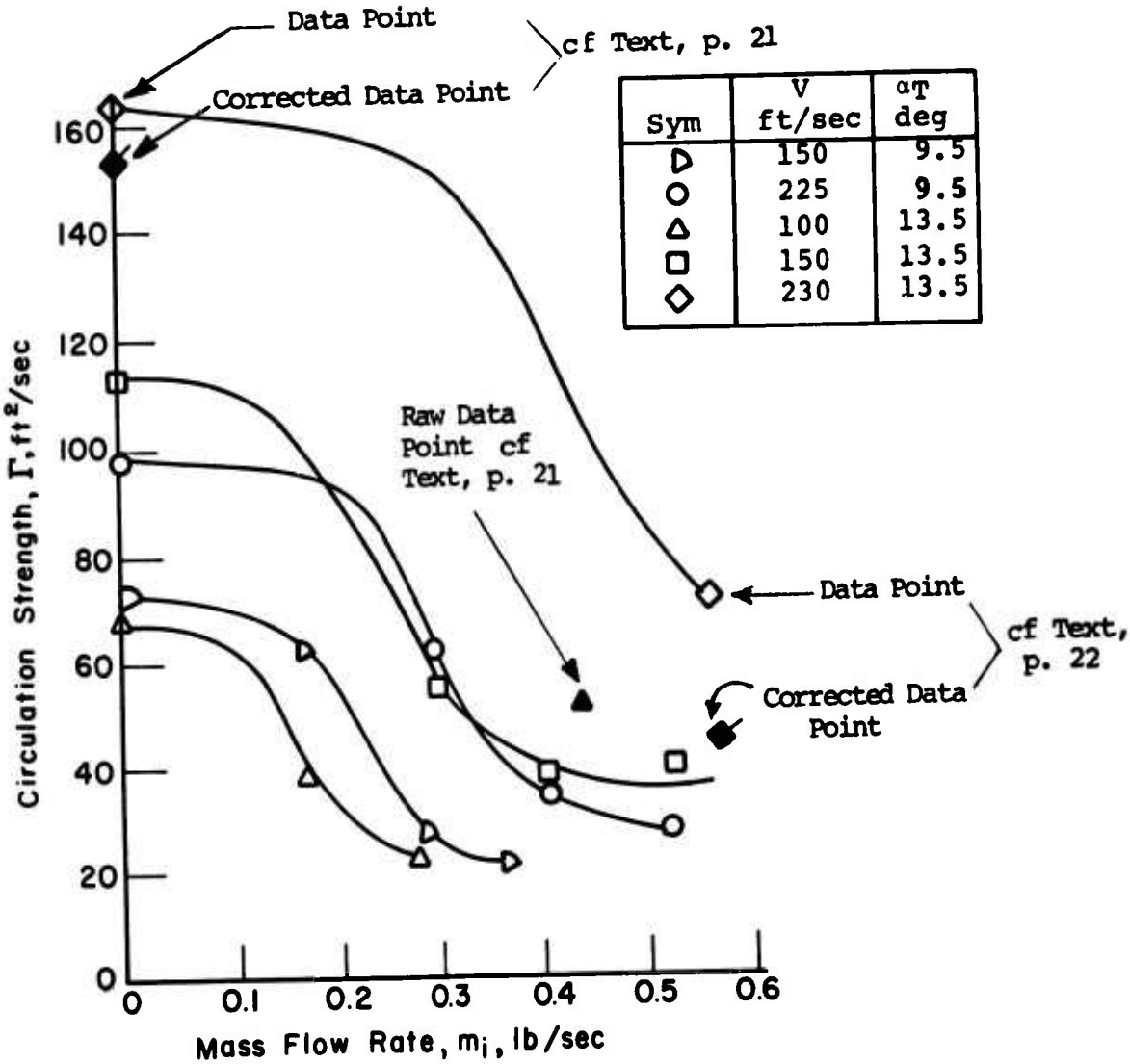

Figure 30. Circulation Versus Mass Flow Rate for Various Test Conditions.

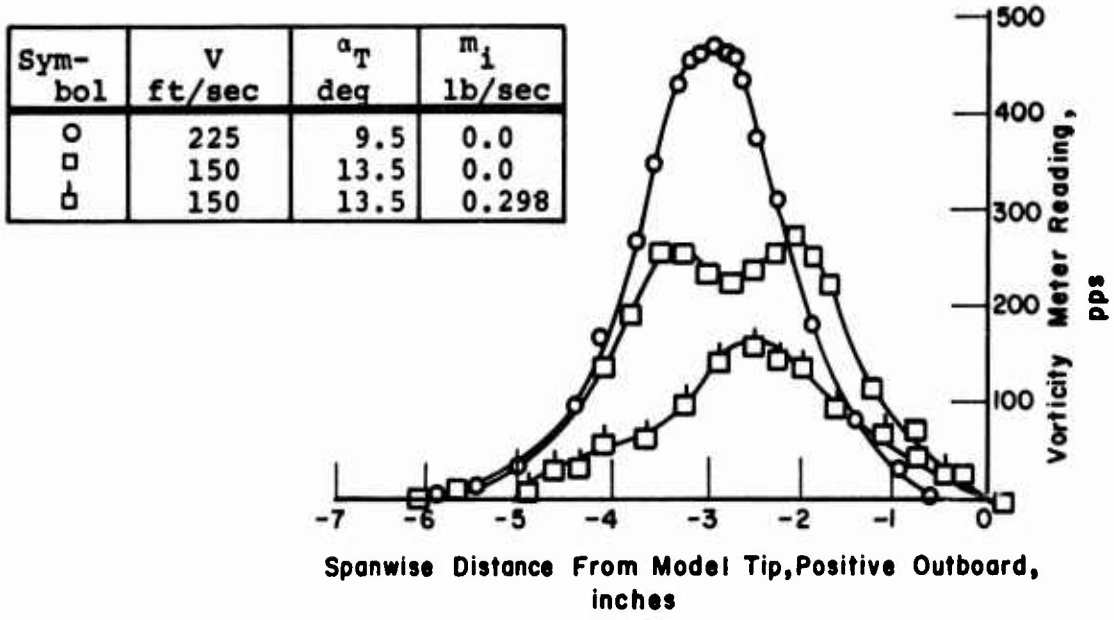

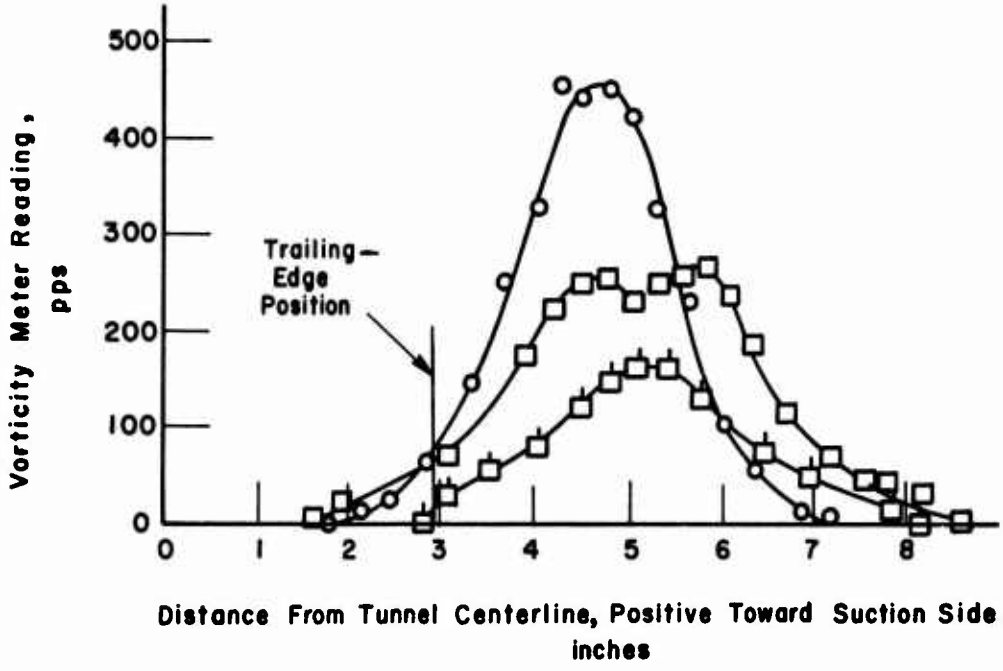

Figure 31. Spanwise and Normal Distribution of Vorticity for Various Test Conditions.

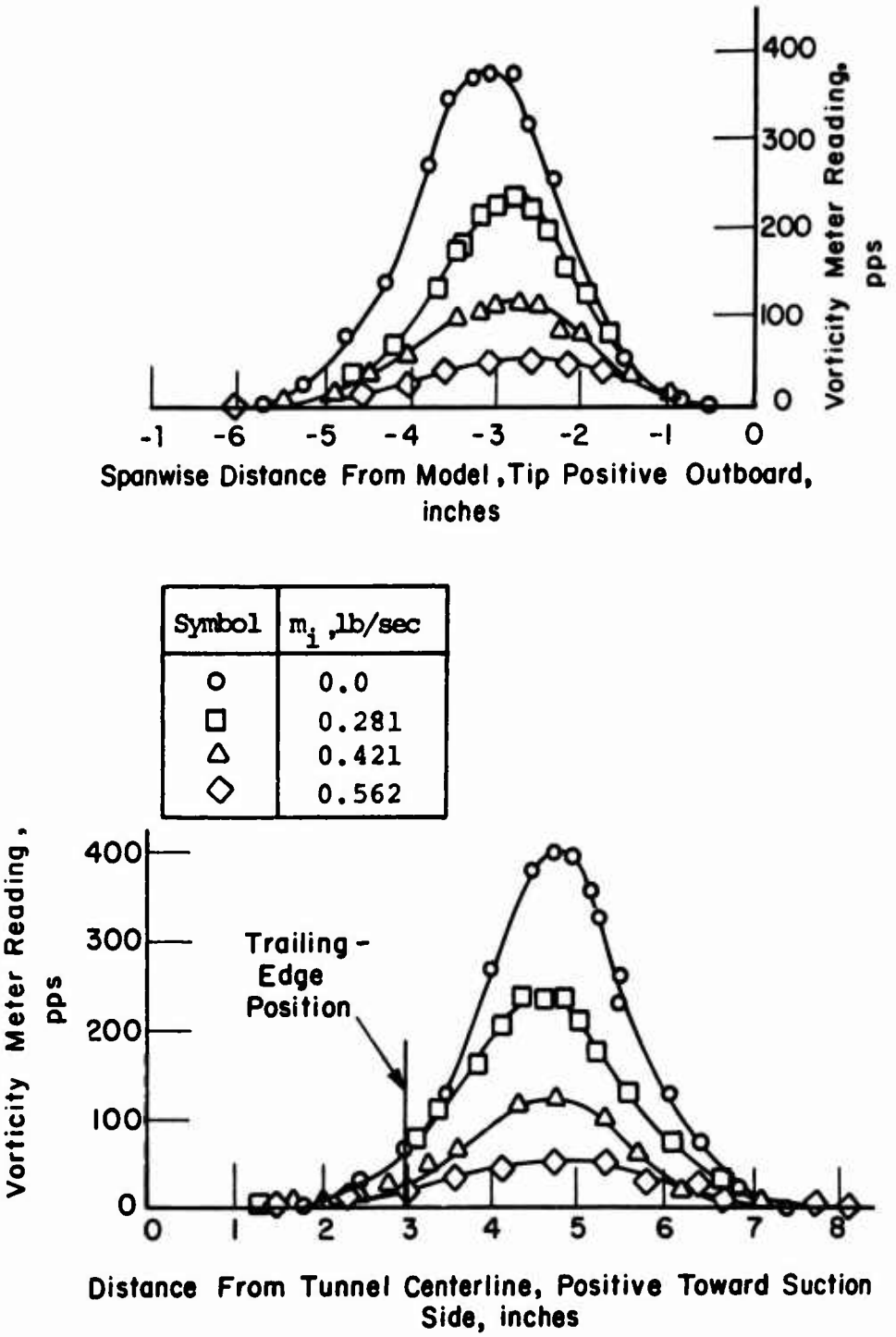

Figure 32. Spanwise and Normal Distributions of Vorticity for Various Rates of Mass Injection, V=225 ft/sec, α_T=9.5°.

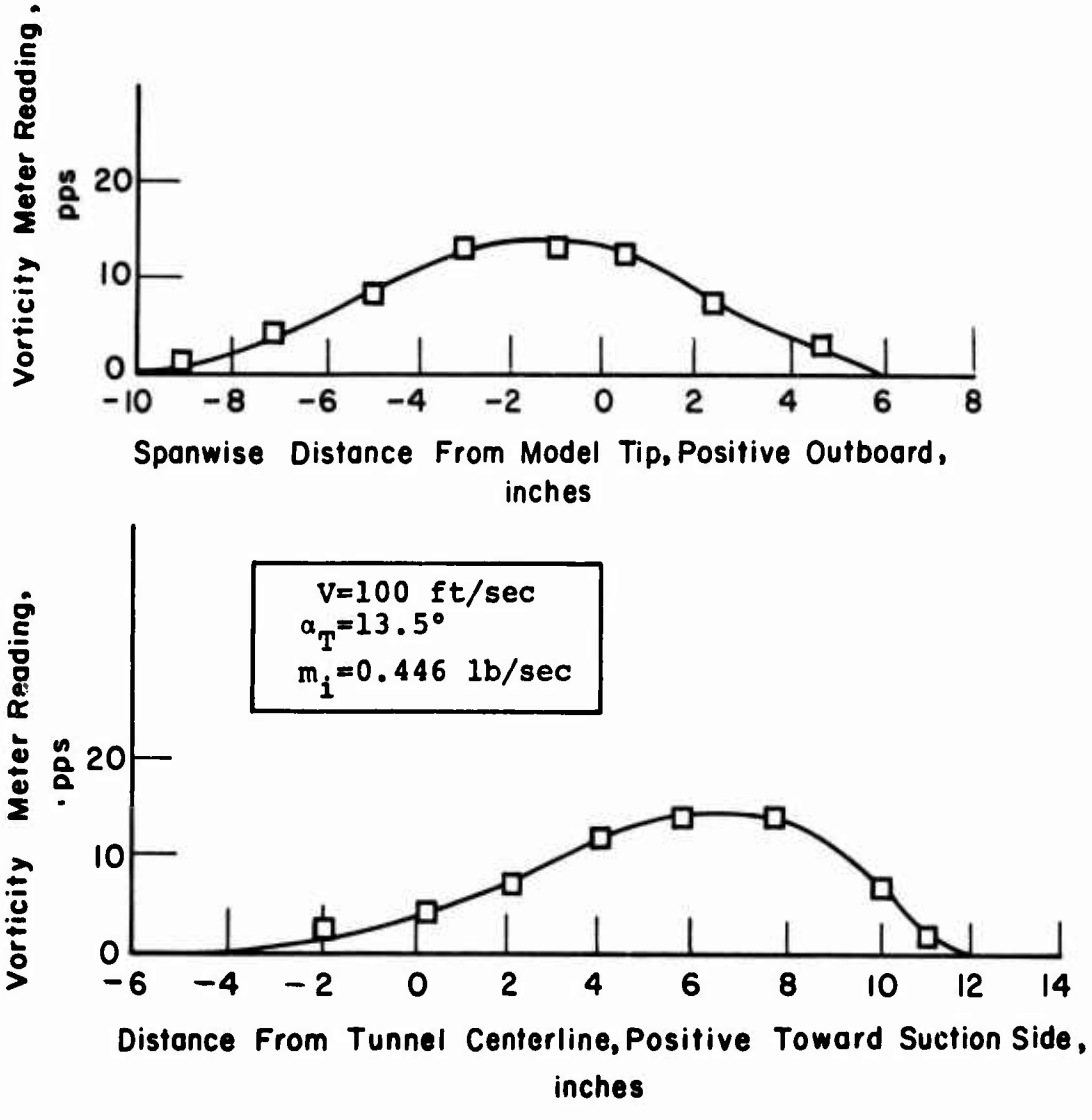

Figure 33. Spanwise and Normal Vorticity Distribution for Vortex Just After Instability.

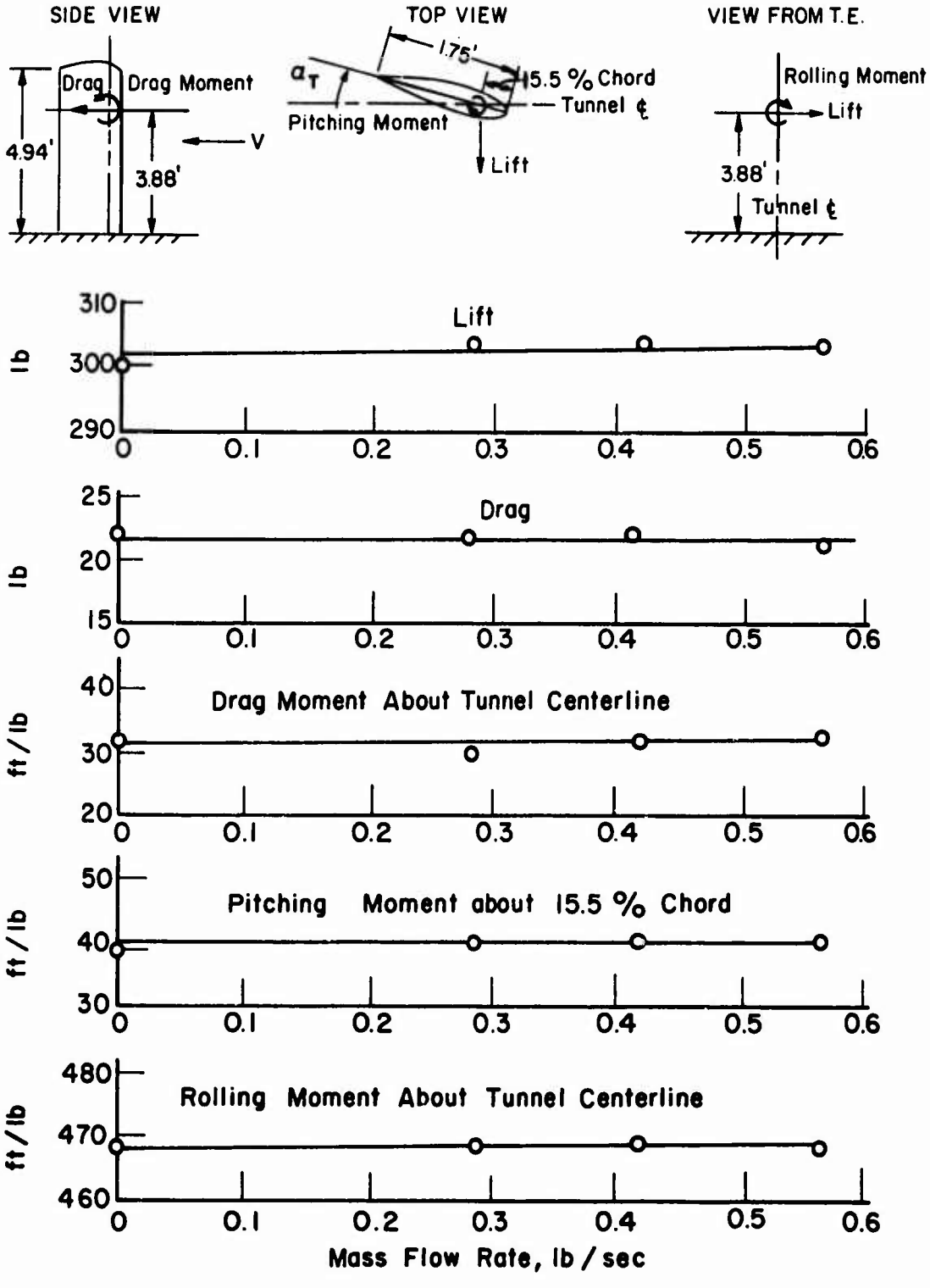

Figure 34. Net Balance Measurements Versus Mass Flow Rate; V=225 ft/sec, α_T=9.5°.

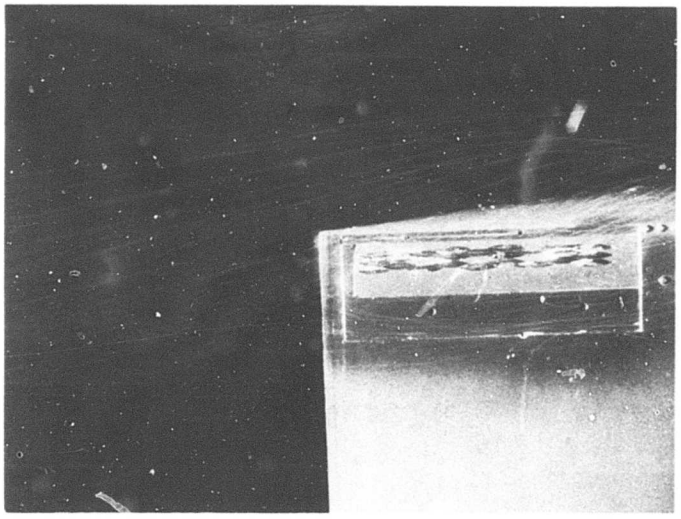

With Mass Injection

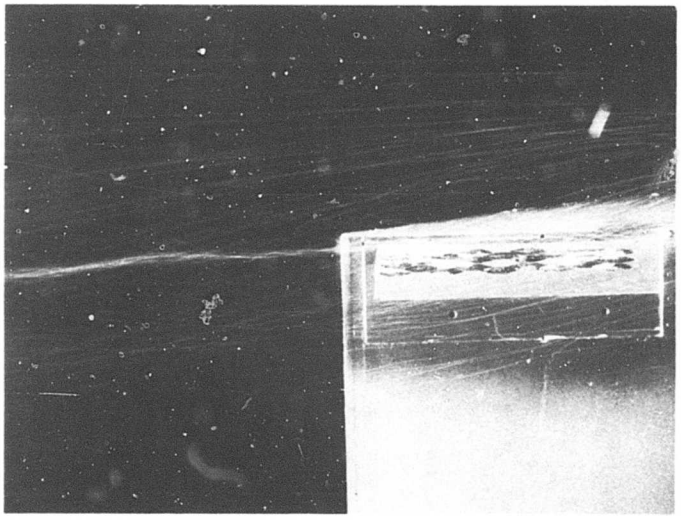

Without Mass Injection

Figure 35. Influence of Mass Injection on the Flow Field in the Proximity of the Model.

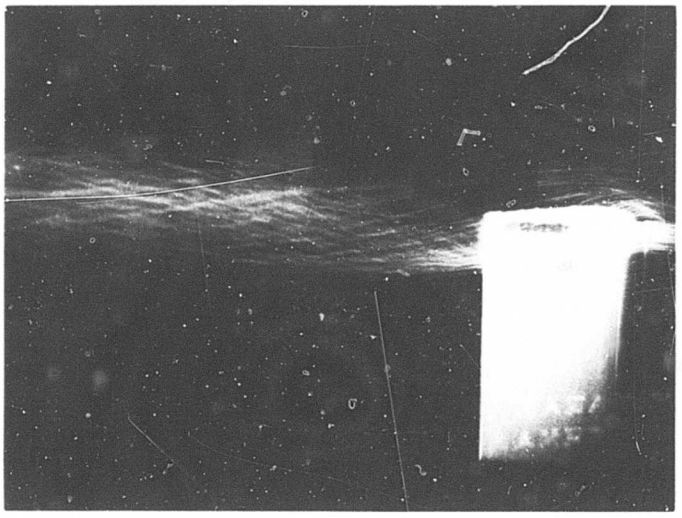

With Mass Injection

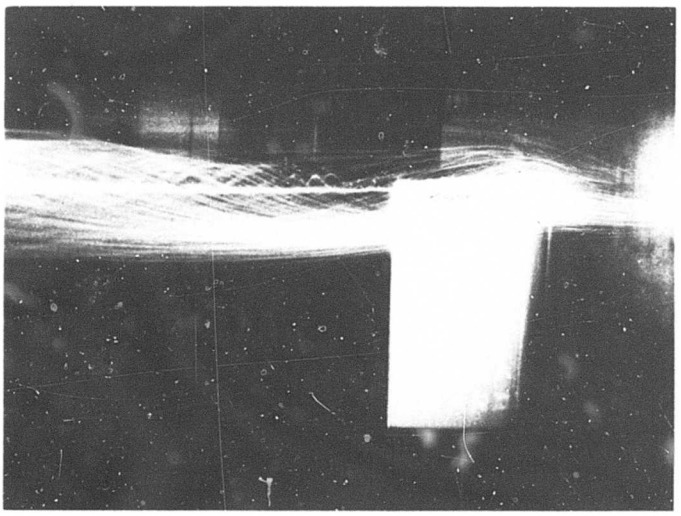

Without Mass Injection

Figure 36. Influence of Mass Injection on the Flow Field in the Near Wake of the Model.

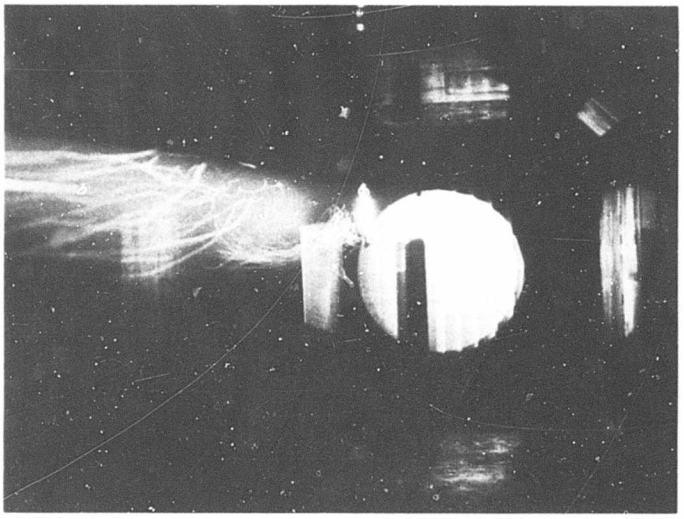

With Mass Injection

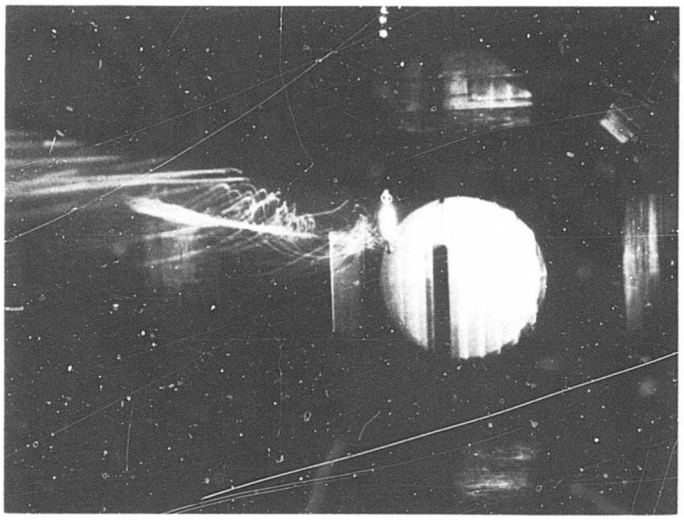

Without Mass Injection

Figure 37. Influence of Mass Injection on the Flow Field in the Wake of the Model, Looking Upstream.

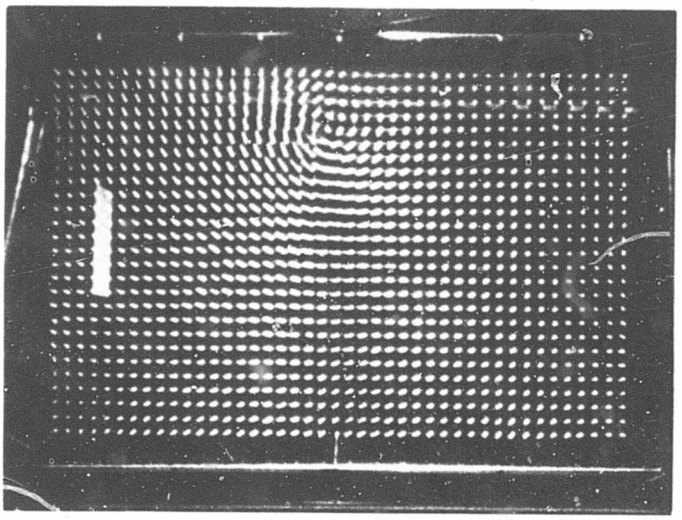

With Mass Injection

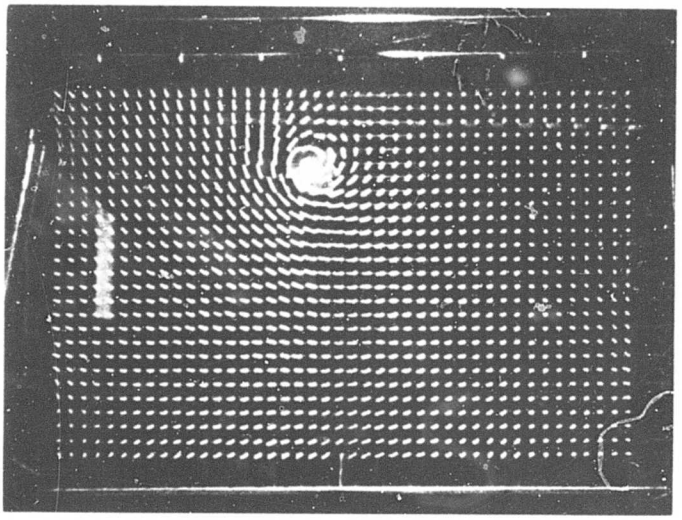

Without Mass Injection

Figure 38. Influence of Mass Injection on Tuft Grid 15 Chord Lengths Downstream of the Model; V=100 fps, α_T=13.5°.

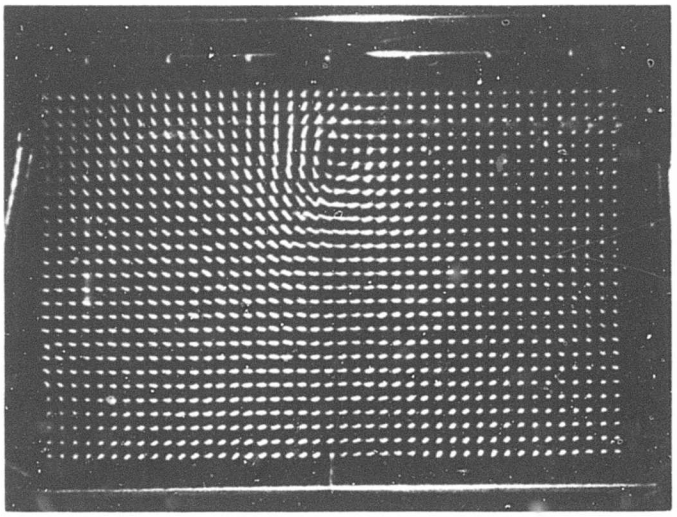

With Mass Injection

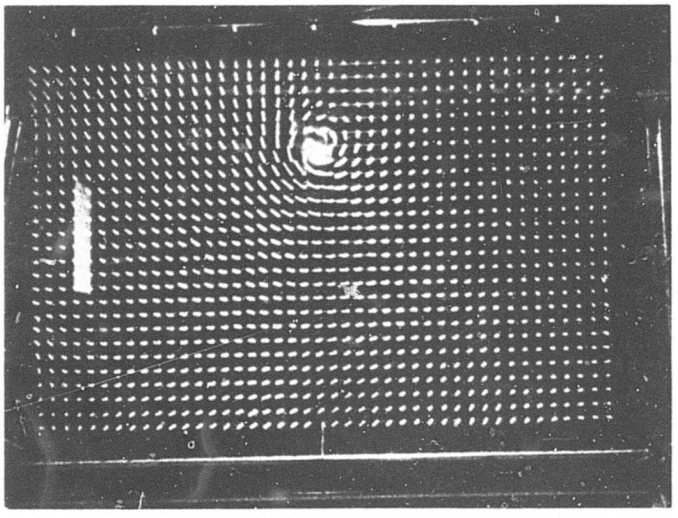

Without Mass Injection

Figure 39. Influence of Mass Injection on Tuft Grid 15 Chord Lengths Downstream of the Model; V=100 fps, α_T=9.5°.

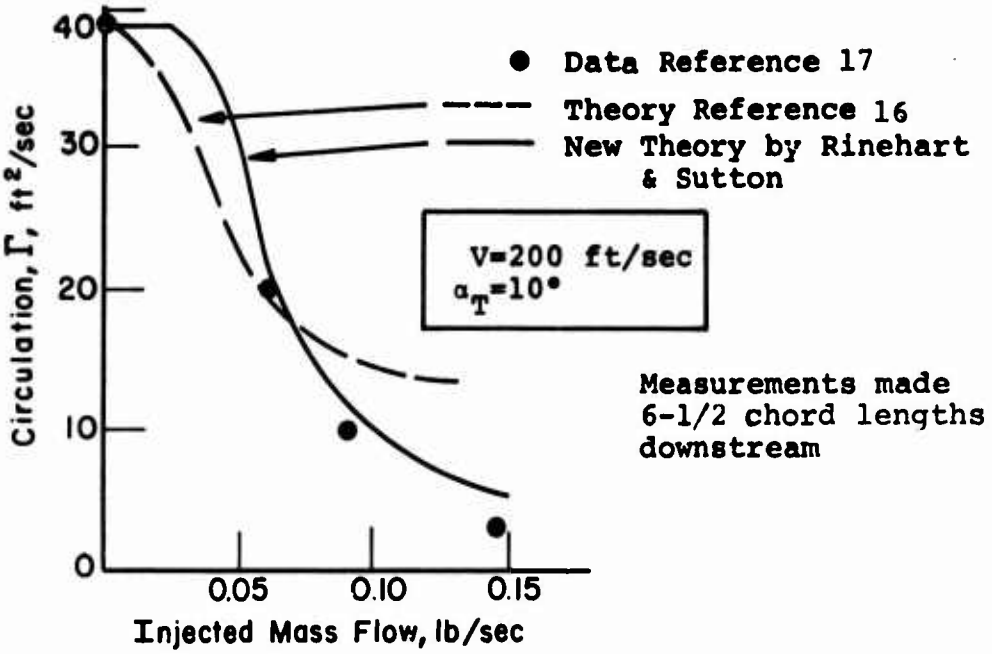

Figure 40. Comparison of Theory and Experiment, AR 4.1 Model (Reference 17).

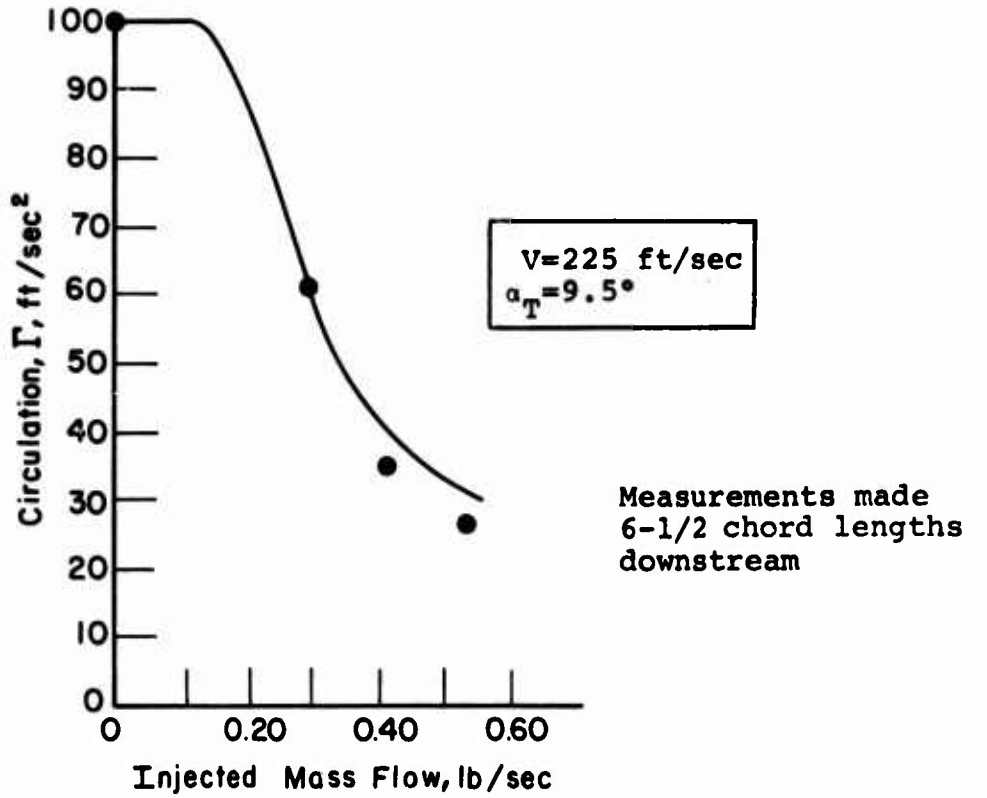

Figure 41. Comparison of Theory and Experiment, AR 2.86 Model.

VIII. LITERATURE CITED

1. Mangler, K.W., CALCULATION OF THE INDUCED VELOCITY FIELD OF A ROTOR, RAE Report No. Aero 2247, 1948.

2. Willmer, M.A.P., THE LOADING OF HELICOPTER ROTOR BLADES IN FORWARD FLIGHT, RAE Report Naval 2-N-76935, No. 8, 1959.

3. Castles, W., and Durham, W.L., THE COMPUTED INSTANTANEOUS VELOCITIES INDUCED AT THE BLADE AXES BY THE SKEWED HELICAL VORTICES IN THE WAKE OF A LIFTING ROTOR IN FORWARD FLIGHT, ASTIA Document No. AD-210613, 1959.

4. Miller, R.H., UNSTEADY AIRLOADS ON HELICOPTER ROTOR BLADES, The Royal Aeronautical Society Fourth Cierva Memorial Lecture, October 1963.

5. Piziali, R.A., and DuWaldt, F.A., COMPUTATION OF ROTARY WING HARMONIC AIRLOADS AND COMPARISON WITH EXPERIMENTAL RESULTS, Presented at AHS Eighteenth Annual National Forum, Washington, D.C., May 1962.

6. Sadler, S. Gene, DEVELOPMENT AND APPLICATION OF A METHOD FOR PREDICTING ROTOR FREE WAKE POSITIONS AND RESULTING ROTOR BLADE AIR LOADS, NASA CR 1911, 1971.

7. Sadler, S. Gene, MAIN ROTOR FREE WAKE GEOMETRY EFFECTS ON BLADE AIRLOADS AND RESPONSE FOR HELICOPTERS IN STEADY MANEUVERS, VOLUME I - THEORETICAL FORMULATION AND ANALYSIS OF RESULTS, Rochester Applied Science Associates, Inc., RASA Report 71-13, NASA Contract NAS1-8448, to be published, 1972.

8. Padakannaya, Raghuveera, EFFECT OF WING TIP CONFIGURATION ON THE STRENGTH AND POSITION OF A ROLLED-UP VORTEX, A Thesis in Aerospace Engineering, NASA CR-66916, March 1970.

9. Spencer, R.H., Sternfeld, H., and McCormick, B.W., TIP VORTEX CORE THICKENING FOR APPLICATION TO HELICOPTER ROTOR NOISE REDUCTION, Vertol Division, The Boeing Company; USAAVLABS Technical Report 66-1, U. S. Army Aviation Materiel Laboratories, Fort Eustis, Virginia, September 1966, AD 644317.

10. Chigier, N.A., and Corsiglia, V.R., TIP VORTICES - VELOCITY DISTRIBUTIONS, Paper presented at the 27th Annual National Forum of the American Helicopter Society, Preprint No. 522, May 19-21, 1971, Washington, D.C.

11. Scheiman, James, and Shivers, James P., EXPLORATORY INVESTIGATION OF THE STRUCTURE OF THE TIP VORTEX OF A SEMISPAN WING FOR SEVERAL WING-TIP MODIFICATIONS, NASA/Langley Research Center, NASA TN D-6101, February 1971.

12. Cornish, J.J. III., HIGH LIFT APPLICATIONS OF SPANWISE BLOWING, Paper presented at the Seventh Congress of the International Council of the Aeronautical Sciences, Consiglio Nazionale Delle Ricerche, Roma, Italy, ICAS Paper No. 70-09, September 14-18, 1970.

13. Olsen, John, AIRCRAFT CONFIGURATION EFFECTS ON WAKE TURBULENCE, Paper presented at FAA Symposium on Turbulence, March 22, 23, 24, 1971, in Washington, D.C.

14. Patterson, James C., Jr., and Flechner, Stuart G., AN EXPLORATORY WIND-TUNNEL INVESTIGATION OF THE WAKE EFFECT OF A PANEL TIP-MOUNTED FAN-JET ENGINE ON THE LIFT-INDUCED VORTEX, NASA TN D-5729, May 1970.

15. McGowan, William A., NASA AIRCRAFT TRAILING VORTEX RESEARCH, Presented at the Federal Aviation Administration Symposium on Turbulence, March 22-24, 1971, Washington, D. C.

16. Rinehart, Stephen A., EFFECTS OF MODIFYING A ROTOR TIP VORTEX BY INJECTION ON DOWNWASH VELOCITIES, NOISE, AND AIRLOADS, Paper presented at AHS/AIAA/UTA Joint Symposium on Environmental Effects on VTOL Designs at Arlington, Texas, November 1970.

17. Rinehart, Stephen A., Balcerak, John C., and White, Richard P., Jr., AN EXPERIMENTAL STUDY OF TIP VORTEX MODIFICATION BY MASS FLOW INJECTION, Rochester Applied Science Assoc., Inc., RASA Report 71-01, ONR Contractor Report, Contract No. N00014-69-C-0169, 1 February 1969 - 31 January 1971.

18. Yuan, S.W., VORTEX POLLUTION, WING-TIP VORTICES: THE HAZARD AND THE REMEDY, J. of the Aeronautical Society of India, Vol. 23, No. 2, May 1971.

19. Poppleton, E.D., EFFECT OF AIR INJECTION INTO THE CORE OF A TRAILING VORTEX, J. of Aircraft, Vol. 8, No. 8, August 1971, pp. 672-673.

20. Kantha, H.L., Lewellen, W.S., and Durgin, F.H., QUALITATIVE RESPONSES OF A VORTEX CORE TO TIP BLOWING AND INTERSECTING AIRFOILS, NASA/Langley Space Research Center Grant No. NGR-22-009-303, ASRL TR 153-4, August 1971.

21. Mason, W.H., and Marchman, J.F., III, INVESTIGATION OF AN AIRCRAFT TRAILING VORTEX USING A TUFT GRID, College of Engineering, Virginia Polytechnic Institute and State University, VPI-E-71-17, NASA Grant No. NGL 47-004-067, September 1971.

22. Fernandez, F.L., and Lubard, S.C., TURBULENT VORTEX WAKES AND JETS, Paper presented at AIAA 4th Fluid and Plasma Dynamics Conference, Palo Alto, Calif., June 21-23, 1971, AIAA Paper No. 71-615.

23. Mager, A., SOLUTION ACROSS VORTEX BREAKDOWN, The Aerospace Corporation, El Segundo, Calif., Report No. ATR-71(9999)-1, April 26, 1971.

APPENDIX I
MASS FLOW RATE VERSUS STATIC PRESSURE AT ORIFICE FOR VARIOUS NOZZLES

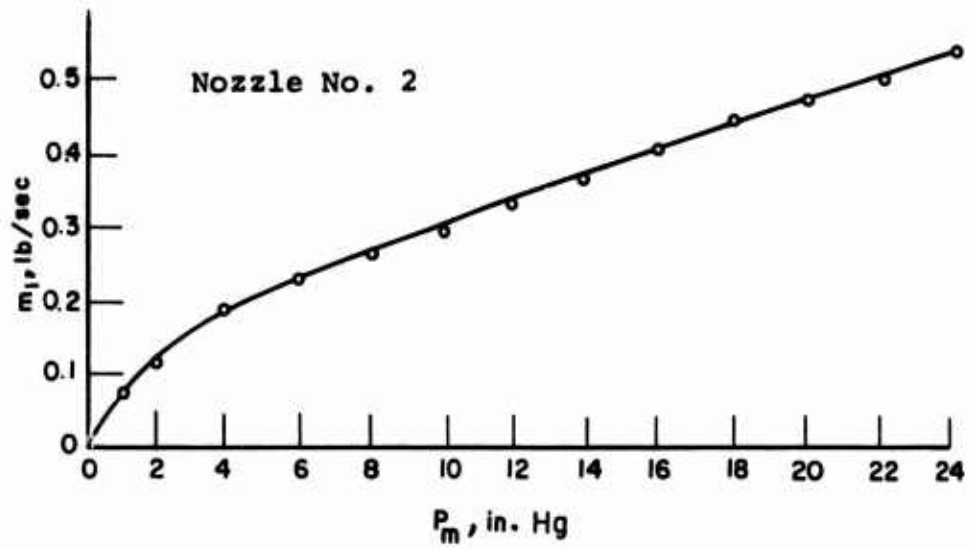

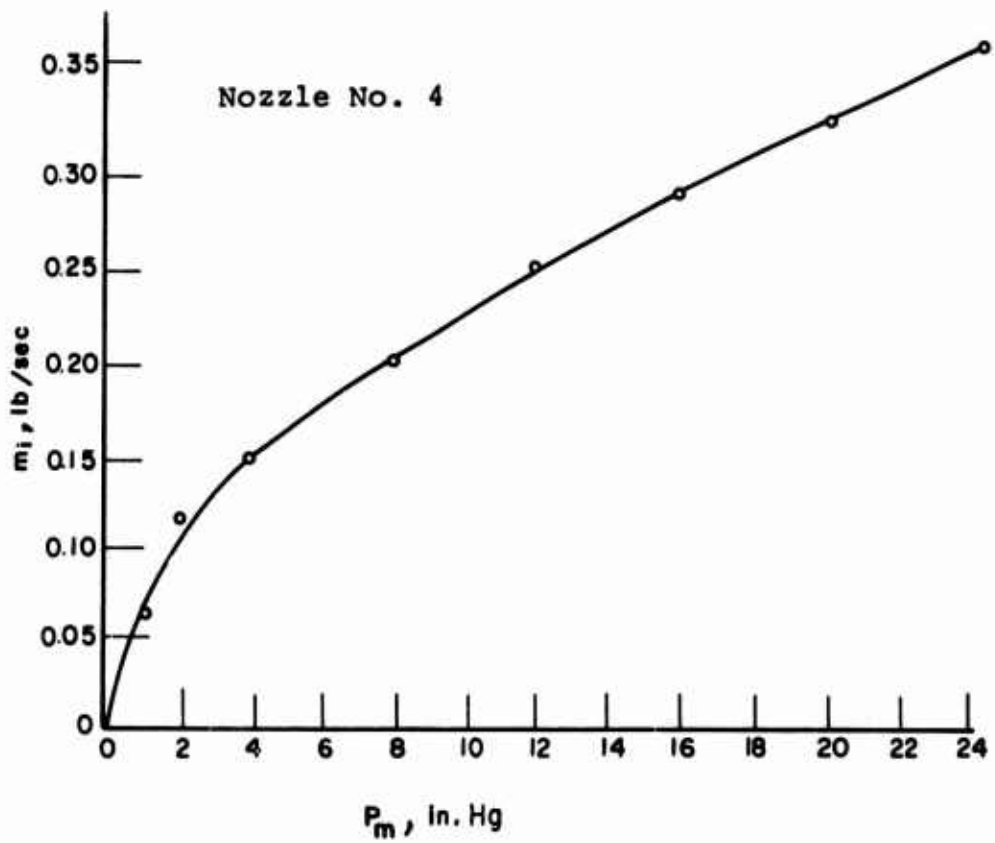

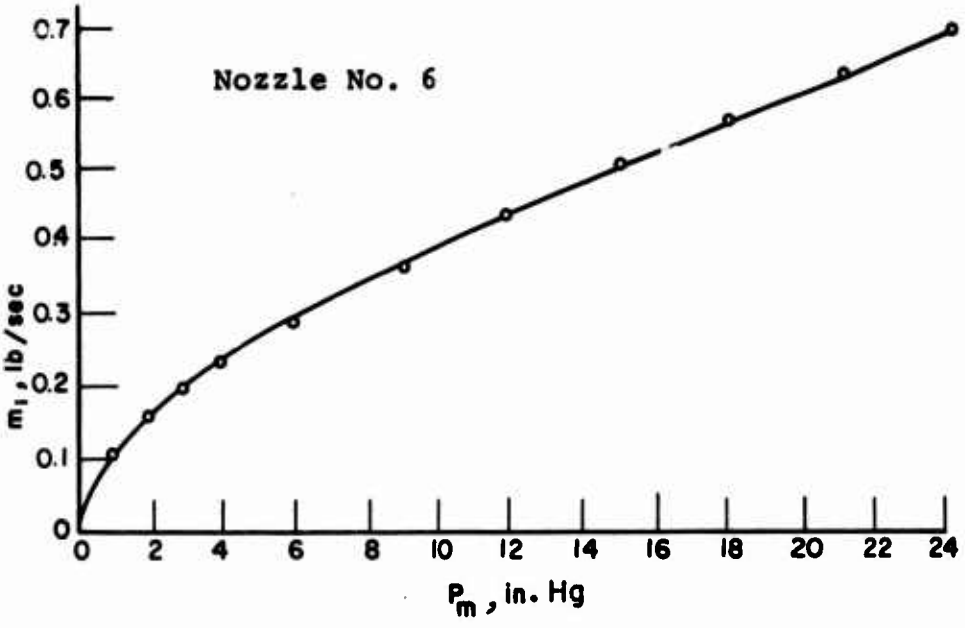
Nozzle No. 6
0.7
0.6
0.5
0.4
0.3
0.2
0.1
0
m_1, lb/sec
0 2 4 6 8 10 12 14 16 18 20 22 24
P_m, in. Hg

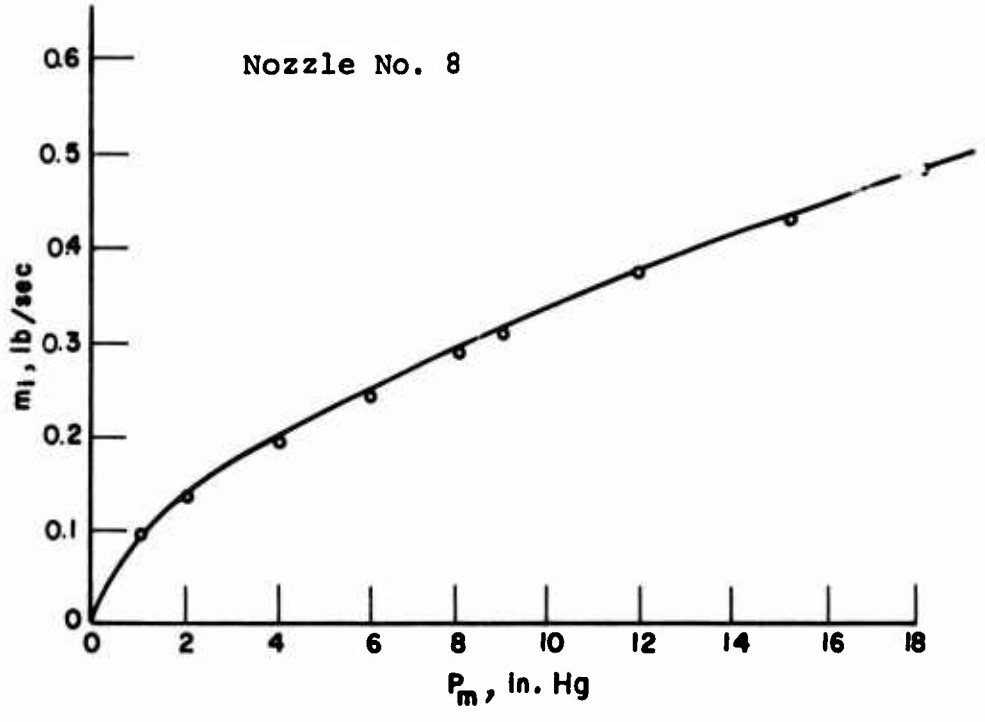
Nozzle No. 8
0.6
0.5
0.4
0.3
0.2
0.1
0
m_1, lb/sec
0 2 4 6 8 10 12 14 16 18
P_m, in. Hg

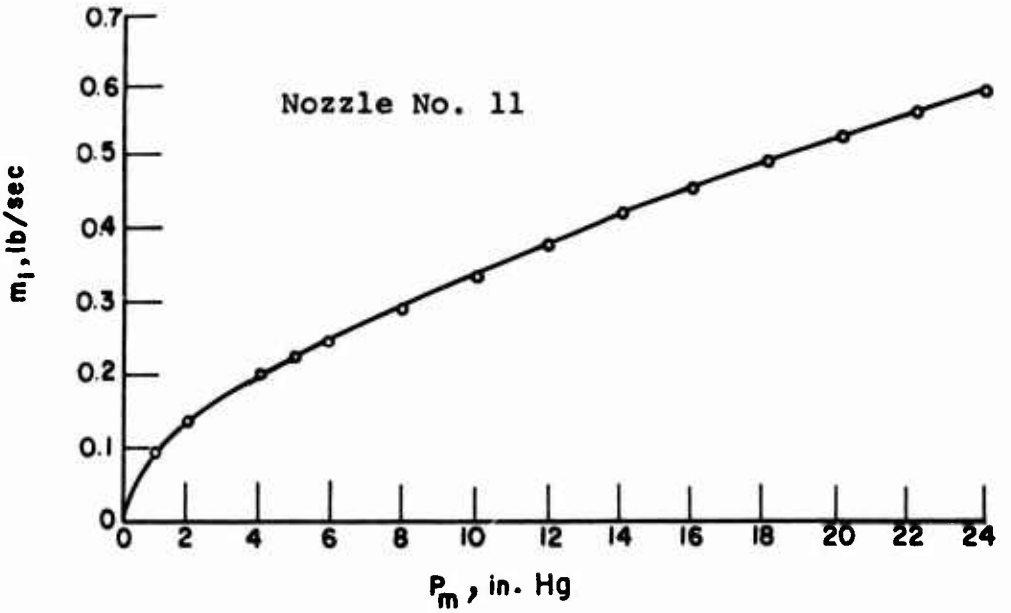
Nozzle No. 11
m_l, lb/sec
0.7
0.6
0.5
0.4
0.3
0.2
0.1
0
0 2 4 6 8 10 12 14 16 18 20 22 24
P_m, in. Hg

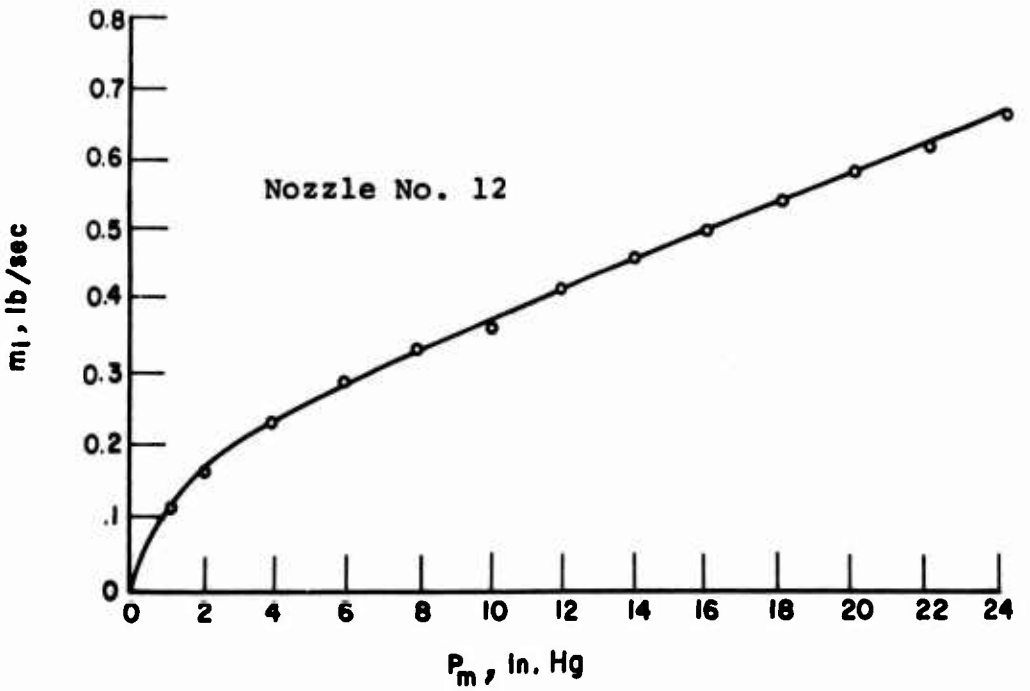
Nozzle No. 12
m_l, lb/sec
0.8
0.7
0.6
0.5
0.4
0.3
0.2
.1
0
0 2 4 6 8 10 12 14 16 18 20 22 24
P_m, in. Hg

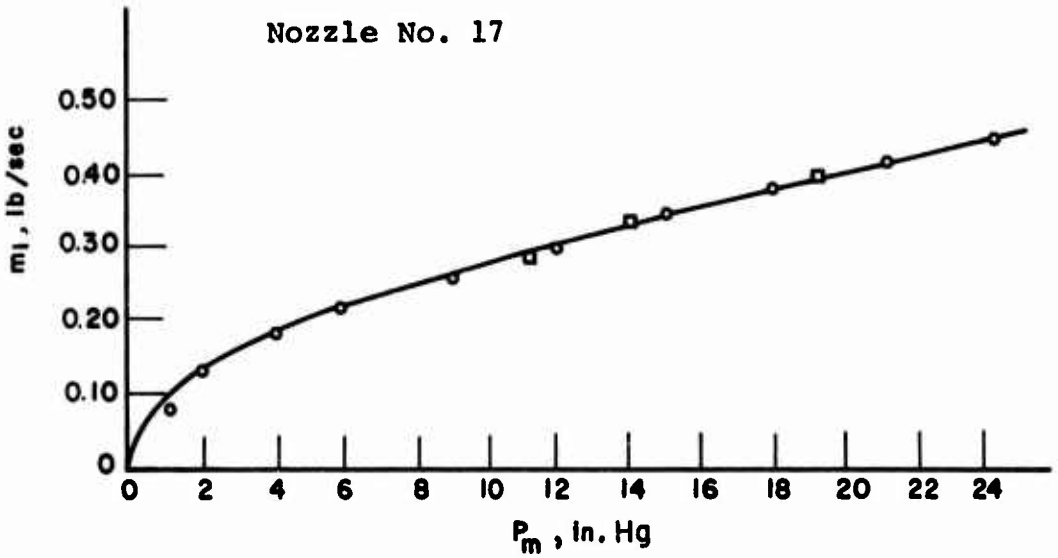
Nozzle No. 17
0.50
0.40
0.30
0.20
0.10
0
m_l, lb/sec
0 2 4 6 8 10 12 14 16 18 20 22 24
P_m, in. Hg

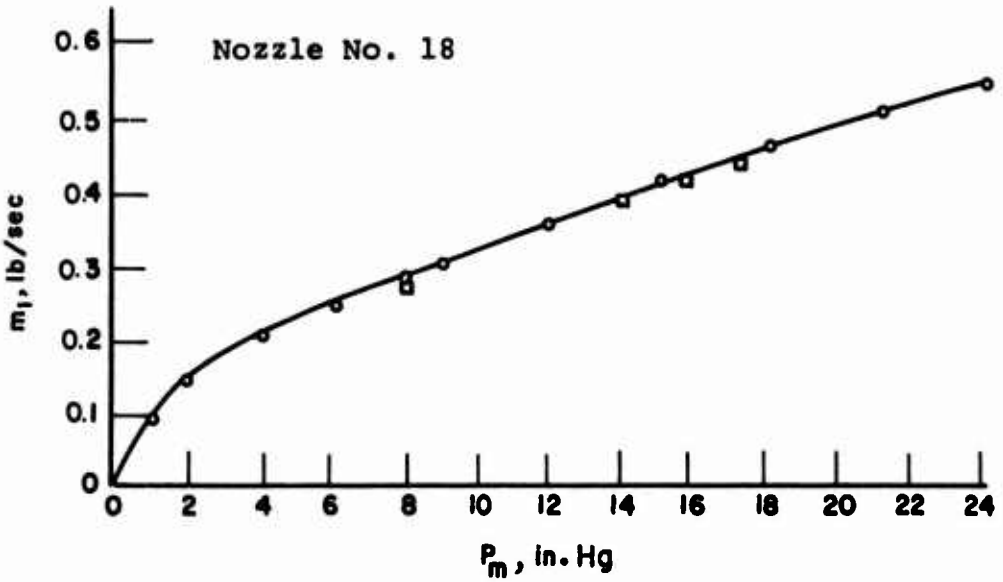
Nozzle No. 18
0.6
0.5
0.4
0.3
0.2
0.1
0
m_l, lb/sec
0 2 4 6 8 10 12 14 16 18 20 22 24
P_m, in. Hg

APPENDIX II
NET BALANCE MEASUREMENTS VERSUS MASS FLOW RATE FOR VARIOUS TEST CONDITIONS

TABLE I. PERFORMANCE PARAMETERS OF ROUND AND SQUARE TIP MODELS, V=75 ft/sec, α_T=9.5°

Tip Configuration	Lift (lb)	Roll Moment* (ft-lb)	Drag (lb)	Drag Moment* (ft-lb)	Pitch Moment* (ft-lb)
Round	36.5	-56.0	1.89	-2.0	-3.9
Square	37.7	-59.0	2.01	-2.0	-4.2

*Roll and drag moments are about the tunnel centerline; pitch moment is about the model 15.5% chord.

TABLE II. PERFORMANCE PARAMETERS OF VARIOUS NOZZLES OF EQUAL AREA, V=150 ft/sec, α_T=9.5°, A=1.24 in.^{2}

Nozzle No.	Nozzle Conf.	Lift (lb)	Roll Moment* (ft-lb)	Drag (lb)	Drag Moment* (ft-lb)	Pitch Moment* (ft-lb)
5	Honeycomb Slot	147.8	-234.7	7.59	-6.9	-16.3
2	Honeycomb Circle	147.5	-237.0	7.28	-7.7	-16.5
11	Open Slot	144.9	-232.8	7.53	-7.2	-15.8
8	Open Circle	149.1	-237.4	7.37	-6.3	-16.5

*Roll and drag moments are about the tunnel centerline; pitch moment is about the model 15.5% chord.

TABLE III. PERFORMANCE PARAMETERS OF SLOTTED HONEYCOMB NOZZLES OF VARIOUS AREA, V=150 ft/sec, α_T=9.5°

Nozzle No.	Nozzle A(in^2)	Lift (lb)	Roll Moment* (ft-lb)	Drag (lb)	Drag Moment* (ft-lb)	Pitch Moment* (ft-lb)
4	0.83	145.9	-233.1	8.69	-7.1	-16.1
5	1.24	147.8	-234.7	7.59	-6.9	-16.3
6	1.66	144.6	-229.0	8.55	-6.9	-16.4

*Roll and drag moments are about the tunnel centerline; pitch moment is about the model 15.5% chord.

TABLE IV. PERFORMANCE PARAMETERS OF SLOTTED HONEYCOMB NOZZLES FOR VARIOUS ANGLES OF INJECTION, V=150 ft/sec, α_T=9.5°, A=1.24 $in.^2$

Nozzle No.	Nozzle α_i deg.	Lift (lb)	Roll Moment* (ft-lb)	Drag (lb)	Drag Moment* (ft-lb)	Pitch Moment* (ft-lb)
17	5.5	148.9	-235.1	7.27	-6.4	-16.8
5	9.5	147.8	-234.7	7.59	-6.9	-16.3
18	13.5	149.6	-242.6	8.24	-6.3	-15.5

*Roll and drag moments are about the tunnel centerline; pitch moment is about the model 15.5% chord.

TABLE V. PERFORMANCE PARAMETERS FOR DETAILED SURVEYS

V (ft/sec)	α_T (deg)	m_i (lb/sec)	Lift (lb)	Roll Moment* (ft-lb)	Drag (lb)	Drag Moment* (ft-lb)	Pitch Moment* (ft-lb)
100	13.5	0	82.2	-119.6	7.74	-10.5	-12.1
100	13.5						
100	13.5	0.169	82.5	-118.1	7.81	-11.4	-12.1
100	13.5	0.281	81.1	-117.7	7.77	-11.0	-12.5
100	13.5	0.446	83.0	-120.8	7.73	-10.6	-12.5
150	9.5	0	131.4	-198.8	9.27	-13.2	-15.8
150	9.5	0.169	133.2	-202.8	9.61	-13.1	-16.8
150	9.5	0.281	132.5	-203.6	9.36	-13.1	-17.6
150	9.5	0.374	133.0	-200.2	9.75	-13.7	-17.6
225	9.5	0	300.2	-468.5	22.19	-31.0	-39.3
225	9.5						
225	9.5	0.296	302.4	-467.3	21.72	-29.7	-40.3
225	9.5	0.421	302.6	-468.7	22.03	-31.0	-40.9
225	9.5	0.562	302.0	-468.2	20.90	-32.0	-41.0
150	13.5	0	187.0	-264.5	17.70	-26.4	-26.5
150	13.5						
150	13.5	0.298	188.9	-275.7	17.75	-25.6	-27.5
150	13.5	0.421	188.6	-275.3	18.07	-25.3	-27.8
150	13.5	0.565	188.6	-275.6	19.92	-26.8	-28.3
230	13.5	0	453.2	-661.2	43.23	-54.9	-65.3
230	13.5						
230	13.5	0.562	454.6	-658.3	42.78	-60.7	-67.2

*Roll and drag moments are about the tunnel centerline; pitch moment is about the model 15.5% chord.